Examining the cell cycle regulator, p21, in the regeneration competent newt species, *Notophthalmus viridescens*

Rachel E. Nottrodt, Hon. BSc.

A thesis submitted to the department of Biological Sciences in partial fulfillment of the requirements for the degree of Master of Science

April 25th, 2016

Abstract

Adult newts are capable of completely regenerating lost structures including limb, tail, and spinal cord tissues after injury. A unique mammal capable of similar epimorphic regeneration is the Murphy Roths Large (MRL) mouse with the ability to fully close ear hole punctures. Examination of these mice revealed that they do not express the protein p21, a cyclin dependent kinase (CDK) inhibitor, which controls cell cycle progression from G1 to S phase by monitoring the cell for DNA damage. Knockout p21 mice were also able to fully close ear hole punctures validating the role of p21 in this phenomenon. Based on these findings, my research seeks to examine p21 during newt tail and caudal spinal cord regeneration. Since a lack of p21 allows for regeneration in these mice, otherwise considered regeneration-incompetent, it is of interest to study p21 in the regeneration-competent newt, *Notophthalmus viridescens*. Using qPCR, I demonstrated that transcripts of a p21-like gene are significantly down-regulated at 14 and 21 days post amputation. Initial Western blots indicated temporal changes in p21 expression across regeneration time points, but at a molecular weight smaller than the predicted 21kDa. The discrepancy in molecular weight led to mass spectrometry protein identification analysis that detected a p16-interacting protein in newt tail that shares 87.5% identity with the *Xenopus* p16-interacting protein. p16 is also a CDK inhibitor, acting at the G1-S transition to specifically inhibit cyclin D and CDK4/6. Continued survey for p21 protein expression was unable to detect p21 within newt tissues tested. This outcome suggests either the tested antibodies are unable to cross-react with the newt p21 protein, or that it is expressed at very low levels in the newt making it virtually undetectable, or the newt lacks p21 protein like the MRL mouse. 5'-3' RACE was unable to determine the newt-specific p21 sequence, but the newt Histone H3a gene was amplified and found to contain some sequence similarity to p21 in other species. This work represents the first attempt to study p21 gene and protein expression in regenerating newt caudal tail and spinal cord tissue. The novel finding of p16-interacting protein suggests the potential for alternative cell cycle regulation methods, via p16, previously thought to be lost in the newt.

Acknowledgements

First and foremost I would like to thank my supervisor, Dr. Robert Carlone, for his unwavering support and guidance throughout this process. I am fortunate to have worked in his lab for the past four years, first as an undergraduate and now as a graduate student. Looking back, there were "easier" projects to pursue for my MSc, but I can honestly say that the roadblocks I encountered challenged me to keep thinking outside the box and have made me a better scientist going forward. Thank you for always encouraging me to continue the pursuit of science and research – even if it meant leaving the lab bench to dig up dinosaur bones instead.

Thank you as well to my thesis committee members, Dr. Spencer and Dr. Stuart, for your invaluable feedback, ideas, and technical assistance.

Graduate school is a unique environment to work, study, and live in, and I am thankful for the many friends I have made in my time here at Brock University. Honourable mentions go to my mentor and friend Dr. Amanda Lepp, my comrade Jonathan Simone, whom I first started grad school with, the ever helpful Dr. Nicholas Vesprini, my long time lab mate of years past David Rozema, my friendly neighbours in the Tattersall lab Susan Wang and Ian Black, and finally, my rock girls – Cait Garner and Rebecca Gunter.

Lastly, I would like to thank my family. The conclusion of my Master's work marks the end of my time at home as I embark on a new journey to pursue a PhD out west. I can never thank my parents enough for the opportunities they have provided me, their enduring support, and their decision to expose me to the wonders of exploration and science from a young age. Thanks to Ben for being an awesome brother and all those fun late night rides home from the lab.

Table of Contents

List of Figures

List of Tables

List of Abbreviations

p19/ARF	Alternative Reading Frame
ATP	Adenosine Triphosphate
BLAST	Basic Local Alignment Search Tool
BrdU	Bromodeoxyuridine
BSA	Bovine Serum Albumin
C57BL/6	C57 Black 6 mouse
CDK	Cyclin Dependent Kinase
CDKN1A	Cyclin-Dependent Kinase Inhibitor 1A
CDKN2A	Cyclin-Dependent Kinase Inhibitor 2A
cDNA	Complementary deoxyribonucleic acid
CIP1	Cyclin Inhibitor Protein/CDK Interacting Protein 1
CIZ1	Cip1 Interacting Zinc Finger Protein
CNS	Central Nervous System
DNA	Deoxyribonucleic acid
dpa	Days Post Amputation
dpi	Days Post Injury
ERK	Extracellular Regulated Kinase
ESCs	Embryonic Stem Cells
EST	Expressed Sequence Tag
Evi5	Ecotropic Viral Integrative Factor
FISH	Fluorescence In Situ Hybridization
GFAP	Glial Fibrillary Acidic Protein
GSP	Gene Specific Protein
Gy	Gray (unit of radiation)
^{3}H	Tritiated thymidine
INK4A	Inhibitor of Kinase 4A
KIP	Kinase Inhibitor Protein
miRNA	MicroRNA
MIQE	Minimum Information for Publication of Real Time Quantitative PCR Experiments
MMPs	Matrix Metalloproteinases
mRNA	Messenger Ribonucleic Acid
MRL	Murphy Roth's Large
NCBI	National Centre for Biotechnology Institute
PBS	Phosphate Buffered Saline
PCNA	Proliferating Cell Nuclear Antigen
pERK	Phosphorylated Extracellular Regulated Kinase
PNS	Peripheral Nervous System
pRb	Retinoblastoma Protein
PVDF	Polyvinylidene fluoride
RACE	Rapid Amplification of cDNA ends
RNA	Ribonucleic acid
RT-qPCR	Reverse transcriptase quantitative Polymerase Chain Reaction
SCI	Spinal Cord Injury
TIMPs	Tissue Inhibitors of Metalloproteinases
WAF1	Wild-Type p53 Activated factor

CHAPTER ONE:
Introduction and Literature Review

1.1 General Introduction

Humans have been fascinated by the phenomenon of regeneration for centuries, with Spallanzani's (1768) work detailing the regeneration of worms, snails, and amphibians like frogs and salamanders. His work represents the first account of complete limb and tail regeneration in the urodele amphibians: newts, axolotls, and salamanders. Following tail amputation, a thickened wound epidermis forms, allowing cells below this surface to proliferate and grow outwards into what is known as a blastema. This highly proliferative cell population associates with the regenerating spinal cord to elongate the regenerate and restore the tail to its original form and functional capacity. Mammals are capable of limited regeneration as seen with human embryonic digit tips and seasonal antler renewal in deer, but they typically lack the ability to fully regenerate lost or injured tissues (Allen et al., 2002; Bryant et al., 2002). Scar formation is thought to be the greatest physical barrier to successful regeneration in mammals, and it is the lack of a scar that aids in creating a permissive environment in urodeles (Whited et al., 2011).

One exemption to the finding that mammals are regeneration-incompetent is the Murphy Roths Large or MRL mouse, first created in 1979 by Murphy and Roths to study autoimmune deficiency disorders such as systemic lupus erythematosus. Serendipitously, while creating ear hole punches for identification purposes, it was observed that after approximately 30 days, the MRL mice no longer had holes in their ears when compared to wild-type mice that underwent the same procedure (Clark et al., 1998). Upon histological examination, punched ears developed a thickened wound covering, with cells below proliferating in a ring-like structure that resembled the blastema seen in regenerating urodele limbs and tails. Further study of this mouse model determined that in addition to regenerating lost ear tissue, the MRL mouse is capable of regenerating heart myocardium, central and peripheral nerves, brain, and other tissues (Buckley et al., 2012; Hampton et al., 2004; Leferovich et al., 2001; Thuret et al., 2012).

Additional examination of MRL mouse ear fibroblasts found that the cells showed a distinct G2/M (gap 2 and mitosis) bias and a high degree of DNA damage – two characteristics

common to the cells of classic regenerators, like hydra and newts, liver tissue, and mouse embryonic stem cells (Bedelbaeva et al., 2010; Buzgariu et al., 2014; Chuykin et al., 2008; Fausto and Webber, 1994; Tanaka et al., 1997). These traits are also indicative of a disruption in cell cycle regulation and led researchers to the discovery that the MRL mouse lacks the cyclin-dependent kinase inhibitor (CKI) known as CDKN1A or p21 (Bedelbaeva et al., 2010). The G1/S (gap 1 and synthesis (replication) phase) transition of the cell cycle is controlled by p21 as the cells prepare for DNA replication. A lack of p21 in the MRL mouse allows for the increased proliferation required for regeneration, but causes the cells to acquire DNA damage from repeated rounds of replication without typical repair. The generation of p21 knockout mice, which were capable of regenerating to the same degree as the MRL mouse strain, demonstrated that a lack of p21 is sufficient to induce regeneration in an otherwise regeneration-incompetent wild-type mouse. Given that a lack of the cell cycle regulator, p21, confers regenerative capabilities in an otherwise regeneration-incompetent species, it is of great interest to determine if and how p21 is involved in the regenerative process in newts.

1.2 Mammalian spinal cord wound healing versus newt caudal spinal cord and tail regeneration

Spinal cord injury (SCI) is characterized by toxic myelin breakdown, the influx of calcium ions, and the formation of a glial scar (Fitch et al., 1999; Silver and Miller, 2004). Following spinal cord injury, mammals undergo primary physical damage that is characterized by hemorrhage and local death of neurons, oligodendrocytes, and astrocytes at the injury site (Lee-Liu et al., 2013). The secondary chemical trauma involves extensive cell death via apoptosis caused by the increased local inflammation. Reactive astrocytes invade the injury site and a glial scar is formed, physically preventing regeneration (Lee-Liu et al., 2013). However, recent evidence suggests that following spinal cord injury in adult mice, axon regeneration can only occur when astrocyte bridges are present (Anderson et al., 2016). When astrocytic scar formation is prevented using a variety of transgenic loss-of-function strategies, a significant

decrease in axonal regrowth is seen, indicating that scar-forming astrocytes facilitate and support robust CNS axon regeneration (Anderson et al., 2016). Interestingly, in the period immediately following a SCI, reactive astrocytes serve a neuroprotective and reparative role, later becoming inhibitory in nature (Lee-Liu et al., 2013). These responses represent both the chemical and physical barriers that prevent mammalian spinal cord regeneration.

Central nervous system (CNS) axonal regenerative capacity exists in mammalian embryos during the early post-natal period, but is restricted as development proceeds (Lee-Liu et al., 2013). The ability of newts to prevent normal scar formation after wounding establishes a permissive environment for regenerative pathways and molecules to initiate and maintain proliferation and outgrowth (Chernoff et al., 2002; Whited et al., 2011). CNS myelin in the newt does not inhibit nerve outgrowth, as it does in the mammal, and less secondary cell death occurs (Chernoff and Stocum, 1995). The newt also experiences calcium influx associated with glutamate excitotoxicity following injury, which would typically kill local neurons and oligodendrocytes, but the injury-reactive ependymal cells are capable of acting as a buffer by sequestering calcium and therefore protecting cells from processes that trigger secondary cell death in the mammal (Chernoff et al., 2003).

Ependymal cells, which line the central canal of the spinal cord in all vertebrates, are thought to contribute the most during spinal cord regeneration as they either maintain the embryonic characteristics of the neuroepithelia or establish the mesenchymal blastema through proliferation and tissue remodeling post injury (Chernoff and Stocum, 1995; Chernoff et al., 2003). These neural progenitor cells acquire broad multipotency and are responsible for creating structures quite distinct from their embryological origins (Tanaka, 2003). The complete regeneration of the amputated tail relies upon the ependymal cells forming a hollow vesicle that remains continuous with the central canal of the cranial, intact spinal cord and provides a scaffold for nerve regeneration (Zukor et al., 2011). This hollow tube becomes the developing spinal cord within the regenerate and extends from the original amputation plane to the caudal

most tip of the blastema (Géraudie et al., 1988; Nordlander and Singer, 1978). Contact between the proliferating cells of the spinal cord and the tail stump lead to the formation of the wound epithelium, thereby driving the process of epimorphic regeneration in the newt tail (Chernoff and Stocum, 1995). Epimorphic regeneration involves the local dedifferentiation of tissues at the injury site and recruitment of progenitor cells to this region, which then undergo extensive proliferation to form a heterogeneous mass of cells (known as a blastema), and eventually differentiate to replace the missing structures (Gawriluk et al., 2016; Stocum and Cameron, 2011). This intricate process of caudal tail and spinal cord regeneration in the newt is an important model to study given that it involves extensive CNS regeneration in addition to epimorphic tissue regeneration of a variety of non-neural structures.

1.3 Stages of tail regeneration in the newt, *Notophthalmus viridescens*

Tail regeneration follows a rostrocaudal pattern and has been described as occurring in five distinct stages, each defined by key morphological and cellular features (Iten and Bryant, 1976). Figure 1.1A-D includes representative histological sections from stages I to IV, respectively. Stage I (Figure 1.1A), representing 1-5 days post amputation (dpa), is characterized by the formation of a thickened wound epithelium that covers the amputation site and the lack of a basement membrane below the wound epidermis. Breakdown of the basement membrane is related to the absence of tissue inhibitors of metalloproteinases (TIMPs) and the related significant increase of matrix metalloproteinases (MMPs), which are found to be highest at two to four weeks post lesioning (Chernoff et al., 2003). The posterior tip of the severed spinal cord retracts and remains proximal to the level of amputation, and the spinal cord meninges extend to make contact with the wound epidermis (Iten and Bryant, 1976). Mitotic figures are not observed in the ependymal cells at this time.

Stage II (Figure 1.1B), encompassed by 6-11 dpa, is the point at which the tail stump takes on a dome shape as it starts out swollen and translucent with a blister-like appearance relative to the firm stump epidermis (Iten and Bryant, 1976). Dead cells and tissue debris are

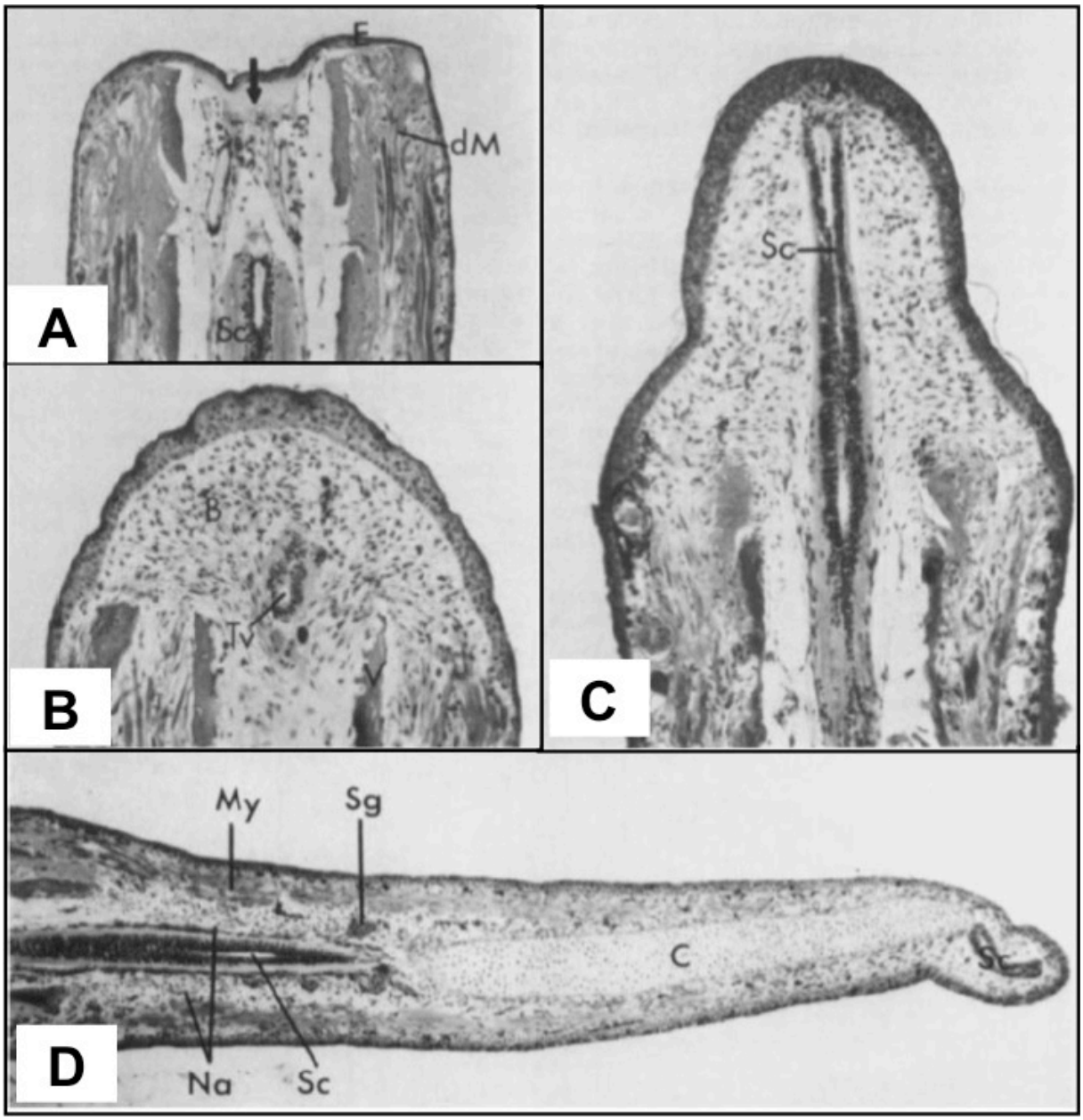

Figure 1.1: Stages of Tail Regeneration in the Adult Newt, *Notophthalmus viridescens.* Figured adapted from Iten and Bryant (1976). A) Frontal section through a regenerate 2 dpa featuring tissue debris (arrow) below epidermis (E), degenerating muscle fibers (dM), and the posterior spinal cord (Sc). B) Median frontal section of a regenerate 10 dpa with the terminal vesicle (Tv) of the ependymal tube present in the accumulation blastema (B). A transected vertebra (V) is also highlighted. C) Frontal section through the spinal cord (Sc) of a regenerate 13 days post amputation. D) Median frontal section of a regenerate 20 dpa featuring the distal half of the cartilaginous rod (C), proximal and distal portions of the regenerating spinal cord (Sc), a myomere (My) amongst new muscle fibers, the neural arch of regenerating vertebra (Na), and spinal ganglia (Sg) surrounding the spinal cord.

found within the wound epidermis and blastema cells are first seen accumulating beneath the regenerate tip. The ependymal tube is formed at this stage caudal to the amputation plane. Ependymal cells exhibit a high degree of mitosis with cells immediately rostral to the amputation site being the area of greatest proliferation (Egar and Singer, 1972; Nordlander and Singer, 1978). Bromodeoxyuridine (BrdU), a thymidine analog that becomes incorporated into the DNA and is used to monitor cell proliferation, indicated that the high levels of mitosis in ependymal cells are also associated with the terminal bulb, with cells distributed along the length of the tube providing a source for new, differentiated neurons (Benraiss et al., 1999; Chernoff et al., 2003). Mesenchymal-like cells surrounding the early ependymal tube are thought to later give rise to muscle and bone in the regenerated tail (Géraudie et al., 1988). The epidermis is innervated, spinal ganglia around the amputation site are growing into the accumulation blastema, and osteoclasts are observed surrounding transected vertebra.

Stage III (Figure 1.1C) from days 11 to 15 encompasses a distinct change in the tail regenerate from dome-shaped to cone-shaped. It is now possible to observe vascularization in the tail, and dead cells and tissue debris have been cleared from the thinning epidermis (Iten and Bryant, 1976). Chondrogenesis is prevalent at this stage, with the developing cartilaginous rod, from which the centrum and new vertebral arches will be derived, is located beneath the cord (Géraudie et al., 1988; Iten and Bryant, 1976). The terminal vesicle of the spinal cord is close to the tip of the regenerating tail, and both myoblast and myotube formation is also occurring at this stage.

Stage IV (Figure 1.1D) covers regeneration from days 16 to 28. At this point, extensive differentiation begins within the tail regenerate, including a gradient of muscle differentiation from the stump. The cartilaginous rod continues to elongate and mature in association with the spinal cord. Numerous mitotic figures are observed along the length of the regenerated ependymal tube, with the establishment of a meningeal layer beginning at the proximal spinal cord (Iten and Bryant, 1976). New neurons are created within the cord itself and spinal cord

regeneration within the tail involves the formation of new segmental nerves and ganglia (Egar and Singer, 1972; Géraudie et al., 1988; Nordlander and Singer, 1978). Peripheral nervous system (PNS) and CNS neurons are produced from the ependymal tube with three week old tail regenerates showing proliferative ependymal cells directly giving rise to glia and neurons (Chernoff et al., 2003). Blastema cells have become confined to the distal tip of the regenerate, condensed between the epidermis and the cartilaginous rod. Spinal ganglia are observed as pairs lateral to the regenerated spinal cord.

Finally in stage V (no image shown), the regenerating tail undergoes full differentiation of remaining tissues. Fine morphological features of the vertebra can be described at this stage. Spinal ganglia are located laterally and ventrally to the regenerated spinal cord and muscle fibers are present along the length of the regenerate (Iten and Bryant, 1976).

One exceptional mammal, known as the MRL mouse, is capable of regenerating a variety of tissues in a mechanism that resembles this epimorphic regeneration seen in the newt.

1.4 The MRL mouse: A mammalian model capable of regeneration

The MRL or Murphy Roths Large mouse was originally created as a mouse line to study autoimmune deficiency disorders, specifically systemic lupus erythematosus (Murphy and Roths, 1979). The mouse line was created from crossing the following strains: AKR, an albino mouse strain with a high incidence of lymphatic leukemia; C3H, an inbred mouse strain with a high incidence of mammary tumors; C57BL/6, or C57 black 6, a common inbred strain of lab mice that is refractory to tumors; and LG/J, or Large, a mouse strain with a compromised immune system that produces antinuclear antibodies and rheumatoid factors (Jackson Laboratory). The last strain, LG/J, contributed to 75% of the MRL mouse's genome and is the only strain included that has regenerative capabilities. Importantly, studies by Kench et al. (1999) demonstrated with reciprocal bone marrow transplants that the ability of the MRL mouse to regenerate is independent of its autoimmunity. The MRL mouse possesses many characteristics that resemble a microenvironment conducive for tumor formation, however the strain has a low incidence of

cancer (Heber-Katz and Naviaux, 2015).

When ear hole punctures were created for identification purposes, it was observed that these mice were able to fully close the holes when compared to wild-type mice (Clark et al., 1998). Ear punctures close in approximately 4 weeks without scarring and normal tissue architecture is reestablished (Clark et al., 1998). Upon closer inspection, it was determined that this closure was facilitated by a highly proliferative cell population mimicking a blastema (Bedelbaeva et al., 2010). This type of regeneration is similar to epimorphic regeneration in urodele species such as the newt because of the prompt re-epithelialization of the wound surface post injury, the formation of a blastema, and the lack of scar formation during healing (Arthur and Heber-Katz, 2011). The circular blastema formed following breakdown of the basement membrane allows local cells to dedifferentiate, proliferate, and eventually re-differentiate into new mouse ear tissue (Figure 1.2).

The discovery of the MRL mouse's ability to regenerate lost ear tissue spurred further research into the extent of the mouse's capacity for regeneration. In MRL mice, innervated ears close almost completely by day 50, but denervated ears become increasingly necrotic with the wound spreading to the ear tip (Buckley et al., 2012). It has since been determined that the MRL mouse is also capable of regenerating heart and brain tissue (Cheng et al., 2013; Hampton et al., 2004; Leferovich et al., 2001; Tucker et al., 2008). Except for rabbits, which have been found to close small ear hole punctures over a 6-8 week period, the MRL mouse is unique in its ability to fully close ear hole punctures in addition to regenerating other tissues (Grimes, 1972; Grimes and Goss, 1970). These mice exhibit high levels of DNA damage, an accumulation of cells at the G2/M stage of the cell cycle, and a lack of p21 protein in both uninjured and injured tissues (Bedelbaeva et al., 2010). The initial finding of cell accumulation in the G2/M phase indicated a possible G1 checkpoint deficiency and led to the specific studies of p21. This G2/M bias, characterized by a lack of p21, leads to unscheduled entry into the synthesis phase of the cell cycle and is common to regenerators as it creates an environment conducive to a proliferative

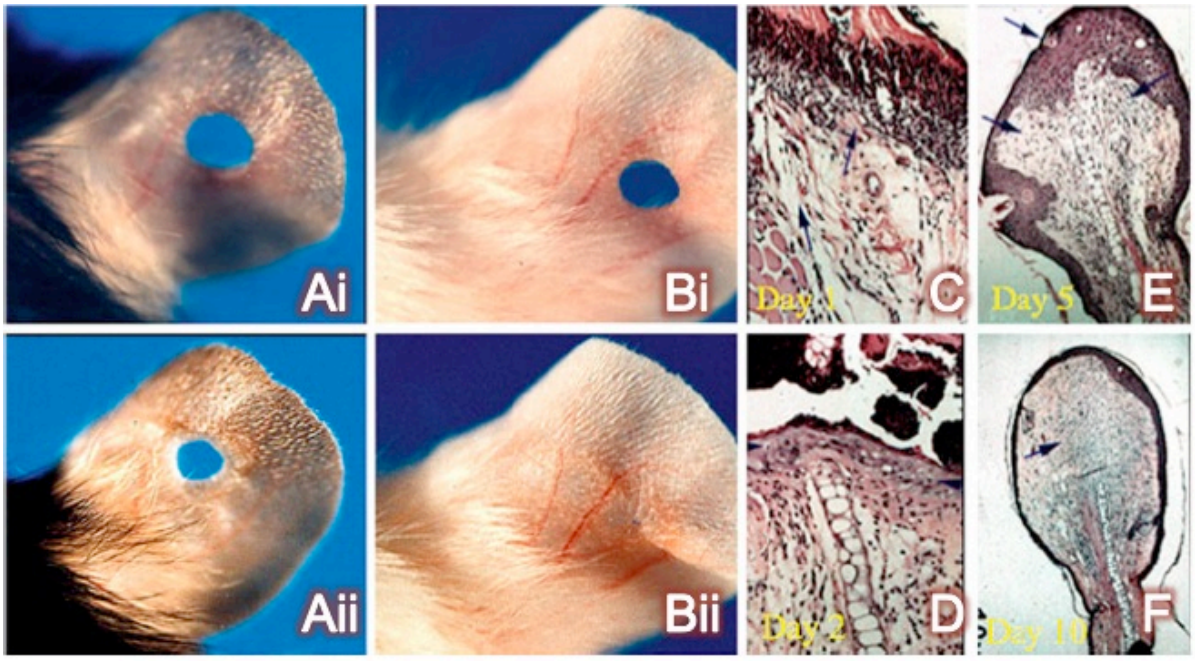

Figure 1.2: The MRL mouse is able to fully regenerate ear hole punctures in a mechanism similar to epimorphic regeneration in the newt. Figure adapted from Heber-Katz et al., (2012). Ai) A control, wild-type mouse (C57BL/6) with initial ear hole punctures and the same ear (Aii) 30 days later. Bi) An MRL mouse ear at the time of ear hole puncture and 30 days later (Bii) showing a closed hole where the puncture used to be.
C-F) Histological changes in the regenerating MRL mouse ear. C) At 1 day post injury (dpi), inflammatory cells line up at the edge of the ear punch (arrows). D) Re-epithelialization of the wound surface is complete by 2 dpi, forming a wound epidermis similar to a regenerating newt tail. E) At 5 dpi, hair follicles begin to form within the new epidermis (uppermost arrow) and cells begin to accumulate in a blastema-like structure beneath the wound epidermis (two lower arrows). F) Ten days post injury the ear tissue contains a highly proliferative cell population (arrow) like that of a blastema, which will eventually close the ear hole by replacing the lost tissue.

response (Bedelbaeva et al., 2010).

Through Western blotting, it was determined that MRL mice do not express the cell cycle regulator p21, and when the p21 gene was ablated in wild-type mice, they too possessed the ability to regenerate lost ear tissue (Bedelbaeva et al., 2010). This demonstrated that a lack of p21 confers regenerative abilities in an otherwise regeneration-incompetent species.

1.5 Cell cycle regulation and p21

The cell cycle contains four main stages (Figure 1.3A) with a quiescent stage, G0; G1, the initial gap before the cell is ready to synthesize DNA; S-phase, DNA synthesis by replication; G2, the second gap during which the cell prepares to divide; and M, the point at which the cell undergoes division through mitosis (Besson et al., 2008; Pajalunga et al., 2008; Vermeulen et al., 2003). p21, also known as CDKN1A (Cyclin-dependent kinase inhibitor 1A), belongs to the Cip/Kip (cyclin inhibitor protein/kinase inhibitor protein) family of CDK (cyclin dependent kinase) inhibitors and acts primarily in the G1 phase to prevent cell cycle progression by binding directly to cyclin-CDK complexes (Albrecht et al., 1997; Harper et al., 1995). The Cip/Kip family includes p21, p27, and p57, all of which contain a conserved amino-terminal CDK inhibitory domain of approximately 80 amino acids (Niculescu et al., 1998).

p21 exhibits preferential binding to the CDK4/6-cyclin D and CDK2-cyclin E complexes causing deformation of and interference with the CDK active site (Niculescu et al., 1998). The related CDK inhibitor, p16 (CDKN2A), is derived from the INK4a locus, and specifically targets D-type cyclins and CDK4/6, rendering the retinoblastoma (pRb) protein inactive (Liggett and Sidransky, 1998; Lukas et al., 1995; Serrano, 1997; Serrano et al., 1993). p16 can only cause cell cycle arrest up until a certain stage in late G1 that most likely correlates with a checkpoint executed by the cyclin D:CDK4/6 complexes (Lukas et al., 1995). The p21 gene contains a p53 binding site in its promoter, allowing p53 to transcriptionally activate p21 gene expression (Besson et al., 2008). p21 is also capable of preventing DNA synthesis by binding to proliferating cell nuclear antigen (PCNA), an interaction that allows for cell cycle arrest in S

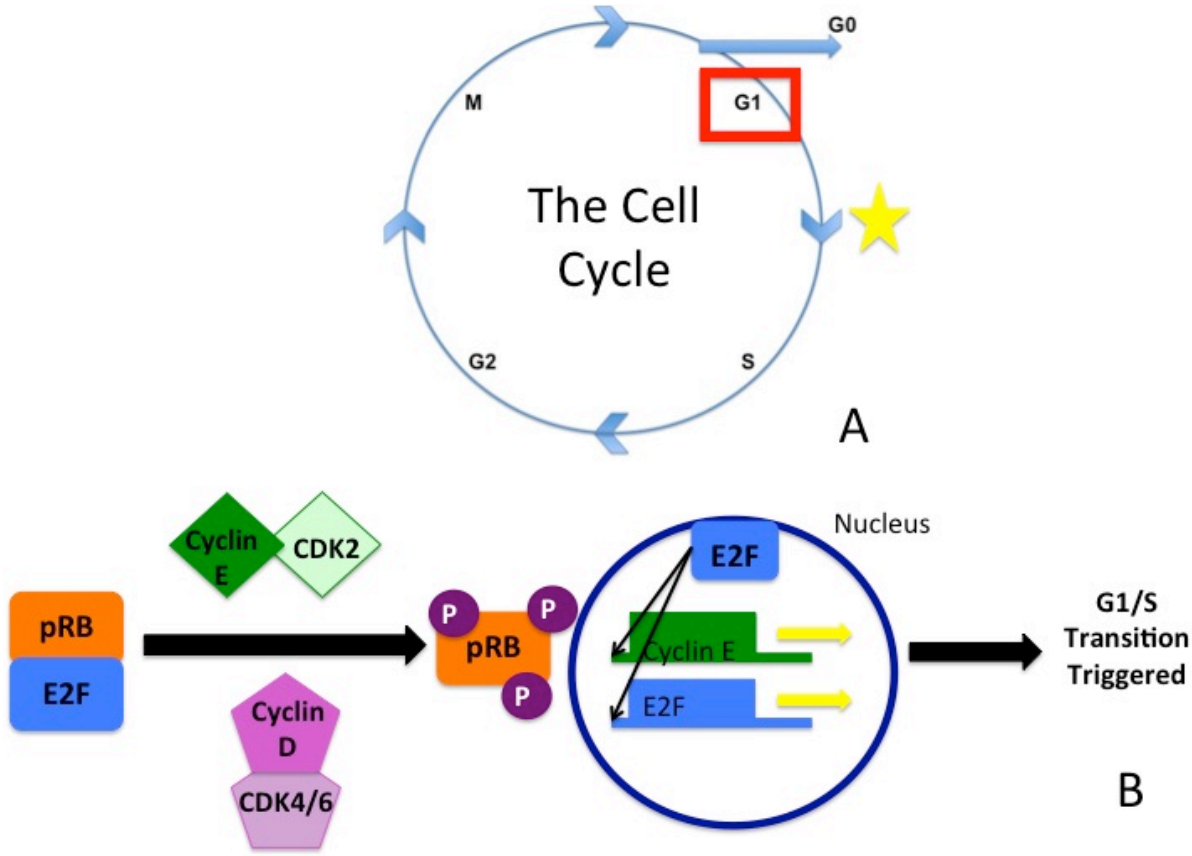

Figure 1.3: The cell cycle and mechanisms triggering the G1/S transition. A) The cell cycle consists of four main stages: G1, S, G2, and M with a quiescent G0 stage. The red box highlights G1 and the yellow star marks the G1/S transition. B) As the cell prepares to transition from G1 to S phase, cyclins and CDKs begin to associate, leading to the phosphorylation of retinoblastoma protein (pRb). Phosphorylated pRb releases the transcription factor E2F, allowing the E2 factor to enter the nucleus and increase its own expression in an autocrine fashion, while enhancing the expression of cyclins, ultimately driving the transition to the synthesis phase.

phase (Arthur et al., 2010). PCNA enhances DNA polymerase α activity, and in p53-deficient cells can trigger both G1 and G2 arrest when activated by p21 (Cayrol et al., 1998; Noda et al., 1994).

In order to proceed through the G1-S checkpoint and enter the synthesis phase of the cell cycle, the concentration of cyclins:CDKs must exceed the available p21 in order to overcome this inhibitory effect (Figure 1.3B). The increasing concentration of cyclins and CDKs triggers the phosphorylation of retinoblastoma (pRb) protein, subsequently removing pRb protein's inhibition of the transcription factor E2F (Lukas et al., 1995; Niculescu et al., 1998). The release of E2F allows its translocation to the nucleus, at which point it acts in both a paracrine and autocrine fashion to increase the expression of the cyclins D and E, and itself. This increased expression of cyclins promotes saturation of p21 with cyclin:CDK complexes, triggering the transition to S phase by overcoming p21-specific inhibition at the G1-S checkpoint.

The classical pathway of cell cycle arrest leads to the activation of the tumor suppressor gene p53 following the detection of DNA damage in the cell. In severely damaged cells, p53 activates the apoptotic pathway. In normal cells, CDKs predominantly exist in quaternary complexes each containing a CDK, cyclin, PCNA, and p21 protein (Xiong et al., 1993). The concentration of p21 in this association has implications for function, with complex assembly being triggered at lower concentrations and inhibition observed at higher concentrations. In a p53-dependent mechanism, p21 expression is triggered, causing it to bind with cyclin:CDK complexes, preventing the phosphorylation of pRb protein and ultimately maintaining the transcriptional repression of E2F (Pajalunga et al., 2008). The progression of the cell cycle into S-phase is blocked by p21 at the G1-S checkpoint until all detected DNA damage is repaired. In normal cycling cells, p21 mRNA is present across the cell cycle with the highest levels seen at G1 and levels re-accumulate as cells complete DNA synthesis and enter G2 (Li et al., 1994). Similarly, p21 protein is expressed throughout the cell cycle with a rapid turnover of protein synthesis (Li et al., 1994). The lack of p21 expression detected in the MRL mouse leads to

unscheduled entry into S phase of the cell cycle, enhancing proliferation (Bedelbaeva et al., 2010). This increase in proliferation is associated with an increase in apoptosis to maintain the high cell turnover rate and clear old cells (Bedelbaeva et al., 2010; Mirzayans et al., 2012; Piccolo and Crispi, 2012).

p21 can also be activated in a variety of p53 independent ways including cytokine production, cell adhesion events, and during the processes of cell growth and differentiation (Arthur et al., 2010; Cayrol et al., 1998; Macleod et al., 1995; Niculescu et al., 1998; Parker et al., 2015). In addition to its repair function, p21 expression is associated with cellular senescence in that its inhibition of cell proliferation is directly linked to the permanent withdrawal from the cell cycle (Arthur and Heber-Katz, 2011; Brugarolas et al., 1995). The localization of p21 can also impact the functionality in that cytoplasmic localization is associated with cell growth and survival as p21 acts as a chaperone for cyclin E, whereas the predominant nuclear localization leads to the canonical function of inhibition of cell division and growth (Gawriluk et al., 2016; Piccolo and Crispi, 2012). Diminished p21 levels are suggestive of significant, widespread DNA damage as the cell cycle proceeds without repair and arrests in G2 instead of the predicted G1 arrest.

1.6 Cell cycling and regulation in common model organisms and regeneration-competent species

In sponges, the ability to heal is associated with the activation of a DNA damage response mechanism that leads to an increase in single strand DNA breaks (Arthur et al., 2010; Bedelbaeva et al., 2010). The freshwater polyp, *Hydra*, a classic model of regeneration, possesses three adult stem cell populations along the central body column that are capable of self-renewal (Buzgariu et al., 2014; David and Gierer, 1974). Myo-epithelial cells (MECs) revealed a very short G1 phase and an extended G2 phase ranging from 24-72 hours, which is uncommon to adult animal cells that typically experience a fixed and short G2. Interstitial cells (ISCs) in the gastric region alternate between the S and G2 phases without pausing in G1. These

cells share properties with mammalian embryonic stem cells (ESCs) that have a short G1 due to the loss of a G1/S checkpoint and subsequently pause in G2 (Chuykin et al., 2008). Cycling progenitor cells are susceptible to pro-apoptotic factors, making cells paused in G2 resistant to these agents. Prolonged pausing in G2 may enhance the DNA repair program and ultimately aid in limiting extensive cell death in the regenerating *Hydra* and other regeneration-competent species (Buzgariu et al., 2014).

Planaria, another excellent model organism for regenerative studies given their simple body plan and stem cell like neoblasts, possess a single p53 family member (Smed-p53) that is chiefly expressed in newly made, postmitotic stem cell progeny (Pearson and Sánchez Alvarado, 2010). When RNAi targeted Smed-p53, increases in the stem cell population were observed and hyperproliferation occurred, but at the expense of daughter cell differentiation, thereby preventing self-renewal (Pearson and Sánchez Alvarado, 2010). This observation demonstrates the tumor suppressor-like function of Smed-p53, similar to human p53, suggesting that p53 expression is important for maintaining the planarian stem cell population. *Drosophila* p53 (Dmp53) shares many sequence features with human p53 including binding sites and the ability to induce apoptosis through the DNA damage response pathway when Dmp53 is overexpressed (Ollmann et al., 2000). Inhibition of Dmp53 renders cells resistant to X-ray induced apoptosis, suggesting an ancestral pro-apoptotic function for p53 (Ollmann et al., 2000).

Apoptosis, or programmed cell death, is essential in the early stages of *Xenopus* tail regeneration as the inhibition of caspase-3, the frequently activated death protease, prevents regeneration. Without apoptosis, the regenerate fails to induce proliferation (Tseng et al., 2007). Similarly, apoptosis is essential to the process of spinal cord regeneration in the brown ghost knifefish, *Apteronotus leptorhynchus,* as it minimizes inflammation of damaged cells at the lesion site (Sîrbulescu and Zupanc, 2009). The intensity of apoptosis detected during the cell replacement phase is equal to levels present at baseline within intact tissues, suggesting that cells are primed to respond to a potential injury (Sîrbulescu and Zupanc, 2009).

Upon exposure to gamma irradiation, an accumulation of p53 protein is seen in the gut epithelium, liver, pancreas, and brain tissues of zebrafish (Lee et al., 2008). In addition to increased p53 expression in the zebrafish, active caspase-3 was detected indicating an elevated apoptotic response and transcriptional up-regulation of p21 was observed (Lee et al., 2008). Further studies with p53 deficient and knockdown zebrafish embryos determined that p21 is a downstream target of p53 as revealed by relative p21 mRNA levels (Langheinrich et al., 2002). Together, these findings indicate similarities in cell cycling between the MRL mouse and regeneration-competent species, such as sponges and *Hydra*, while highlighting the conserved roles of p53 and apoptosis across a variety of invertebrate and vertebrate species.

1.7 Cell cycling and regulation in the axolotl and newt

Urodele amphibians are capable of undergoing multiple rounds of cell cycle re-entry without increased susceptibility, but rather, enhanced resistance to tumor formation. For example, newt limb blastema cultures can cycle through nearly 200 generations without showing signs of senescence (Ferretti and Brockes, 1988). The reentry response underlies the ability to dedifferentiate during regeneration. Upon amputation, dedifferentiation and entry of mesodermal cells into the cell cycle occurs leading to DNA replication and mitosis. Newt limb blastema cells spend approximately 40 hours in S phase making up 83% of the cell cycle (McCullough and Tassava, 1976). Tritiated (^{3}H) thymidine labeling, which is incorporated into the DNA and can be used to determine the rate of replication, showed approximately 30% of blastema cells are labeled by the accumulation blastema stage, but continuous studies have indicated that as high as 80% of the cells can be labeled (McCullough and Tassava, 1976; Mescher and Tassava, 1975). Not all cells of the blastema are actively cycling, instead a number of cells exist in a transient quiescent state with a population size dictated by the degree of innervation present in the regenerating limb (Tassava et al., 1987). In the absence of nerves, cells arrest in G2, whereas cells arrest in G1 without an associated wound epithelium (Tassava and Mescher, 1976; Tassava et al., 1987). Most cells involved in forming the accumulation limb blastema are thought to arrest

in G2 after completing DNA replication, and remain there until the growth phase begins, based upon the blastema cell profile of high levels of DNA replication and very low levels of mitosis (Mescher and Tassava, 1975).

Salamander myotubes remain responsive to proliferative cues because they are able to re-enter the cell cycle upon serum stimulation either in culture or after implantation into the regenerating limbs (Tanaka et al., 1997). Re-entry into the cell cycle is dependent on the phosphorylation of retinoblastoma protein and the down-regulation of p53 activity. Sustained ERK1/2 (extracellular regulated kinase) activation is also essential to this process as it is directly responsible for the decrease in p53 and promotes S-phase re-entry of newt A1 myotubes (Yun et al., 2014). The continued activation of ERK has also been implicated as a negative regulator of antiproliferative genes, such as p21, until the onset of S phase to allow for G1 phase progression (Yamamoto et al., 2006).

Newt A1 myotubes exhibit basal levels of p53 expression with little change post exposure to 10 Gy (Gray) of irradiation (Linklater, 2011). When p53 expression was blocked in the axolotl using the p53-specific inhibitor, pifithrin-α, limb regeneration was inhibited (Villiard et al., 2007). More detailed studies revealed that p53 expression in the limb blastema is under tight regulation, with an initial decrease in expression required for the formation of the blastema, followed by an eventual up-regulation to basal levels for the process of redifferentiation (Yun et al., 2013). Protein levels of p53 were significantly decreased in mid-bud blastemas and differentiated muscle and epidermis showed strong p53 expression, but no change in p53 mRNA expression occurred, suggesting that p53 undergoes post-transcriptional regulation (Yun et al., 2013). Cloning of the axolotl p53 gene allowed for sequence comparison to human p53 that revealed multiple amino acid changes that are thought to have evolved specifically for maintaining tumor suppressor ability in the regeneration-competent species (Villiard et al., 2007). It is further speculated that these changes to p53 may aid the axolotl in withstanding drastic variations in both oxygen level and temperature within their environment (Villiard et al.,

2007). Perhaps a more extreme example of evolutionary distinct genes is the salamander-specific gene, Prod1, a retinoid-inducible gene expressed during newt limb regeneration (Garza-Garcia et al., 2010; Geng et al., 2015). With no ortholog present in *Xenopus* or zebrafish, Prod1 is an orphan gene that either evolved independently in the newt, or was retained in newts and lost in other tetrapods over time (Geng et al., 2015).

An axolotl EST (expressed sequence tag) sequencing project detected a variety of cell cycle inhibitor contigs including p27, p28, and p57 (Habermann et al., 2004). Mass spectrometry analysis of proteome changes during axolotl limb regeneration determined that the significant up-regulation of the cell cycle-related oncoprotein, ecotropic viral integrative factor 5 (Evi5), is associated with the low mitotic index observed during limb blastema formation (Rao et al., 2009). In early G1, the centrosomal protein Evi5 accumulates within the nucleus to stabilize the protein Emi1, an association that is later responsible for preventing premature entry into mitosis. The strong expression of Evi5 in the axolotl limb blastema is thought to restrict dedifferentiated cells from entering mitosis, instead pausing in G2 until sufficient numbers of cells exist to form the accumulation blastema (Rao et al., 2009; Stocum and Cameron, 2011).

The administration of human p16 to urodele regenerating systems is a common method for understanding the function of cell cycle inhibition. When human p16 was expressed in newt myotubes, BrdU uptake was abolished after serum stimulation, establishing the importance of retinoblastoma protein phosphorylation for cell cycle re-entry (Tanaka et al., 1997). It has been proposed that the INK4a locus first arose in mammals and is not actually present in salamanders, contributing to the restricted regenerative capacity of mammals (Pajcini et al., 2010). The induced over-expression of p16 suppresses axolotl spinal cord regeneration by reducing the ependymal tube length (Khattak et al., 2013). p16 may be required for normal development, but the induction of p16 just before the onset of regeneration negatively impacts the regenerative process, suggesting that a lack of p16 gene products allows for robust regeneration in the axolotl (Khattak et al., 2013). Overall, this collection of research indicates that cell cycle regulation, via

a number of different mechanisms, is an integral part of regeneration in urodele amphibians like axolotls and newts.

1.8 p21 in mammals and conflicting roles in mammalian regeneration

In mouse tissues, p21 is not expressed at appreciable levels in heart, liver, or lung tissues until after exposure to gamma irradiation. Strong p21 expression often correlates with an absence of apoptosis (Bouvard et al., 2000). In the adult mouse, expression of p21 is restricted to terminally differentiating cells, with the highest expression levels detected in tissues such as the skin and gastrointestinal tract lining that experience a high cell turnover rate (Boonstra, 2003). Terminally differentiated cells are defined by specialized functions, which are acquired from tissue specific gene expression associated with irreversible growth arrest (Tanaka et al., 1997). Wild-type mice demonstrate expression of p21 in the thymus, spleen, testes, and brain with very high levels in the small intestine (Macleod et al., 1995). No induction of p21 is seen in tissues of irradiated p53-deficient mice indicating that p53 is essential to triggering the DNA damage response (Macleod et al., 1995). p21 acts to inhibit cell proliferation in order to protect cells from undergoing stress-induced apoptosis and contributing to oncogenesis (Boonstra, 2003).

p21 is essential to the *in vivo* healing process of muscle injury as *p21* knockout mice experienced delayed muscle regeneration (Chinzei et al., 2015). The *p21* deficiency extended the length of the cell cycle and led to increased muscle cell proliferation, but the expression of muscle synthesis genes was too low, halting muscular differentiation (Chinzei et al., 2015). Similar to this finding, after dorsal hemisection of the thoracic spinal cord in rats, the administration of cytoplasmic p21 to the injury site leads to increased axonal regeneration, hindlimb functional recovery, and inhibition of cavity formation within the spinal cord (Tanaka et al., 2004). The increased local expression of p21 prevented apoptosis and macrophage infiltration to the injury site, while enhancing immunoreactivity to glial fibrillary acidic protein (GFAP) indicating the presence of astrocytes that contribute to wound healing in this context (Tanaka et al., 2004). As mentioned previously, the specific cytoplasmic localization of p21 in

this context implies that the functionality of p21 changes from inhibitory to promoting cell growth and survival instead (Piccolo and Crispi, 2012).

Conversely, a lack of p21 expression is essential for successful liver regeneration as increased p21 protein levels are correlated with impaired hepatocyte proliferation (Stepniak et al., 2006). The up-regulation of p21 protein leads to increased phosphorylation of p38, a stress kinase that stabilizes p21, thereby prolonging p21 expression (Stepniak et al., 2006). Recent work by Gawriluk et al., (2016) has identified successful ear hole closure in the African spiny mouse, *Acomys cahirinus,* and the New Zealand white rabbit, *Oryctolagus cuniculus*, confirming prior findings of rabbit ear hole closure, and identifying this epimorphic regenerative ability in other mammals (Grimes and Goss, 1970). Following transcriptome, histological, and cell cycle analyses, *A. cahirinus* demonstrated the formation of a newt-like blastema in regenerating ear tissue, with no nuclear localization of p21 detected in proliferating mesenchymal cells (Gawriluk et al., 2016). *Mus musculus* controls run in parallel to *A. cahirinus* were unable to regenerate, producing only scarred ear tissue and demonstrating strong nuclear localization of p21 that increased over the time course studied (Gawriluk et al., 2016).

The presence of p21 expression in cases of muscle and spinal cord regeneration represent tissue-specific examples that require p21 for successful regeneration. In contrast, the absence of p21 during liver regeneration and in the blastema-mediated epimorphic regeneration of ear tissue in the African spiny mouse indicate that a lack of p21 in these instances plays a similar role to p21 in the regeneration-competent MRL mouse.

1.9 p21 in regeneration-competent and related newt species

Xenopus possess 3 CDK inhibitors, including p16Xic2, which is the structural and functional ortholog of human p21 (Daniels et al., 2004). The carboxy terminal region shows good homology with the PCNA binding domain of human p21, suggesting that p16Xic2 may regulate the cell cycle by changing PCNA activity in addition to inhibiting CDK and cyclin complexes (Daniels et al., 2004). p16Xic2 is found in *Xenopus* somites, tail bud, lens, and

cement gland and like mammalian p21, Xic2 expression is greatly induced post irradiation (Zhu et al., 2013).

Work in the marbled newt, *Triturus marmoratus marmoratus*, which experiences limited regeneration in response to injury, examined the expression of p53, p21, and pRb across the annual testicular cycle (Towle, 1901; Weismann, 1893). Maturation of testis is a synchronous and well-controlled process defined by three stages: proliferation, spermiogenesis, and quiescence (Ricote et al., 2002). The strongest expression of p21 protein was observed during the quiescent phase of the cycle, as it had previously been shown in rat and mouse testicular cells, as no cell proliferation is occurring at this stage (Ricote et al., 2002). In a similar cyclical fashion, the circadian clock is responsible for daily timing of the cell cycle, specifically restricting S phase and M phase to certain times of the day (Laranjeiro et al., 2013; Peyric et al., 2013).

The cell cycle regulators, p21 and the related p20, are expressed in the brain and gut of developing zebrafish and their differential patterns of expression regulate the daily timing of entry into S phase (Laranjeiro et al., 2013). These examples indicate the presence of the cell cycle inhibitor, p21, in regeneration-competent species such as *Xenopus* and zebrafish, and demonstrate a role for p21 in the regeneration-compromised newt species, *T. marmoratus*, suggesting the cell cycle regulator, p21, is conserved in other vertebrates beyond mammals.

1.10 Objectives

Given that the unique abilities of the MRL mouse to regenerate a variety of tissues can be attributed directly to a lack of, or down-regulation of the cell cycle regulator, p21, it is fundamental to understand if a similar mechanism exists in regeneration-competent species. This question forms the basis of my thesis, which seeks to examine the role of p21 during caudal spinal cord and tail regeneration in the Eastern Red-Spotted newt, *Notophthalmus viridescens.* Using real-time quantitative polymerase chain reaction (RT-qPCR), Western blotting, and 5'-3' Rapid Amplification of cDNA end (RACE) techniques, I sought to provide novel data regarding the expression of p21 in the newt. Determining the newt-specific p21 sequence would allow for

the examination of potential evolutionary differences in cell cycle regulation and its role in regeneration. Overall, this collection of work represents the first exploration of p21 expression in the regeneration-competent newt.

CHAPTER TWO:
p21 is down-regulated and a p16-interacting protein, not p21, is detected during caudal spinal cord and tail regeneration

Abstract

Regeneration is considered a unique characteristic of urodele amphibians such as newts and salamanders. The ability to completely regenerate lost structures including the limbs, spinal cord, and parts of the heart as an adult makes the newt, *Notophthalmus viridescens,* a useful model organism to study the process. Typically, mammals are unable to undergo epimorphic regeneration, however, the MRL mouse is a rare exception, able to fully close ear hole punctures with the formation of a highly-proliferative cell population known as a blastema. MRL mice do not express the cell cycle regulator p21, and when the p21 gene is ablated in wild-type mice, they too acquire the ability to regenerate lost ear tissue. This p21 knockout mouse demonstrated that a lack of p21 confers regenerative abilities in an otherwise regeneration-incompetent species. The transition from G1 to the S-phase of the cell cycle is regulated by p21 binding to cyclin and CDK complexes, preventing continuation of the cycle until any detected DNA damage is repaired. A p21 gene has not been identified in the newt; however, a CDK inhibitor with sequence similarity to human p21 was found in the closely related axolotl, *Ambystoma mexicanum*. Using this partial axolotl sequence to design primers, qPCR analysis revealed that expression of a p21-like gene was down-regulated at 14 and 21 dpa. A series of Western blots were performed in order to find a suitable antibody that cross-reacted with newt p21. Unfortunately, p21 protein was not detected in any tested newt sample suggesting that either the antibodies used were unable to recognize p21 in the newt, p21 is expressed at very low levels in the newt, or the newt completely lacks p21 protein expression. During these studies, a cell cycle related protein, CDKN2A interacting protein N-terminal like, or p16 interacting protein, was detected in both regenerating and unamputated newt tail tissue with changes in expression over the course of regeneration. Similar to p21, p16 is a CDK inhibitor that specifically targets Cyclin D and CDK4/6 to inhibit cell cycle progression, but previous research has been unable to identify this gene in regenerators such as the newt and axolotl. Overall, this work represents the first exploration of p21 expression and the first evidence of p16-related proteins in the regeneration-competent newt.

Introduction

The Murphy Roths Large mouse is capable of epimorphic regeneration in ear tissue injured by identification hole punctures (Clark et al., 1998). Further examination has determined that these mice can regenerate damaged heart and brain tissue as well (Hampton et al., 2004; Heber-Katz et al., 2004; Leferovich and Heber-Katz, 2002; Leferovich et al., 2001). Understanding why this otherwise regeneration-incompetent species possesses this ability is paramount in establishing the factors required for successful regeneration. Similarly, the continued study of how regeneration-competent species, such as the newt, are capable of replacing lost limbs and organs is vital to determine the elements necessary for this process. Together, this information can help define the features essential for regeneration and the molecular differences that exist between regeneration-incompetent and regeneration-competent organisms.

It was established by Bedelbaeva et al (2010) that a lack of p21 protein expression in the MRL mouse was linked to the ability to regenerate. Subsequent p21 knockout experiments, performed by the same research group, demonstrated that the abolishment of p21 expression in an otherwise normal mouse conferred the same regenerative capabilities (Bedelbaeva et al., 2010). Given that a lack of p21 conferred regenerative abilities in mice, which are typically considered regeneration-incompetent animals, it is of interest to understand the role that p21 plays in the regeneration-competent newt species, *Notophthalmus viridescens*. Would a lack of p21 also be found in this species, potentially highlighting the importance of this cell cycle regulator to regeneration in a variety of organisms? Or, if p21 protein is expressed in the newt, why would the lack of p21 confer regenerative abilities in these mice? To provide insight into these questions, I first examined the temporal expression patterns of both p21 mRNA and protein during caudal tail and spinal cord regeneration in the newt. mRNA transcript expression of p21 was not originally studied in the MRL mouse, so it is of interest to determine if p21 gene expression varies between intact and amputated tails. As well, I wanted to account for potential

issues in detecting p21 protein expression in the newt since in a previous study by Dolezalova et al (2012) looking at p21 expression in human embryonic stem cells (hESCs), changes were found in p21 RNA expression, but p21 protein was not detected whatsoever. p21 mRNA was up-regulated after the DNA damage response was triggered in hESCs, but no subsequent increase in p21 protein expression was observed (Dolezalova et al., 2012). If a lack of p21 is involved in the newt's ability to regenerate caudal tail and spinal cord tissue, then it is expected that there will be low to virtually undetectable p21 transcript and protein expression across unamputated and regenerate time points, as in the MRL mouse. Given that the MRL mouse exhibits a mechanism of regeneration very similar to that of the newt, it is predicted that p21 expression will be minimal in basal and regenerating tail.

The regenerating caudal tail and spinal cord of the newt were chosen for this investigation as the tail tissue undergoes epimorphic regeneration; characteristics of which are observed in the MRL mouse's regenerative process, making it an ideal comparison tissue. Furthermore, the regenerating spinal cord is unique to the adult newt and offers the greatest potential for future medical applications, highlighting the importance of establishing the role of p21 in this process. Time points of 7, 14, and 21 days post tail amputation were examined for both p21 gene and protein expression studies as these time points define three distinct stages of tail regeneration, representing significant morphological changes in the regenerating tail (Iten and Bryant, 1976). At seven days post amputation, blastemal cells are first seen accumulating below the thickened wound epidermis, and the terminal vesicle of the ependymal tube appears caudal to the amputation plane (Iten and Bryant, 1976). Several mitotic figures are present along the ependymal tube, confirming active cell cycling within the regenerate at this time (Iten and Bryant, 1976). By fourteen days after amputation, the process of chondrogenesis is apparent as a cartilaginous rod, which provides a scaffold for the regenerating spinal cord, develops within the narrowed and elongated blastema (Iten and Bryant, 1976). Twenty-one days post amputation, the regenerating tail is undergoing extensive differentiation of a variety of tissue types and the final

stages of morphogenesis occur (Iten and Bryant, 1976). In addition to these hallmark stages of regeneration, changes in gene expression triggered by injury can be transient events, underlining the need for an examination of earlier time points at 1, 2, and 3 days post amputation as well. This phenomenon was previously illustrated when studying the expression of p21 in response to induced mouse liver damage (Fan et al., 2014). Upon administration of damage-inducing concentrations of acetaminophen, p21 was only shown to be up-regulated at 24 hours post exposure, immediately returning to nearly undetectable basal levels by 48 hours post injection, demonstrating that changes in p21 expression have the potential to be very brief events (Fan et al., 2014).

Examination of mRNA transcripts determined that expression of a p21-like gene changes over the course of regeneration. Extensive Western blotting analysis determined that none of the commercially available anti-p21 antibodies tested were able to detect p21 protein in unamputated or regenerating newt tail samples. A peptide sequence matching a p16 interacting protein, which associates with the p21-related CDK inhibitor p16, was detected in newt tissues. These findings represent the first look at mRNA and protein expression of p21 in the regenerating newt, and indirectly suggest a role for the related cell cycle regulator, p16, in this regenerative process.

Materials & Methods

Animal Care and Surgery

All handling and surgical procedures were approved by the Brock University Animal Care and Use Committee (Protocol #13-05-01). Adult Eastern red-spotted newts, *Notophthalmus viridescens*, were obtained from Boreal Northwest in St. Catharines, Ontario and were utilized in all experiments. Animals were housed in plastic containers with dechlorinated water for the duration of experiments. Water changes occurred after every liver feeding, 3 days per week. Prior to each surgery, newts were anesthetized by bathing in a 0.1% solution of m-aminobenzoic acid ethyl ester methane sulfonate (pH=7.0, MS-222, Sigma). Tail amputations were performed caudal to the cloaca, ensuring that any incisions made on previously amputated animals were

made rostral to prior tail amputations. Studies have shown that repeated rounds of regeneration lead to no adverse effects on tissue architecture, gene expression, and regenerative capacity (Eguchi et al., 2011). The tail tissue removed during the initial amputation surgery represents the unamputated (day 0) tail tissue sample. Tail blastema tissue recovery involved a second amputation a few millimeters rostral to the original wound plane, with focus on obtaining regenerated tissue primarily. Newts recovered on ice for approximately ten minutes post surgery, and then were placed on a damp paper towel to fully recover before being re-immersed in water. *Xenopus,* zebrafish, and rat tissues were obtained from euthanized animals used in other research protocols and all tissue was taken post-mortem.

Reverse Transcription – Quantitative Polymerase Chain Reaction (RT-qPCR) Analysis

Newt tail tissues were collected following amputation and immediately placed in liquid nitrogen to be stored as individual samples at -80°C until needed. RNA isolation was performed using the Norgen Biotek Animal Tissue RNA Purification Kit and the NanoVue Plus spectrophotometer (General Electric) was used to assess the 260/280 nm absorbance ratios and RNA concentrations. Only those samples with 260/280 ratios greater than 1.8 and concentrations above 100ng/µL were utilized. Synthesis of cDNA required 500ng of each RNA sample and was performed with the BioRad iScript cDNA Synthesis Kit. In accordance with the Minimum Information for Publication of Quantitative Real-Time PCR Experiments (MIQE) guidelines, 3 biological and 3 technical replicates were run following primer validation using standard curves (Taylor et al., 2009). An additional 4 biological replicates of newt tail tissue were added to the study for each time point, increasing the overall sample size to 7. Real-time qPCR was performed using the BioRad CFX Connect Real-Time detection system using BioRad SsoAdvanced SYBR Green Supermix for the detection of amplified DNA. Data were analyzed using the $\mathbf{\Delta\Delta C_T}$ method (BioRad CFX Manager program) normalizing all samples from the target p21 to the reference genes alpha tubulin and caspase 3, and then reporting expression relative to the calibrator of unamputated (Day 0) control tail. PCR product was sent to Nanuq – McGill

University and Genome Quebec Innovation Centre for sequencing to confirm identity. Primers were designed using Primer3 and can be found in Table 2.1.

Table 2.1: Primer Sequences for Reverse Transcription-Quantitative Polymerase Chain Reaction Analysis

Primer Name	Primer Sequence (5' to 3')
Alpha Tubulin Forward	ACTGGAGTCAGGTGGACGAC
Alpha Tubulin Reverse	ATTGAGGGTTGCCTTCAGTG
Caspase 3 Forward	CAACAGGACCACAGCAAAAG
Caspase 3 Reverse	AATCTCCTCCACTGTCTGCC
p21 Forward	ATAGGACAGTGTGGGTGAGC
p21 Reverse	CTTAATACGTGTGTGGGCGG

Western Blot Analysis

Newt tail tissues were obtained under the same procedure as for RT-qPCR analysis and stored as individual samples at -80 ° C until needed. Protein isolation involved homogenizing individual tissue samples in lysis buffer for 30 seconds, followed by 30 minutes of centrifugation to pellet cellular debris. Supernatant was collected and analyzed using the Pierce BCA protein assay kit to determine protein concentration. Equal amounts (μg) of total protein from each sample were used after combination with a Laemmli protein loading dye. Samples were loaded onto 12% resolving and 4% stacking polyacrylamide gels along with protein molecular weight standards (Thermo Scientific PageRuler Prestained NIR Protein Ladder) and run for 2-3 hours at 80V. Gels were then transferred to Polyvinylidene fluoride (PVDF) membranes (Millipore) at 100V and below 0.35A for 60 minutes.

In separate trials, blots were then incubated overnight with shaking at 4 °C, with each primary antibody following 1 hour shaking in blocking buffer (1xPBS/3% Milk powder/0.1% Tween 20 or 1xPBS/5% BSA/0.1% Tween 20). Primary anti-p21 antibodies used included: Abcam anti-p21 rabbit polyclonal antibody (ab7960), Acris rabbit anti-human CDKN1A/p21 WAF1 p21 Antibody (AP06263PU-N), Sigma monoclonal anti-p21Waf1/Cip1 mouse antibody (P1484), and Cell Signaling Technology p21 Waf1/Cip1 (12D1) Rabbit mAb (2947)**.** Control primary antibodies used were an Abcam anti-beta actin antibody (ab8227) and a Developmental

Studies Hybridoma Bank (DSHB) anti-alpha tubulin antibody (AA4.3 was deposited to the DSHB by Walsh, C. (DSHB Hybridoma Product AA4.3)). Additional antibodies utilized: DSHB anti-*Drosophila melanogaster* p53 antibody (Dmp53 H3 was deposited to the DSHB by Ollmann, M. (DSHB Hybridoma Product Dmp53 H3)), DSHB anti-Cip1-interacting zinc finger protein antibody (PCRP-CIZ1-1A2 was deposited to the DSHB by Protein Capture Reagents Program, produced by JHU/CDI (DSHB Hybridoma Product PCRP-CIZ1-1A2)), Abcam Anti-active + pro Caspase 3 antibody (ab13847), Cell Signaling Technology (CST) total ERK p44/42 MAPK (4696) and Phospho ERK p44/42-Thr202/Tyr204 (4370), and CST anti-Caspase 3 antibody. Following washes, blots were incubated for 45 minutes with either the Alexa Fluor 680 goat anti-rabbit or goat anti-mouse secondary antibody in a 1:15000 dilution of blocking solution. Blots underwent a final 1xPBS wash and were stored with 1xPBS at 4°C protected from direct light until visualization using the Odyssey Infrared Imaging system at 700 nm.

HeLa human epithelial carcinoma cell line whole cell lysate, used as a control sample for the p21 antibodies, was obtained from Abcam (ab150035). Mouse C2C12 muscle cell lysate protein, SHSY5Y neuroblastoma cell lysate protein, and rat hippocampus protein samples were donated from labs of Drs. Stuart and McCormick. Various *Xenopus*, rat, and zebrafish tissues were obtained from euthanized animals post-mortem.

In order to assess each primary anti-p21 antibody's ability to recognize p21 protein in newt tissue, a number of parameters were altered including: protein concentration, antibody concentration, gel percentage, imager used, blocking solution, and secondary antibody utilized. Protein sequencing and identification was carried out by Harvard University's Mass Spectrometry and Proteomics Resource Lab.

Protein Identification Analysis of the detected low molecular weight band

Unamputated (day 0) tail protein sample was run on a 12% resolving and 4% stacking polyacrylamide gel along with protein molecular weight standards (Thermo Scientific PageRuler Prestained NIR Protein Ladder) for 30 minutes at 80V until the samples reached the interface of

the stacking and resolving gels, followed by 3 hours at 100V. From this point on sterility was of the utmost importance to minimize skin-derived keratin contamination of the protein sample. The gel was stained with Coomassie Brilliant Blue R250 overnight, with 3 solution changes. The next morning the gel was incubated with destain solution two times for 30 minutes each in order to remove the dye without disturbing the sample. Careful excision and isolation of the target band was performed, placing the sample in a sterile 1.5mL eppendorf tube. At this point the sample was shipped on dry ice for Protein Identification Analysis to Harvard's Mass Spectrometry and Proteomics Resource Lab. The data obtained from the analysis were provided as a detailed excel file indicating the peptide fragments detected in the low molecular weight band. Upon further analysis using the National Center for Biotechnology Information's (NCBI) Basic Local Alignment Search Tool (BLAST), 418 unique peptide fragments were identified from the protein sequence data.

Custom Peptide Synthesis and Analysis

Using sequence information for the Human p21 epitope, the *Xenopus* p16 interacting protein, and the *Xenopus* p16 protein (that is homologous to human p21), three custom peptides were designed and sent to ThermoFisher Scientific for synthesis (Table 2.2). Upon arrival,

Table 2.2: Amino acid sequences for three custom peptides designed to test the Sigma anti-p21 antibody.

Peptide name	Amino acid sequence
Human p21 epitope	ALMAGCIQEARERW
Xenopus p16 interacting protein	MAEGIVVEDAPHFTTR
Xenopus p16	EFMQKSNEEAKAKW

lyophilized peptides were centrifuged and reconstituted with sterile water to achieve a final concentration of 1ug/mL. First, PVDF membranes were activated in methanol and saturated in 1xPBS/0.1% Tween 20 in order to run a series of dot blots. A grid was created on each membrane to separate and distinguish the tested samples. Various concentrations of each peptide were applied to the membrane in tight droplets with dye-free unamputated (day 0) tail protein

being used as a control sample. After all samples were absorbed into the PVDF membrane, the dot blot was blocked for one hour in 1xPBS/3% BSA/0.1% Tween 20 solution followed by overnight incubation with the primary Sigma anti-p21 antibody in the same solution. The next morning, the dot blot was washed with 1xPBS/0.1% Tween 20 and then incubated for 45 minutes with the Alexa Fluor 680 goat anti-mouse antibody in blocking solution. Blots underwent a final 1xPBS wash and were visualized using the Odyssey Infrared Imaging system at 700 nm.

The Western blotting protocol for testing the peptides followed those steps described above with a few distinct differences: first, the gel was only run for 1 hour at 80V to prevent the peptides from running off the gel as they were much smaller than denatured protein samples; second, the peptides were mixed with normal protein loading dye instead of Laemmli in order to maximize the amount of peptide sample (in micrograms) that could be loaded on the gel; and third, a 15% resolving gel was used rather than a 12% gel to increase the resolution of the peptides given their low molecular weight.

Statistical Analysis

A one-way ANOVA was performed using GraphPad Prism 6 to examine temporal expression differences in mean p21 gene expression, normalized to alpha tubulin and caspase 3 expression and reported relative to time zero ($\Delta\Delta C_T$ method). A post-hoc Tukey test was run for each ANOVA. A p-value less than 0.05 was considered significant.

Densitometric analysis was performed on Western blots using ImageJ software, however normalized mean band density could not be determined using statistical analysis due to the inconsistency of the anti-beta actin antibody in unamputated and regenerating newt tissues. Instead, the raw, unnormalized density values calculated using ImageJ were compared using a one-way ANOVA in GraphPad Prism 6 to simply indicate if visual band differences were associated with numerical differences in band density. A sample size of at least two blots was required for this analysis. A post-hoc Tukey test was run for each ANOVA. A p-value less than

0.05 was considered significant.

Results

Transcripts of a p21-like gene are down-regulated during regeneration

Reverse-transcription qPCR analysis was performed across the six regenerative time points of 1, 2, 3, 7, 14, and 21 dpa comparing relative expression to unamputated (day 0) control tissue. A newt-specific p21 sequence is not available in the literature, so primers were designed from the closely-related regeneration-competent axolotl, *Ambystoma mexicanum*, partial contig sequence that shares approximately 44% identity with Human p21 (Heber-Katz et al., 2012). The CDK binding domain is the site of greatest similarity between these two sequences, making it the ideal location at which to design primers. Figure 2.1 depicts the results of the RT-qPCR analysis, showing the expression of the newt p21-like gene relative to the two housekeeping genes alpha-tubulin and caspase-3 ($N=7$, $F_{(6,42)}=6.935$, $p < 0.0001$). A significant down-regulation of p21 transcripts relative to day 0 is seen at both 14 and 21 days post amputation (post-hoc Tukey test $p<0.05$ and $p<0.01$, respectively). There appears to be a gradual decline in p21 mRNA across regeneration stages, although statistical significance relative to unamputated tissue is only seen at 14 and 21 days. Additionally, post hoc analysis revealed a significant down-regulation of p21 expression between day 1 and days 7, 14, and 21 regenerates, and a statistically significant difference between day 2 and day 21 regenerates. In order to confirm the identity of the amplified sequence as p21, qPCR products were run on a gel and sent to Nanuq – McGill University and Genome Quebec Innovation Centre for sequencing. Figure 2.2 depicts the sequence alignment of 46.8% identity and similarity between the p21 qPCR product and the axolotl p21 contig. Nucleotides 96 to 112 match the complementary sequence to the reverse primer designed from the axolotl contig for the qPCR reaction, suggesting that the amplified product contains a series of bases that are identical to the axolotl p21 sequence. The predicted 184 base pair newt product encompassed the axolotl CDK binding domain that, as mentioned above, is the region of p21 sequence that shares the greatest similarity with human and other

known p21 sequences such as *Xenopus* (Heber-Katz et al., 2012). This is a fairly short sequence for comparison, and when excluding the sequence that is identical to the reverse primer (which

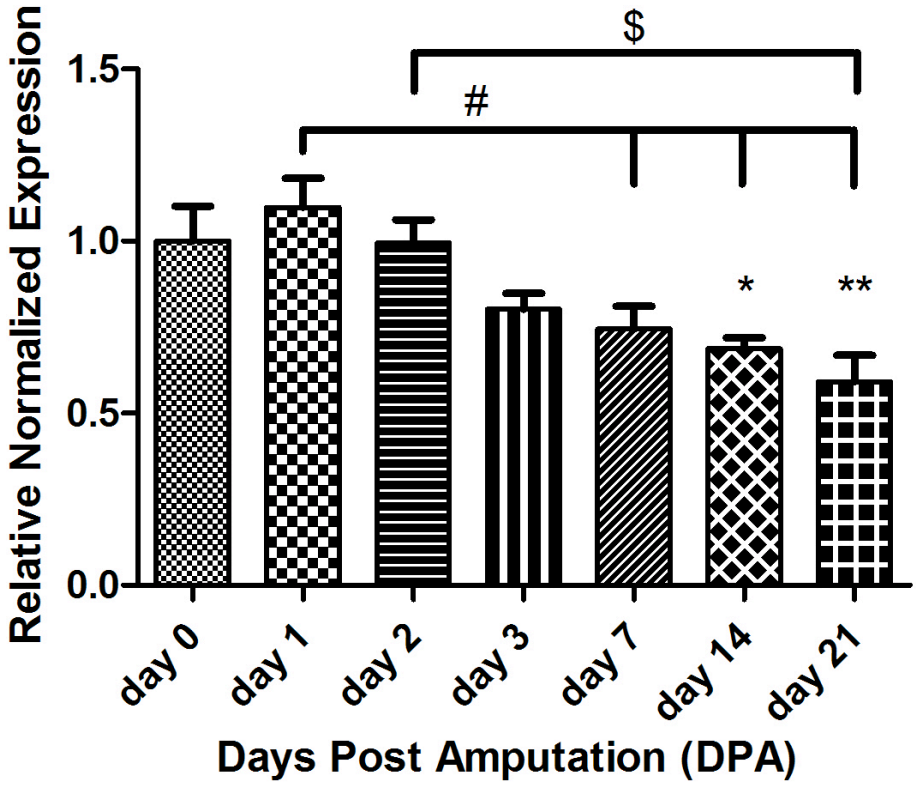

Figure 2.1: Expression of a p21-like gene is down-regulated at 14 and 21 days post tail amputation. Relative normalized expression of p21-like mRNA transcripts to the two reference genes Alpha Tubulin and Caspase-3. Day 0 (unamputated) tissue is used as the calibrator control (N=7, $F_{(6,42)}$=6.935, $p < 0.0001$; * $p<0.05$, ** $p<0.01$ compared to Day 0). p21 expression at days 7, 14, and 21 all differ significantly from day 1 regenerate tissue (#; $p<0.05$, $p<0.01$, and $p<0.001$, respectively). Day 21 is significantly down-regulated when compared to day 2 tail regenerate samples ($; $p<0.01$).

```
newtp21pcrpro     46 catg--tgaacggtcag----------gannnnnnnanctccgcccacac     83
                     ||||  |||  |||.||          ||           |||
Axolotlp21con    389 CATGTTTGA--GGTGAGTGCTTAACTTGaG----------CGC------    419

newtp21pcrpro     84 acgtattnnnnngcccacacacgtattaa    112
                        |||      ||||||||||||||||||
Axolotlp21con    420 ---TAT----CCGCCCACACACGTATtAA    441
```

Figure 2.2: Validating that the amplified qPCR product is p21. Sequence alignment shows 46.8% identity and similarity of the qPCR product (newtp21pcrpro) with the *Ambystoma mexicanum* (Axolotlp21con) p21 contig. The sequence present from nucleotides 96 to 112 of the newt sequence matches the complement of the reverse primer.

would be amplified in subsequent rounds of the qPCR reaction) minimal newt-specific sequence remains that matches the axolotl p21 sequence. This qPCR data represents the most complete newt sequence obtained from a p21-like gene, but the data is insufficient to conclude newt-specific p21 has been amplified, stressing the need for more extensive study of the newt genome.

All commercially available p21 antibodies fail to recognize newt p21 protein

To begin the process of identifying p21 protein in the newt, an anti-p21 antibody from Acris was chosen as the first commercial antibody because it was raised in rabbit, showed specificity for human, rat, and mouse, and its epitope was predicted to bind to the CDK binding domain of human p21 - the region of greatest sequence similarity to the known axolotl contig. Samples from the mouse C2C12 muscle cell line, HeLa cervical carcinoma cell line, and pooled rat hippocampus brain tissue were run alongside unamputated (day 0) newt tail tissue on a Western blot (Figure 2.3). Using 40ug of newt tail and all other protein samples, a band was not detected at the expected molecular weight of 21 kDa with either 1/500 or 1/1000 primary anti-p21 antibody dilutions. There was, however, a single band detected for only the newt tail sample at each dilution used that measured between 10 and 15 kDa. Continued testing of this antibody was unable to identify p21 protein in any of the tested samples at 21 kDa. Notably, the product information for this Acris p21 antibody indicated that in a HeLa cell extract sample, a single band was recognized below 25 kDa at approximately 21 kDa, but I was unable to detect p21 protein in the HeLa cell sample I tested with this same antibody.

An anti-p21 antibody from Abcam was tested next because it was shown to cross react in human, mouse, and rat tissues, with a consistent band detected at approximately 18-20 kDa indicating p21 expression. Figure 2.4 is a representative Western blot of mouse C2C12 muscle cell lysate, HeLa cells, rat hippocampus brain tissue, and unamputated tail tissue probed with this anti-p21 antibody. After repeatedly testing this antibody by changing a number of variables such as the amount of protein loaded, the primary antibody dilution, and the gel percentage, it was decided that the Abcam anti-p21 antibody failed to recognize p21 protein in any of the tested

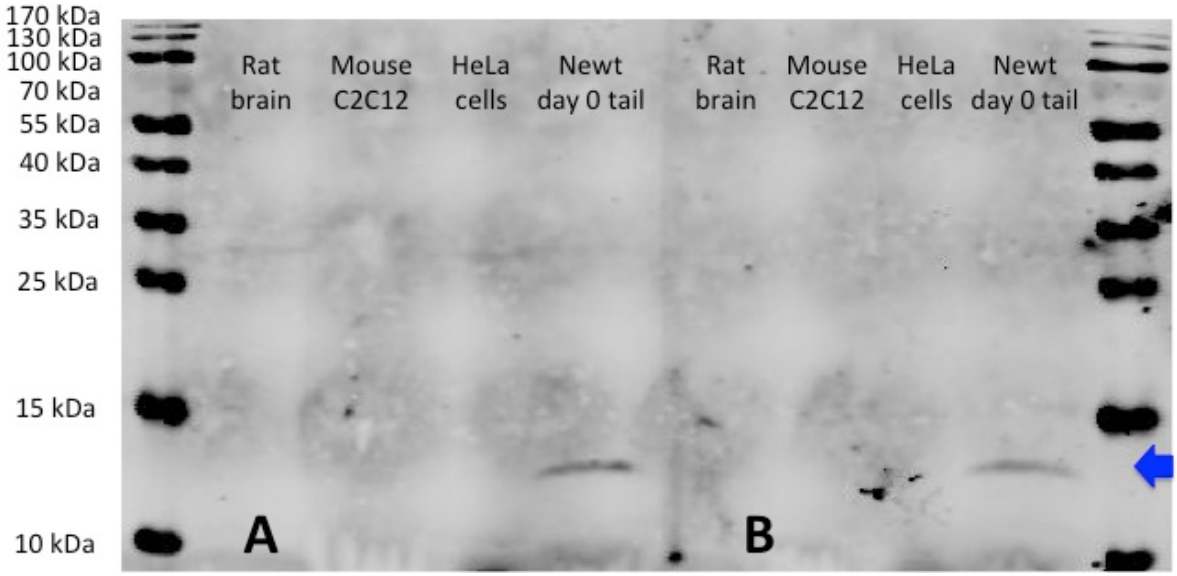

Figure 2.3: Representative Western blot image of various mammalian and newt tissue samples probed with the Acris anti-p21 antibody. A) The Acris anti-p21 antibody used at a 1/500 dilution and B) The Acris anti-p21 antibody used at a 1/1000 dilution. Protein from various tissues are as follows: rat hippocampus, mouse C2C12 muscle cell lysate, HeLa cells, and unamputated (day zero) newt tail tissue. The arrow on the right highlights a low molecular weight band detected at approximately 14 kDa in only the unamputated newt tail samples at both tested antibody dilutions.

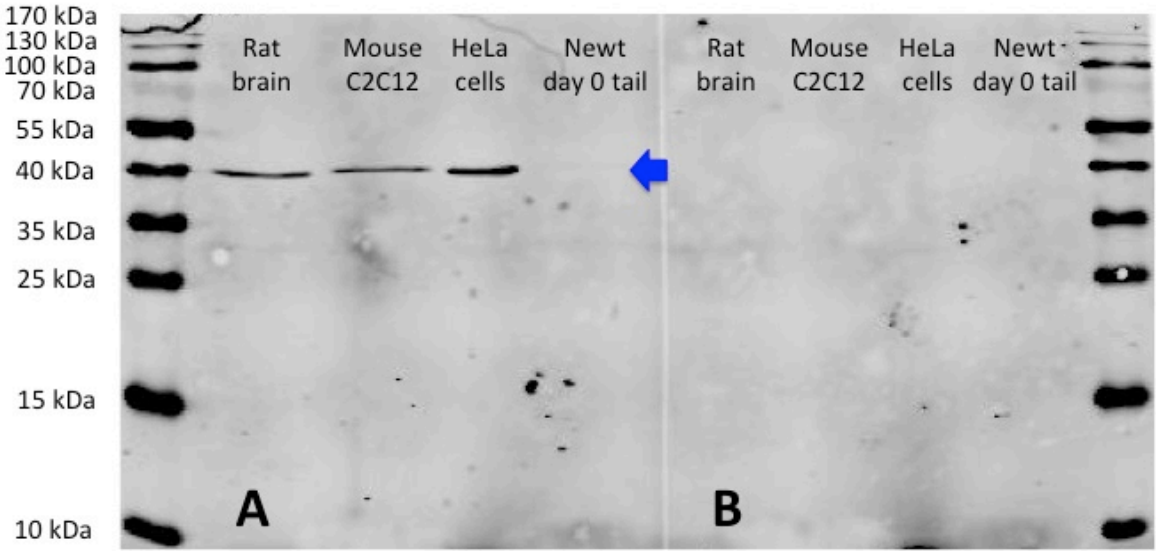

Figure 2.4: Representative Western blot image of various mammalian and newt tissue samples probed with the Abcam anti-p21 antibody and anti-beta actin control.
A) The Abcam anti-beta actin control antibody used at a 1/500 dilution and B) The Abcam anti-p21 antibody used at a 1/500 dilution. Protein from various tissues are as follows: rat hippocampus, mouse C2C12 muscle cell lysate, HeLa cells, and unamputated (day zero) newt tail tissue. The arrow at the middle highlights actin expression in lanes 1, 2, and 3 at approximately 40 kDa. The faint band that suggests a lack of beta actin expression in the time zero newt sample was a common observation with unamputated newt tails, which were always less than regenerate newt tail samples.

newt and mammalian samples, making it an unusable antibody for this study. It is worth noting that this antibody has since been discontinued from Abcam's product line and is no longer available for purchase.

A mouse monoclonal anti-p21 antibody from Sigma was chosen as the next antibody to test as the epitope is located at amino acids 17-30 of the CDK binding domain of human p21. The CDK binding region represents the most highly conserved portion of the p21 amino acid sequence between common model organisms like the mouse, rat, and *Xenopus* (Heber-Katz et al., 2012). As with the two previous antibodies, a variety of antibody and protein concentrations with different mammalian and tail regenerate protein samples at various time points were tested.

Upon first use of the Sigma anti-p21 antibody, it was clear that it recognized a low molecular weight protein of approximately 14/15 kDa, only in newt samples, that demonstrated temporal changes in expression (Figure 2.5). The protein recognized by the p21 antibody was highly expressed at day 0 with downregulation seen at 7 and 14 dpa followed by an increase at 21 dpa (see appendix for quantification, N_{Day0}=8 and N=5). As with the previous two antibodies, the mouse C2C12 muscle cells, HeLa cell lysate, and rat hippocampus brain samples did not show expression of p21 at the expected weight of 21 kDa. The lack of a band at 21 kDa in any of the tested mammalian samples was concerning, but the low molecular band in the newt samples represented an intriguing possibility of a unique p21-like protein in the newt that could be differentially expressed during regeneration. As well, a protein with similar molecular weight was initially detected in unamputated newt tail tissue with the Acris anti-p21 antibody, further supporting the notion that this band could represent a p21-related newt protein.

Before continuing with this antibody for the purposes of establishing p21 expression in the newt, it was essential to verify that the antibody is accurately recognizing the appropriate antigen by finding a reliable positive control protein sample. In the adult mouse, p21 is typically restricted to terminally differentiating cells like those in the heart, lungs, and brain, with the greatest expression seen in tissues with high turnover cell populations such as the linings of

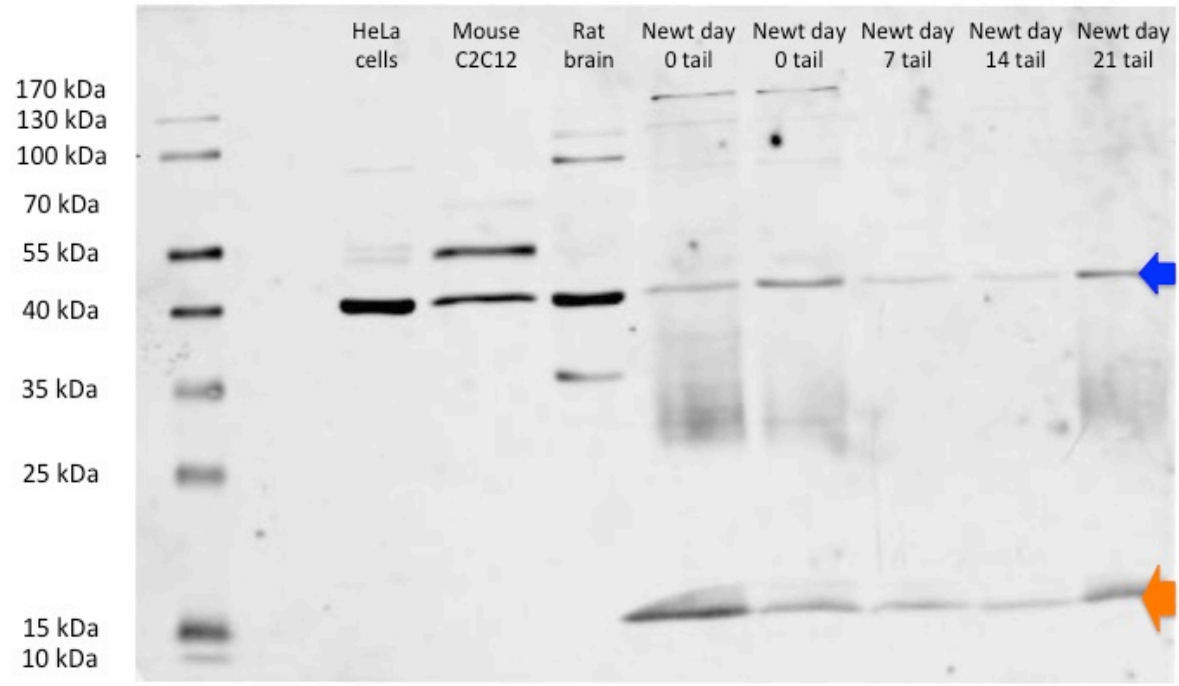

Figure 2.5: Representative Western blot image of various mammalian and newt tissue samples probed with the Sigma anti-p21 antibody and later reprobed with the Abcam anti-beta actin control antibody. The anti-p21 antibody used at a concentration of 5 ug/mL. The anti-beta actin antibody used at a 1/500 dilution. Protein from various tissues are as follows: HeLa cells, mouse C2C12 muscle cell lysate, rat hippocampus, two biological replicates of unamputated (day zero) newt tail tissue, day 7 regenerate newt tail tissue, day 14 regenerate newt tail tissue, and day 21 regenerate newt tail tissue. The orange arrow on the right highlights a low molecular weight band recognized by the Sigma anti-p21 antibody at 14/15 kDa in only newt tissue at all stages of regeneration in the tail. The blue arrow on the right indicates beta actin expression in each of the tested tissues.

intestinal walls (Bouvard et al., 2000; Gartel and Tyner, 2002; Macleod et al., 1995). With access to euthanized rat and *Xenopus* specimens, a variety of tissue types were collected for the purpose of testing these antibodies. *Xenopus* lung, rat liver, and human buccal cells were tested alongside newt tail regenerate time points with the Sigma Anti-p21 antibody in an attempt to find a suitable positive control (Figure 2.6). Once again, the p21 antibody recognized a low molecular weight band of approximately 15 kDa in the regenerating newt tail tissue. As well, smeared bands were detected at slightly above 25 kDa in newt tail tissue, as they were in Figure 2.5, with visible changes in expression over time that parallel those in the smaller band around 15 kDa. Interestingly, continued use of the antibody solution on additional blots resulted in a gradual disappearance of these smears, without changes to the signal strength in the low molecular weight band, suggesting that the smears were related to initial non-specific binding of the antibody to proteins in the newt tissue.

Unfortunately, none of the newly tested human, rat, *and Xenopus* tissues exhibited p21 expression at the expected molecular weight of 21 kDa, removing them as options for potential control mammalian or amphibian samples to use with the Sigma p21 antibody. The consistent expression of a band at approximately 35 kDa in both rat hippocampus (Figure 2.5) and rat liver (Figure 2.6) samples were similar to the band observed in the PC12 (rat adrenal medulla pheochromocytoma) cell lysate sample included in the Sigma p21 antibody product information.

It should be noted that in continued testing of this antibody (which included nearly 20 additional blots, some of which can be found in the appendix), the Western blot loading control was eventually switched from beta actin (Abcam) to alpha tubulin (DSHB) as it was more consistently expressed over the course of regeneration. Beta actin was typically expressed at very low levels at day zero and would exhibit increased expression in response to amputation, making it an unreliable control from which to normalize protein expression (Figures 2.5 and 2.6). Alpha tubulin, on the other hand, was consistently expressed at relatively the same density in unamputated and regenerating newt tail samples, making it an ideal control sample (Figure 2.7).

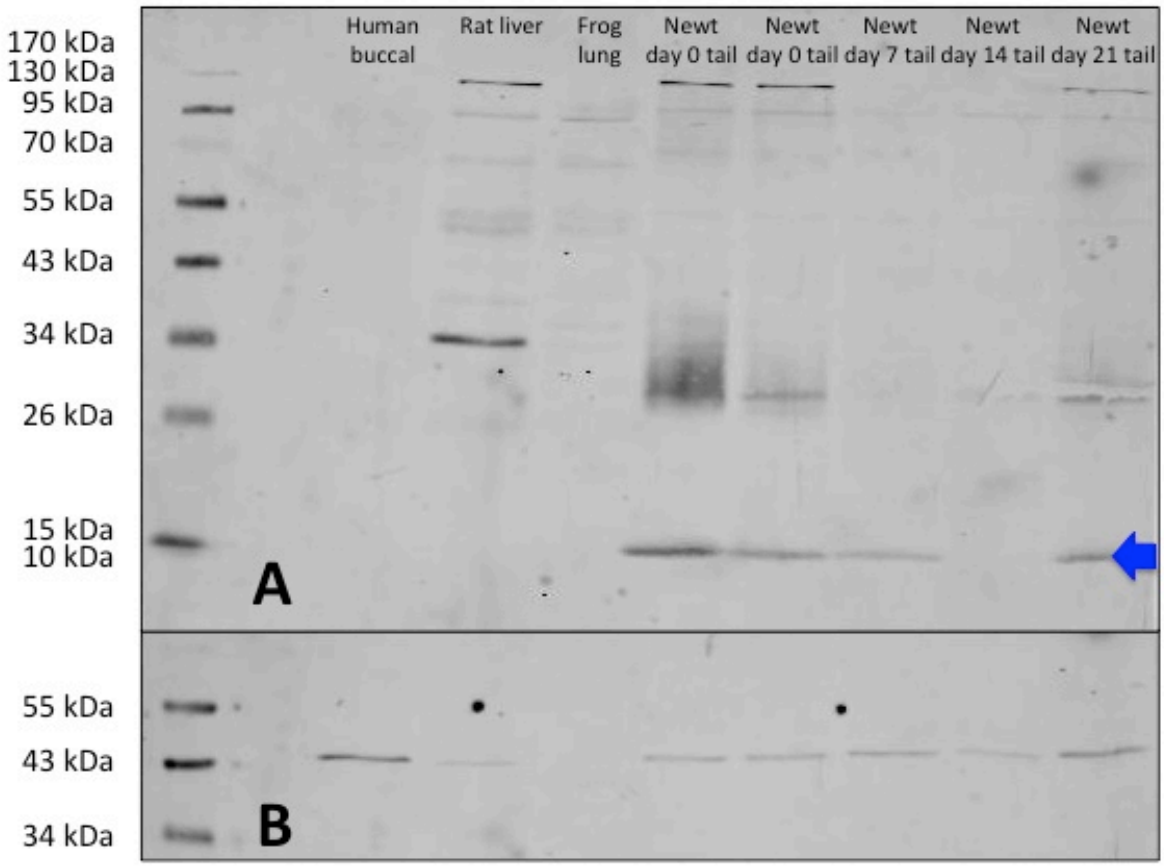

Figure 2.6: Representative Western blot image of additional mammalian and newt tissue samples probed with the Sigma anti-p21 antibody. A) The anti-p21 antibody used at a concentration of 5 ug/mL. B) The anti-beta actin antibody used at a 1/500 dilution. Protein from various tissues are as follows: human buccal cell lysate, rat liver tissue, *Xenopus* lung tissue, two biological replicates of unamputated (day zero) newt tail tissue, day 7 regenerate newt tail tissue, day 14 regenerate newt tail tissue, and day 21 regenerate newt tail tissue. The arrow on the right highlights a low molecular weight band recognized by the Sigma anti-p21 antibody at 14/15 kDa in only newt tissue at all stages of regeneration in the tail.

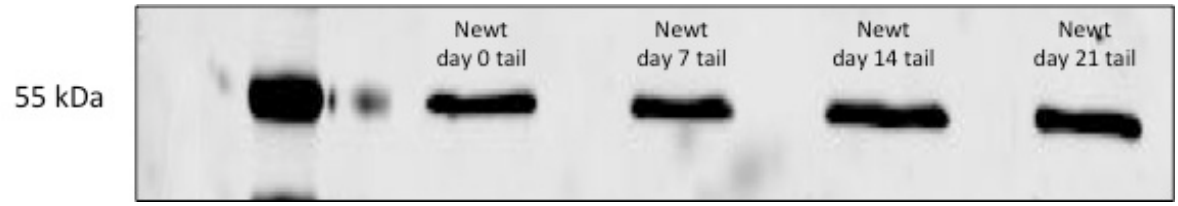

Figure 2.7: Alpha Tubulin is consistently expressed during newt regeneration. Western blot probed with the Cell Signaling Technology anti-alpha tubulin antibody demonstrating consistent tubulin expression in newt tail tissues at 55 kDa. Protein from various tissues are as follows: unamputated (day zero) tail tissue, day 7 regenerate tail, day 14 regenerate tail, and day 21 regenerating tail.

To further examine this putative newt protein, and determine if it is solely expressed in newt tail tissue, protein from unamputated and regenerating newt limbs was also tested (Figure 2.8). Comparable to the tail, the Sigma anti-p21 antibody recognized a low molecular weight protein in unamputated and regenerating newt limbs. This protein also demonstrated temporal changes in abundance (see appendix for quantification, N=2), suggesting that this p21-like protein may play a role in the regenerative response of both the tail and limb. The inability to find a suitable control sample and confirm that the antibody was accurately recognizing a p21-like protein in the newt samples led to three separate lines of investigation: first, testing if the low molecular weight band represents a cleaved fragment of p21; second, isolating the low molecular weight band and submitting it for protein sequencing; and third, synthesizing the peptide epitope used to produce the antibody and directly testing its ability to bind to the antibody on a blot.

Previous studies by a number of research groups have shown that in the presence of active caspase-3, p21 may be cleaved into a smaller p14/p15 fragment (Chai et al., 2000; Gervais et al., 1998; Park et al., 1998; Zhang et al., 1999). Caspase-3 plays a major role in the cell's apoptotic pathway. Originally present as an inactive proenzyme, cleavage of caspase-3 by caspases 8 and 9 activates the protein, allowing it to function in apoptosis as the 'executioner' (Connolly et al., 2014). The cleavage activity is concentration dependent in that the greater the expression of caspase-3, the more likely that p21 will be cleaved (Zhang et al., 1999). Bedelbaeva et al. (2010) demonstrated that caspase-3 is only expressed in the MRL mouse and not wild-type mice, suggesting the necessity of apoptosis to the regenerative process. Furthermore, caspase activity has been linked to both early *Xenopus* tail regeneration and forelimb regeneration in *N. viridescens* (Tseng et al., 2007; Vlaskalin et al., 2004). In order to indirectly test if cleavage by caspase-3 may be linked to the low molecular weight band present in newt tissue, two different caspase-3 antibodies that recognize both the proenzyme and active forms (at 32 and 15 kDa, respectively) were tested on a variety of tissues. The Cell Signaling

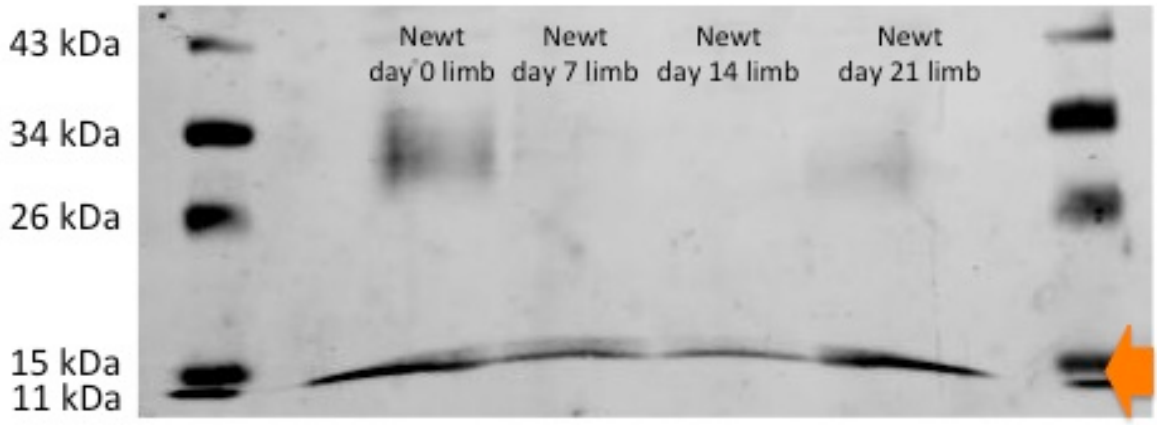

Figure 2.8: Representative Western blot image of newt limb samples probed with the Sigma anti-p21 antibody. The anti-p21 antibody used at a concentration of 5 ug/mL. Protein from various tissues are as follows: unamputated (day zero) newt limb tissue, day 7 regenerate newt limb tissue, day 14 regenerate newt limb tissue, and day 21 regenerate newt limb tissue. The arrow on the right highlights a low molecular weight band recognized by the Sigma anti-p21 antibody at 14/15 kDa in these limb tissue samples that mirrors the results seen with regeneration in the tail.

Technology anti-caspase-3 antibody recognized the proenzyme of caspase-3 in the tested HeLa cell and mouse C2C12 muscle cell samples, but none of the newt samples cross-reacted with the antibody.

A caspase-3 antibody from Abcam was then chosen after a series of *in silico* alignments predicted there was potential for the antibody to recognize caspase-3 in the newt. Original observations of these Western blots noted the location of bands in newt tail tissue at weights double or triple the expected 35 kDa weight of pro-caspase-3; however, upon review of an additional blot with increased exposure, it would appear that the proenzyme of caspase-3 is expressed between 24 and 32 kDa in day 7 regenerating tissue (Figure 2.9). A band at approximately 11 kDa can be seen in newt tail samples 0, 7, and 14 dpa, which is close to a small 12 kDa fragment that can be created when caspase-3 is cleaved (Abcam product info), but it is unclear whether these bands represent active caspase-3. As expected, the expression of both pro-caspase-3 and active caspase-3, at approximately 32 kDa and 15 kDa, respectively, can be seen in the rat hippocampus sample that was run as a control. Although this antibody was originally abandoned for use in Western blotting, recent immunofluorescence work in our lab has demonstrated extensive protein expression in day 7 regenerating newt tails utilizing this caspase-3 antibody (Wlodarek, BSc. Honours Thesis), suggesting that it may be worth testing the antibody again in the future. In order to confirm that both the western blot and immunofluorescent signals are caspase-3 expression, a blocking procedure using the commercially available peptide could be performed. For the purposes of my project, the focus shifted from establishing caspase-3 expression during regeneration to instead determining the identity of the low molecular weight band detected in the newt samples.

Low molecular weight band identified as related cell cycle protein

After carefully excising the low molecular weight band, the sample was sent to Harvard University's Mass Spectrometry and Proteomics Resource Lab for Protein Identification Analysis. The band was found to contain 418 unique peptide sequences. Each sequence was

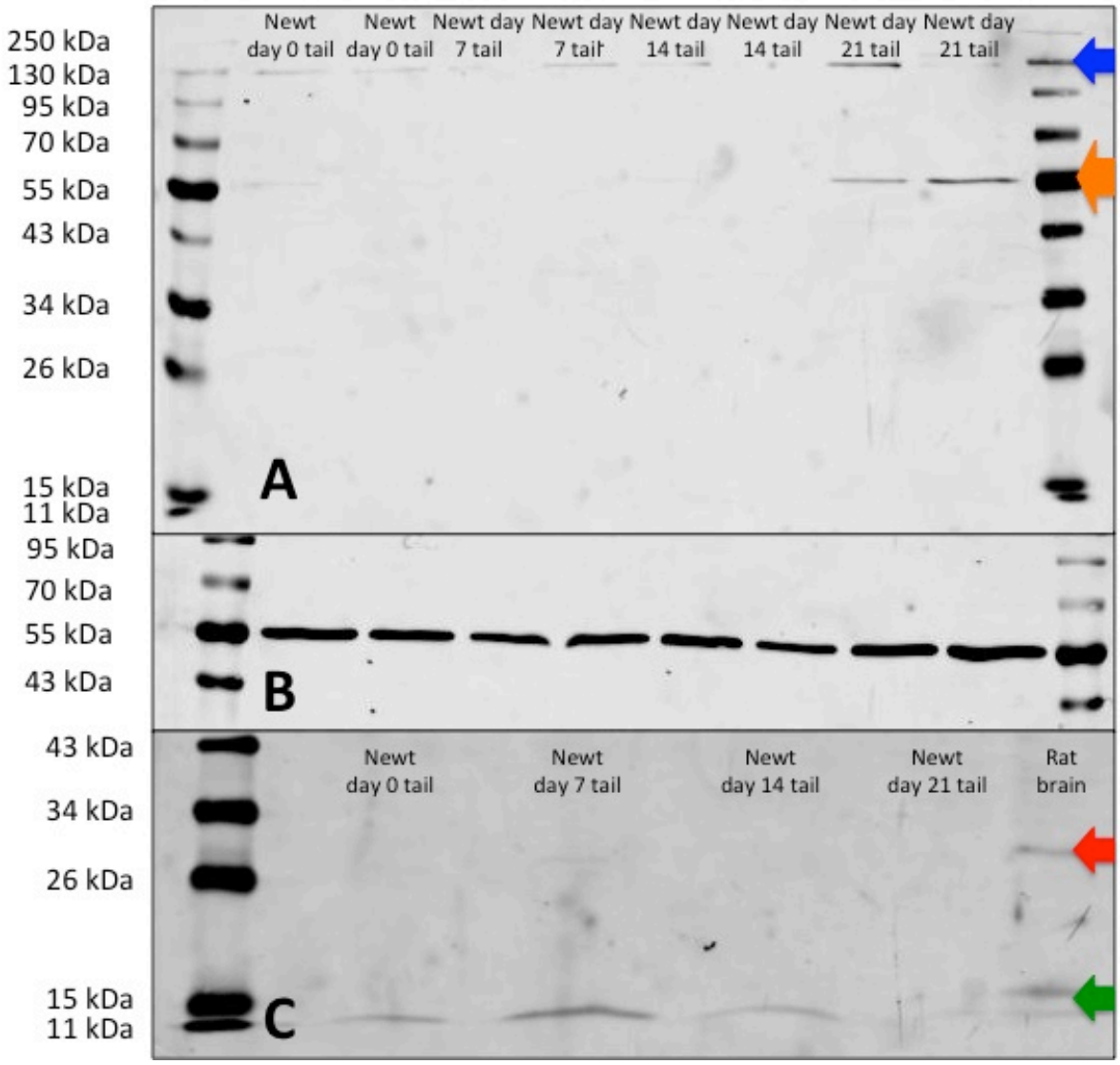

Figure 2.9: Representative Western blot image of rat hippocampus and newt tissue samples probed with the Abcam anti-caspase-3 antibody. A) The anti-caspase-3 antibody used at a 1/500 dilution. The blue and orange arrows denote large proteins recognized by the antibody that are 2-3 times greater than the expected molecular weight of procaspase-3 at 32 kDa. B) The anti-alpha tubulin antibody used at a 1/500 dilution. Protein from various tissues are as follows: two biological replicates of unamputated (day zero) newt tail tissue, two biological replicates of day 7 regenerate newt tail tissue, two biological replicates of day 14 regenerate newt tail tissue, and two biological replicates of day 21 regenerate newt tail tissue. C) The anti-caspase-3 antibody used at a 1/500 dilution and subjected to a higher exposure (+3) when imaging. Protein from various tissues are as follows: unamputated (day zero) newt tail tissue, newt tail tissue from days 7, 14, and 21 dpa, and rat hippocampus. The red arrow highlights the approximately 32 kDa band that most likely represents procaspase-3 expression in the rat brain sample with a faint band present at a similar weight in the 7 dpa newt tail tissue sample. The green arrow points to a roughly 15 kDa band that represents active caspase-3. Newt tail samples at days 0, 7, and 14 recognize a band at approximately 11 kDa.

analyzed by hand using NCBI BLAST and one sequence was identified as sharing similarity with CDKN2A interacting protein N-terminal like or p16 interacting protein. p16 is a cyclin dependent kinase inhibitor that belongs to the INK4a family of inhibitors and specifically targets cyclin D and CDK4/6 (Lukas et al., 1995; Ruas and Peters, 1998; Serrano, 1997). This result represented the only cell cycle related protein to be detected in the newt tail sample. Alignment analysis determined that the identified peptide is 87.5% identical and 93.8% similar to *Xenopus* (*X. laevis*) p16 interacting protein (Figure 2.10). Further comparison between the newt (*N. viridescens*) peptide sequence and p16 interacting protein sequences from mouse (*M. musculus*), human (*H. sapiens*), and zebrafish (*D. rerio*), which are all evolutionarily conserved, demonstrates the remarkable degree of sequence similarity (Figure 2.11). It is worth mentioning that the *Xenopus* p21 gene is called p16Xic2 and is the functional ortholog of Human p21 (Daniels et al., 2004; Zhu et al., 2013). The findings of the protein identification analysis indicate the potential for this antibody to be recognizing p16 interacting protein, which appears to be differentially expressed during regeneration, rather than p21 in the newt. In order to continue using the Sigma p21 antibody to examine p21, or p16 interacting protein expression in the newt, it was essential to validate the antibody and ensure it accurately recognizes p21 protein in other samples.

The Sigma p21 antibody is unable to be validated

The peptide for the human p21 epitope, encompassing amino acids 17-30 of the CDK binding domain, was unavailable for purchase commercially, prompting the design of a series of custom peptides. The first peptide was identical to the human p21 epitope for the Sigma p21 antibody to specifically test the antibody's ability to recognize the sequence for which it was designed. The second peptide was designed to the *Xenopus* p16 interacting protein. The orthologous relationship between *Xenopus* p16 and human p21 formed the basis for the third peptide, utilizing the *Xenopus* p16Xic2 sequence in order to determine if the Sigma p21 antibody was recognizing a p21-like protein in the newt with similarities to the *Xenopus* sequence.

```
Xlaevis           70 MAEGIVVEDAPHFTTR     85
                     |||||.:|||||||||
Nviridescens       2 MAEGIHIEDAPHFTTR     17
```

Figure 2.10: Sequence alignment of *Notophthalmus viridescens* peptide and *Xenopus laevis* p16-interacting protein N-terminal like. Sequence alignment using EMBL-EBI EMBOSS Water Pairwise Sequence Alignment program. CDKN2A interacting protein N-terminal like *Xenopus* sequence obtained from NCBI. (|) = positions with a single, fully conserved residue, (:) = conservation between groups of strongly similar properties, and (.) = conservation between groups of weakly similar properties.

```
Hsapiens          MVGGEAAAAVEELVSGVRQAADFAEQFRSYSESEKQWKARMEFILRHLPDYRDPPDGSGR
Mmusculus         MVGGEASAAVEKLVSGVRQAADFAEQFRSYSESEKQWKARMEFILRHLPDYRDPPDGGGR
Drerio            ----MASMDVEEFIGQNRQLADRVEAFRGFSESDKHWKGRREFIFRNMADFPEP-----Q
Nviridescens      ------------------------------------------------------------
Xtropicalis       -----------------MAAEFVGQFQSFSESDKQWQAREEFIIRNLKHFEDES----A

Hsapiens          LDQLLSLSMVWANHLFLGCSYNKDLLDKVMEMADGIEVEDLPQFTTRSELMKKHQS-
Mmusculus         LDQLLSLSMVWANHLFLGCSYNKDLLDKVMEMADGIEVEDLPQFTTRSELMRKHQS-
Drerio            VDHLLALSMVWQNHVFMGCRYSSELLQRVMEMAEGIEVEDAPVFKTRDEIIRQQKQR
Nviridescens      ----------------------------RMAEGIHIEDAPHFTTR----------
Xtropicalis       LDRLLALSMVWANHVFMGCRYSNELLEKVFSMAEGIVVEDAPHFTTRDEIMKQNR--
                                              **:** :** * *.**
```

Figure 2.11: Sequence alignment of *Notophthalmus viridescens* peptide and various p16-interacting protein N-terminal like sequences. Sequence alignment using EMBL-EBI MUSCLE Multiple Sequence Alignment program. CDKN2A interacting protein N-terminal like sequences for *Homo sapiens, Mus musculus, Danio rerio,* and *Xenopus tropicalis* were obtained from NCBI. (*) = positions with a single, fully conserved residue, (:) = conservation between groups of strongly similar properties, and (.) = conservation between groups of weakly similar properties.

In order to test the custom peptides, a series of dot blots were performed in which the peptides, in 3 increasing concentrations, were pipetted onto a PVDF membrane in addition to control newt tail protein samples. After exposure to the Sigma p21 antibody overnight, only the newt tail samples showed a dot, likely representing the same protein recognized at the low molecular weight on a Western blot (Figure 2.12). A series of Western blots were then performed as an additional method to potentially identify antibody recognition of any of the custom peptides, particularly the one matching the antibody's epitope. Despite efforts to alter the gel percentage, run time, and the concentration of peptide and antibody used, none of the Western blots were able to demonstrate positive recognition of any of the custom peptides when exposed to the Sigma p21 antibody. There is the possibility that the lack of a visible dot or band could be attributed to the differences in how the epitope interacts with the antibody on its own versus how it interacts with the antibody when part of a larger protein/peptide. However, this inability to directly validate the Sigma p21 antibody led first to the examination of cell cycle related proteins, and the continued search for a p21 antibody capable of recognizing p21 protein expression in the newt.

Testing other cell cycle related proteins

The struggle to successfully and accurately detect p21 protein expression in the newt using a p21 antibody led to the decision to study a variety of p21 related proteins to indirectly explore p21 expression. The first protein studied was p53, the canonical activator of p21 expression in response to DNA injury. In mammals, p53 is responsible for maintaining stability of the genome by regulating gene expression in response to detected DNA damage, leading to either cell cycle arrest, senescence, or cell death (Vousden, 2000; Yun et al., 2013). A p53 antibody, Dmp53, derived from the *Drosophila melanogaster* p53 peptide sequence was utilized because *Drosophila p53* is the structural and functional homolog of the human tumor suppressor, *p53* (Ollmann et al., 2000). The role of p53 in axolotl limb regeneration has been studied, indicating that early down-regulation of p53 is associated with blastema formation and its

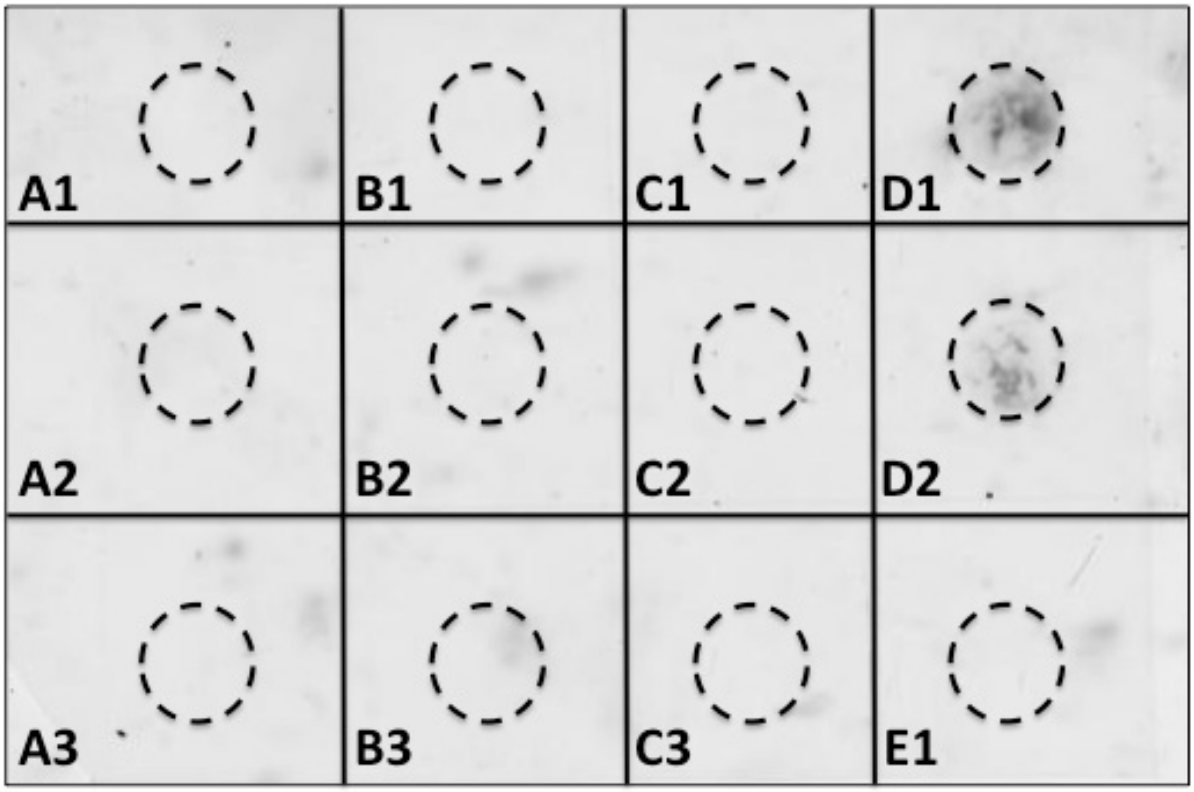

Figure 2.12: Dot blot image of three custom peptides and newt tissue samples probed with the Sigma anti-p21 antibody. A) 1, 2, and 3 represent application of 10uL, 5uL, and 2uL, respectively, of the custom peptide designed to match the epitope for the Sigma anti-p21 antibody named p21. B) 1, 2, and 3 represent application of 10uL, 5uL, and 2uL, respectively, of the custom peptide designed to match the *Xenopus* p16-interacting protein N-terminal like sequence named p16int. C) 1, 2, and 3 represent application of 10uL, 5uL, and 2uL, respectively, of the custom peptide designed to match the *Xenopus* p16Xic2 (human p21 ortholog) sequence named Xp16. D) Newt day 0 (unamputated) tail protein sample with 1 and 2 each representing individual biological samples. E1) 20uL of the custom peptide designed to match the epitope for the Sigma anti-p21 antibody named p21. Dashed circles indicate areas of application to the PVDF membrane. Only the unamputated tail tissue samples show reactivity to the anti-p21 antibody.

subsequent up-regulation is required for later redifferentiation of the limb (Yun et al., 2013). It is key to note that in the study by Yun et al (2013), a custom axolotl p53 antibody raised against the peptide was used to examine the expression of p53. After testing unamputated and regenerating newt tail samples, there was no recognition of p53 expression with the Dmp53 antibody suggesting that a newt-specific antibody may be required to study p53 expression in the newt.

The next protein examined was Cip1-interacting zinc finger protein, or CIZ-1, which has been shown to interact with the p21 protein in human tissues (Copeland et al., 2010; Coverley et al., 2005; Mitsui et al., 1999; Nishibe et al., 2013). CIZ1 can induce cytoplasmic distribution of p21, and although no similar structure is found in yeast, *C. elegans*, or *Drosophila*, the presence of CIZ1 in humans and the Japanese pufferfish, *Fugu rubripes,* suggests conservation in vertebrates (Mitsui et al., 1999). It was uncertain if this antibody would cross-react in the newt, especially given our previous difficulties in detecting p21 expression, but it was worth testing this antibody in the event we could detect the interacting protein. Following similar testing as the Dmp53 antibody, there was no expression of CIZ-1 protein detected in any of the unamputated or regenerating newt tail samples.

The final p21 related proteins studied were extracellular signal-regulated kinase (ERK) and phosphorylated or phospho-extracellular signal-regulated kinase (p-ERK), which are involved in the control of cell proliferation in response to mitogenic signals. It has previously been shown that sustained ERK activation, indicated by p-ERK expression, is required for the cell cycle re-entry of postmitotic newt A1 myotubes, in part by down-regulating p53 expression (Yun et al., 2014). Continuous activation of ERK also causes the down-regulation of antiproliferative genes during the course of the G1 phase, contributing to cell cycle progression and entry into S phase (Yamamoto et al., 2006). A sample of rat hippocampus tissue was run alongside newt tail tissue and showed the expected two bands of total ERK protein expression, which includes ERK1 and ERK2, at 44 and 42 kDa, respectively. Total ERK1/2 protein expression was detected in unamputated newt tail and regenerate tail samples at 7, 14, and 21

days after amputation (Figure 2.13A) as one band at approximately 43 kDa. The presence of a single band in the newt samples could be explained by the previous observation that *Xenopus* only possesses one ERK that is orthologous to human ERK2 (Lefloch et al., 2008; Lefloch et al., 2009). Both ERK1 and ERK2 are present in fish such as *Danio rerio*, suggesting that *erk1* has been lost in vertebrates like *Xenopus* and the chicken, *Gallus gallus*, as fish are evolutionarily closer to the common ancestor vertebrates (Lefloch et al., 2008). However, when newt A1 myotube extracts were incubated by Yun et al. (2014) with an ERK antibody two bands were detected, with the 44 kDa band showing greater abundance. This finding in newt A1 myotubes could also illustrate the differences in determining ERK protein expression in a homogeneous cell culture versus the heterogeneous cell populations of the unamputated and regenerating newt tails.

When incubating the same samples with the pERK antibody overnight, only the rat brain sample showed cross-reactivity with the antibody, indicating activated ERK (Figure 2.13B). As it has been previously demonstrated that activated ERK is directly involved in the ability of newt myotubes to re-enter the cell cycle *in vitro*, it is possible that this phosphorylation leading to activation occurs on different amino acids in the newt than those recognized by this antibody (Yun et al., 2014). A further consideration for the lack of a phosphorylated ERK signal is that the lysis buffer used to process the newt protein samples did not include phosphatase inhibitors, leaving the phosphate groups susceptible to cleavage or degradation during tissue processing. Of these four p21-related proteins tested, extracellular signal-regulated kinase represents the most promising result with two blots showing no difference in expression across regenerated and unamputated tail tissues (see appendix for quantification, N=1 and N=2), suggesting its utility as a possible control antibody for Western blots in addition to alpha tubulin. At this point in time, these results provide little information regarding the role of p21 in the newt, but further exploration of activated ERK expression *in vivo* during tail regeneration could provide valuable information on cell cycle regulation and cell proliferation in this process.

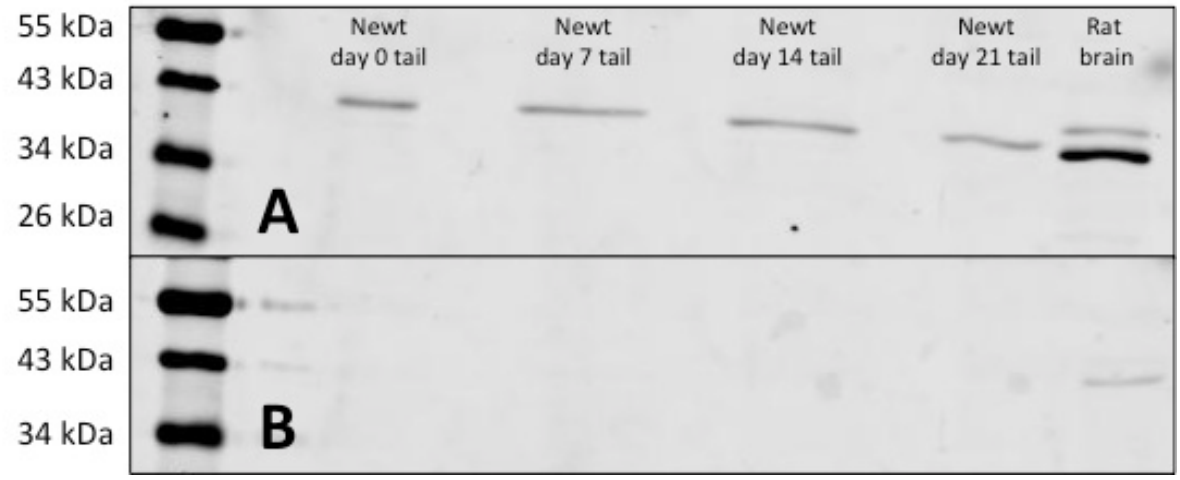

Figure 2.13: Representative Western blot image of mammalian and newt tissue samples probed with Cell Signaling Technology anti-ERK and anti-pERK antibodies. A) The anti-ERK antibody used at a dilution of 1/2000. B) The anti-pERK antibody used at a 1/1000 dilution. Protein from various tissues are as follows: unamputated (day 0) newt tail tissue, day 7 regenerate newt tail tissue, day 14 regenerate newt tail tissue, day 21 regenerating newt tail, and rat hippocampus. Only one band is seen in all tested newt tissues at approximately 42 kDa using the anti-ERK antibody, whereas the rat tissue shows the two expected bands for ERK1 and ERK2 at 42 and 44 kDa, respectively. After probing with the anti-phosphoERK antibody (B), only the rat sample recognizes a single band at approximately 43 kDa.

Cell signaling technology p21 antibody recognizes positive control

After testing three p21 antibodies with little success in identifying p21 expression in newt tissue, or any mammalian samples, a final antibody from Cell Signaling Technology (CST) was tested. This specific p21 antibody was chosen given its prior success in Western blotting applications with a variety of cell types, a few of which were available for us to test together with newt tissue. Despite the antibody's specific epitope sequence being unavailable, the antibody previously identified p21 in human and monkey samples, with expected reactivity in dog tissue (CST product information). The antibody was created using a synthetic peptide that corresponds to the carboxy-terminus of human p21. An alignment of a p21-like sequence from the Japanese newt, *Hynobius retardatus*, and the human p21 sequence was performed (37% identity and 51% similarity), indicating likeness at the carboxy-terminus and suggesting the potential for cross-reactivity in my newt, *N. viridescens*. The sequence from *H. retardatus* was found as an unidentified contig in the DNA database of Japan during the later stages of this project and I categorized it as a p21-like sequence given the high degree of similarity it shares with the human p21 protein sequence, specifically within the CDK-binding domain.

The first test of the CST p21 antibody involved utilizing a series of cell lysates from SHSY5Y cell cultures grown in media enriched with either glucose or galactose. SHSY5Y cells were selected because they were one of the cell types used successfully in the CST p21 antibody product information. They are human neuroblastoma cells and it has been shown that the sustained expression of p21 is required for the survival of differentiating SHSY5Y cells (Poluha et al., 1996). When testing the CST p21 antibody for the first time, four SHSY5Y samples (three cultured in galactose and one cultured in glucose) and two different day 0 newt tail samples were used (Figure 2.14). All four SHSY5Y samples recognized a band at approximately 21kDa representing p21, with a faint band at a lower molecular weight of approximately 15kDa**.** The CST p21 antibody failed to recognize protein in either of the newt tail samples. Five additional Western blots (see appendix for a few examples) were run, using differing antibody and sample

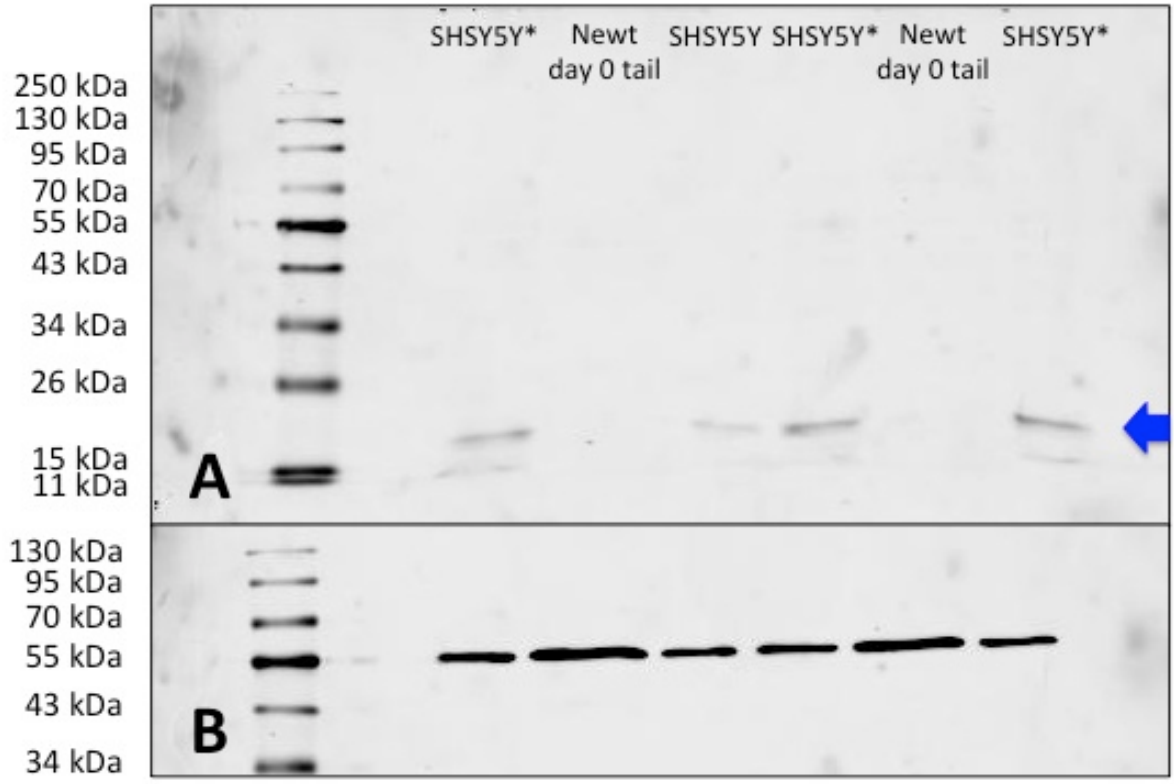

Figure 2.14: Representative Western blot image of human neuroblastoma (SHSY5Y) cells and newt tissue samples probed with the Cell Signaling Technology anti-p21 antibody. A) The anti-p21 antibody used at a dilution of 1/500. B) The anti-alpha tubulin antibody used at a 1/500 dilution. Protein from various samples are as follows: SHSY5Y* cell lysates cultured with galactose, two biological replicates of unamputated (day zero) newt tail tissue, and SHSY5Y cell lysate cultured with glucose instead. The arrow on the right highlights p21 at approximately 20 kDa in all SHSY5Y cells tested. Neither of the newt samples tested recognize any proteins in response to being probed with the CST anti-p21 antibody.

concentrations, and detection methods, with no success in detecting p21 protein expression in any newt tail sample. This inability to detect p21 protein in any of the tested regenerating newt tail samples led to the examination of p21 in a variety of other newt tissues, in addition to similar tissue types from other species.

No newt tissues tested demonstrate reactivity with the CST anti-p21 antibody

The final attempt at Western blotting with the CST p21 antibody involved the use of tissues from the following four animals: newt, zebrafish, rat, and *Xenopus*. Newt tissues included both unamputated and pooled regenerating tail (from various time points), miR-1 and miR-133a mimic-injected tail, as well as brain, gut, and heart collected from newts that previously underwent tail amputation. Mimic-injected tail tissue samples are regenerate samples that were collected after microRNA mimics had been injected into the spinal cord, followed by electroporation. The microRNAs miR-1 and miR-133a have been previously shown in our lab to significantly inhibit newt tail regeneration (Lepp and Carlone, 2015). If the original hypothesis that a lack of p21 or very low basal expression contributes to the regenerative phenotype of newts is correct, then the use of mimic-injected tissue could help to determine if inhibiting the regeneration process alters the expression of p21 in the regenerating tail. Gut tissue from the newt was included in this analysis because previous research in our lab has shown the greatest expression of several proteins in the gut and this tissue's cell population experiences a high turnover rate, which characteristically indicates the potential for prominent p21 expression.

Brain, spinal cord, and heart tissue were also used from zebrafish, rat, and *Xenopus* since they contain significant numbers of terminally differentiated cells and could express p21. The tail and fin tissues from the zebrafish were used such that the expression of p21 could be examined in two regeneration competent species simultaneously. Similarly, hindlimb tissue from *Xenopus* was run on the gel to represent a regeneration-competent species that undergoes a reduction in regenerative ability following metamorphosis. As a tadpole, *Xenopus* has what is considered unlimited regenerative potential, however after metamorphosis, this capacity diminishes, and in

the event of a hindlimb amputation, the missing limb is instead replaced by a hypomorphic cartilaginous rod or spike (Dent, 1962). Together, this collection of samples was chosen to represent a diversity of species and tissue types in order to provide the best chance of detecting p21 protein expression using the CST p21 antibody.

As can be seen in Figure 2.15A, of all the tested samples, only the SHSY5Y cell lysates recognized p21 protein at approximately 21 kDa. The corresponding alpha tubulin control for each sample, shown below in Figure 2.15B, indicated that all protein samples were intact and at a concentration suitable to at least be detected by the alpha tubulin antibody. Similar findings for the remaining rat, frog, and newt tissue samples can be seen in Figure 2.16B. This alpha tubulin blot was reprobed with the CST p21 antibody (Figure 2.16A), and none of the tested tissues recognized a band at approximately 21 kDa that was not previously there from exposure to the alpha tubulin antibody. Upon closer inspection, however, the *Xenopus* heart and hindlimb samples may show faint expression at approximately 25 kDa suggesting there could be p21 related bands since they were not present on the initial alpha tubulin probed blot. Further examination will be required to determine if in fact the CST p21 antibody is recognizing a protein in the frog that is presumably related to p21 at approximately 25 kDa. None of the tested newt tissues showed p21 protein expression in response to being probed with the CST p21 antibody. The inability to find a human or mouse anti-p21 antibody capable of cross-reacting with newt tissues emphasizes the need for a newt-specific p21 antibody. Moreover, the difficulty in finding a suitable antibody suggests that the human and newt p21 peptide sequences may be more distinct than previously thought.

Discussion

This research focused on defining the temporal patterns of expression of both p21 mRNA and protein in the regenerating newt compared to the Murphy Roths Large mouse. The down-regulation of this protein in MRL mice is suggested to be sufficient to confer epimorphic regenerative abilities in a previously non-regenerative species. Both the newt and the MRL

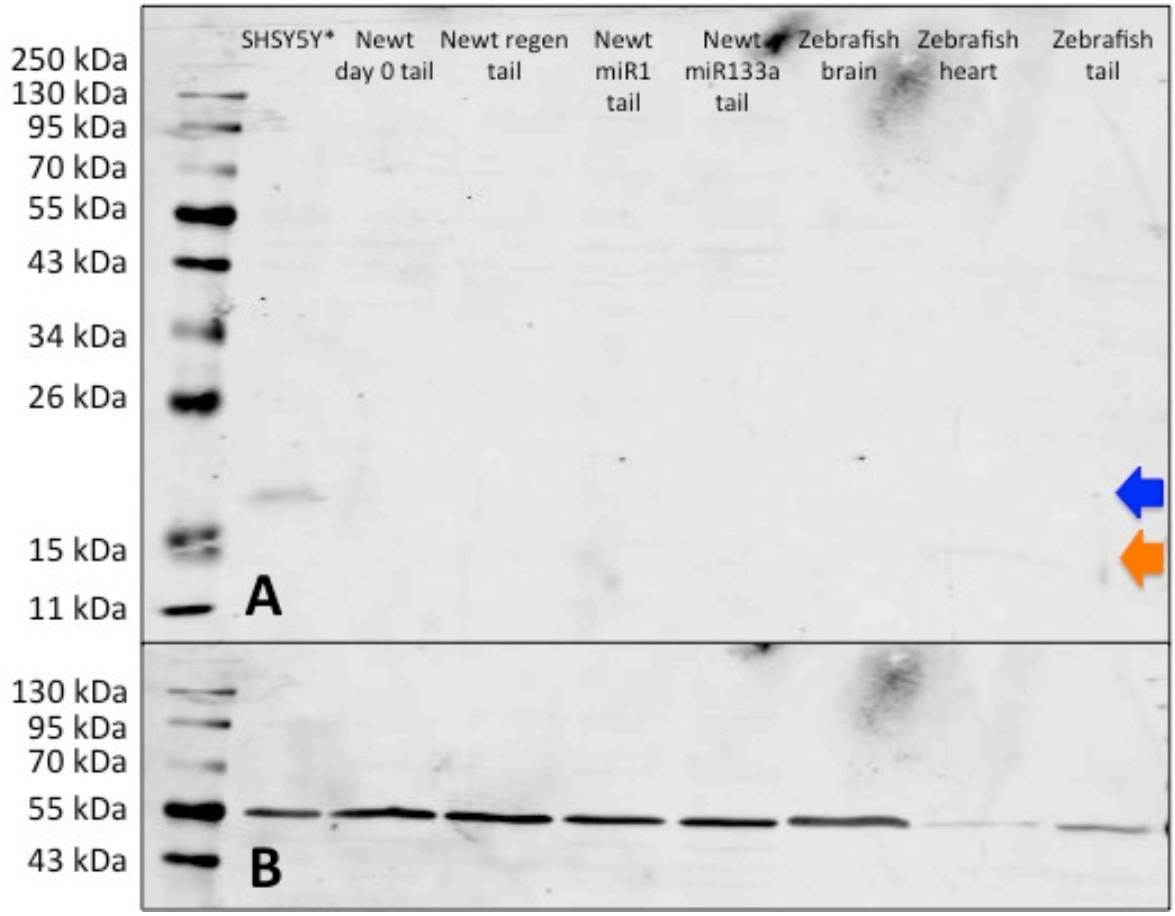

Figure 2.15: Western blot image of human neuroblastoma (SHSY5Y) cells, newt tissue, and zebrafish tissue samples probed with the Cell Signaling Technology anti-p21 antibody. A) The anti-p21 antibody used at a dilution of 1/500. B) The anti-alpha tubulin antibody used at a 1/500 dilution. Protein from various tissues are as follows: SHSY5Y* cell lysate cultured with galactose as a food source, unamputated (day 0) newt tail, regenerating newt tail pooled from various stages, newt tail tissue injected with microRNA mimics miR1 and miR133a, and zebrafish brain, heart, and tail tissues. The blue arrow on the right highlights p21 expression at approximately 20 kDa in the SHSY5Y cell sample and the orange arrow highlights the faint band at approximately 15 kDa that appears to be recognized in the zebrafish heart sample by this p21 antibody.

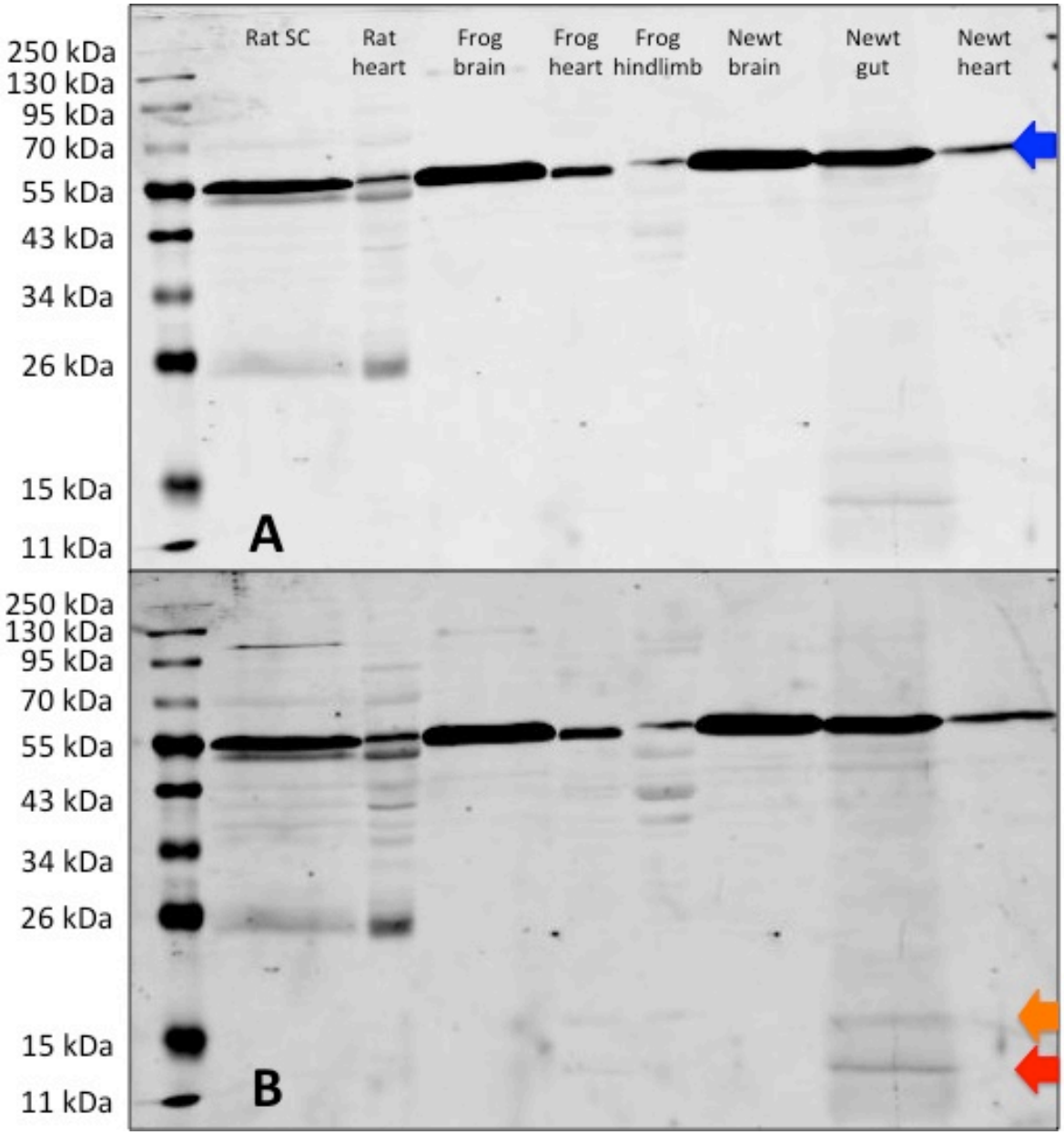

Figure 2.16: Western blot image of rat, *Xenopus*, and newt tissue samples probed with the Cell Signaling Technology anti-p21 antibody. A) The anti-alpha tubulin antibody used at a 1/500 dilution. B) The anti-p21 antibody used at a dilution of 1/500 and subjected to a higher exposure (+3) when imaging. Protein from various tissues are as follows: rat spinal cord, rat heart, *Xenopus* brain, heart, and hindlimb, and newt brain, gut, and heart. The blue arrow on the right highlights alpha tubulin expression at the expected molecular weight of 55 kDa. Notably, some of the samples contain multiple bands in addition to the one at the predicted tubulin weight. The orange arrow denotes the presence of a single band at approximately 15 kDa in both *Xenopus* heart and hindlimb in response to probing with the p21 antibody. Additionally, the red arrow marks a second faint band in the *Xenopus* heart tissue sample.

mouse undergo epimorphic regeneration, therefore comparisons of p21 in both phenomena will be vital to understand the differences between these models.

Studies of both MRL and p21 knockout mice show that p21 protein is down-regulated, allowing for regeneration of lost ear tissue; however, the expression of p21 mRNA transcripts was never examined. In the regenerating newt, mRNA transcripts of a p21-like gene are down-regulated at 14 and 21 days post amputation when compared to day zero p21 expression. Furthermore, this p21-like gene is down-regulated at 7, 14, and 21 dpa when compared to day 1 regenerating tail tissue transcript expression. The contact between the regenerating spinal cord and the tail stump wound epithelium is essential for creating an environment capable of epimorphic regeneration (Chernoff et al., 2003). By 7 days post amputation, extensive breakdown of the extracellular matrix has occurred, with cells undergoing dedifferentiation and the formation of a wound epidermis covering the amputation site (Iten and Bryant, 1976). The blastema, characterized by an accumulation of proliferating cells, can be seen at day 7 with extensive cell proliferation detected in the ependymal cells that form a hollow terminal vesicle that remains continuous with the stump cord as regeneration proceeds (Benraiss et al., 1999; Egar and Singer, 1972). In order to be a proliferating cell population, cells will need to re-enter the cell cycle and be actively cycling, hence why a decrease in the expression of p21 would be logical at 7 days post amputation. It is, however, worth mentioning that studies of the regenerating axolotl limb have indicated that blastema cells undergo a 'punctuated' phenomenon, existing as a mixture of actively cycling cells and a transient quiescent population (Tassava et al., 1987; Tomlinson et al., 1985). The composition of this mixture is dependent upon the degree of innervation to the limb and shifts to a primarily cycling population as regeneration proceeds (Tassava et al., 1987).

The continued, and greater down-regulation of p21-like transcripts at 14 and 21 dpa are suggestive of sustained extensive proliferation within the mesenchymal tail blastema that can be seen predominantly at 14 days post amputation. Day 14 is characterized by the formation of the

cartilaginous rod that is continuous with the regenerating spinal cord, growth of the accumulation blastema as the regenerate lengthens, and apoptosis required to clear dead cells and maintain the proliferative state of the regenerate (Iten and Bryant, 1976). The ependymal cells, which line the central canal of the spinal cord, contain numerous mitotic figures and blastema cells become restricted to the caudal portion of the regenerate as proliferative ependyma gives rise to new neurons (Chernoff et al., 2003; Iten and Bryant, 1976). By day 21, the regenerate length has elongated and is undergoing differentiation in a variety of tissue types. The physical changes occurring at 21 dpa contradict my finding of significantly decreased *p21* expression at this time point. This disparity could indicate that the signals for differentiation in the newt tail are related to another gene. However, it is more likely that the gene amplified from the newt is not p21, instead resembling a p21-like gene, which does not exhibit the changes in p21 expression that would presumably occur in response to the various stages of regeneration (ie. proliferation, differentiation). In order to better understand this mechanism and the pattern of expression, examination of later time points such as 28 and 35 days post amputation would help determine mRNA expression of this p21-like gene throughout regeneration.

The observed decrease in transcript expression of the p21-like gene could be p53-dependent as the down-regulation of p53 protein in the early stages of axolotl limb regeneration is necessary for blastema formation to proceed, whereas its later upregulation to baseline expression is necessary for redifferentiation of the limb (Yun et al., 2013). Additionally, the use of newt A1 myotubes to further examine this relationship determined that a decrease in p53 activity is crucial for the postmitotic, differentiated cells to reenter the cell cycle, followed by a final increase in p53 to trigger muscle differentiation (Yun et al., 2013). A series of experiments using the p53 inhibitor, α-pifithrin, demonstrated that blocking p53 signaling significantly inhibits axolotl limb regeneration (Villiard et al., 2007). The p53 antibody utilized in the Villiard et al. (2007) study was able to successfully cross react in newt tissue and was subsequently used by Linklater (2011) when observing that newt A1 myotubes had basal p53 expression that

underwent little change post irradiation. This result was unexpected given that irradiation directly triggers DNA damage, and control mouse cell lines tested concurrently demonstrated significant changes in p53 expression in response to this stress (Linklater, 2011). These findings suggest that the basal expression of DNA damage proteins, like p53, may prime the cell to repair DNA damage accumulated as a result of the extensive proliferation required during regeneration.

In my study, four anti-p21 antibodies were assessed under a variety of conditions, with two antibodies – termed Sigma p21 and CST p21 – representing the most promising ones. The Sigma p21 antibody consistently recognized a low molecular weight peptide only in newt tissue that was later identified as CDKN2A interacting protein N-terminal like or p16 interacting protein. Though not p21, this result suggested that, at the very least, there are cell cycle proteins related to p21 present in newt tissue, and these proteins may cross-react with a p21 antibody. p16, also known as p16Ink4a as an inhibitor of CDK4, specifically inhibits CDK4/6 to block G1 and cause cell cycle arrest, whereas p21 (Cip/Kip) is capable of inhibiting all cyclin/CDK complexes (Sherr, 1996; Tam et al., 1994). The INK4a locus, which encodes p16Ink4a and Alternate Reading Frame (p19ARF), is absent in lower organisms, proposed to have first arisen in mammals, and is thought to have evolved at the expense of regenerative capabilities (Pajcini et al., 2010). Homologs of p16 exist in fish such as the puffer fish, *Fugu rubripes*, with zebrafish possessing the closely-related and functionally similar gene *p15* (CDK2NB), but the earliest (evolutionarily) identified p19ARF can be found in chickens (Gilley and Fried, 2001; Kazianis et al., 1999; Pajcini et al., 2010).

In order to test if ectopic p16 expression affects regeneration, researchers utilized Cre-mediated induction of p16 in axolotl tails and found that spinal cord regeneration was suppressed, with the length of the ependymal tube being significantly reduced (Khattak et al., 2013). Similarly, if newt A1 myotubes are injected with a plasmid containing mammalian p16, the cells are blocked from re-entering the cell cycle following serum treatment (Tanaka et al., 1997). Taken together, these results suggest that the lack of p16 in salamanders creates an

environment conducive for robust regeneration. However, the presence of a peptide sequence in regenerating newt tail resembling p16-interacting protein N-terminal like does create questions as to why a p16-interacting protein would exist if p16 is presumably not present in the newt.

Upon closer examination, the CDKN2A interacting protein N-terminal like gene is conserved in chimp, Rhesus monkey, dog, cow, mouse, rat, zebrafish, and frog species, with a total of 120 organisms possessing orthologs as determined by an extensive search of NCBI. However, no function has been identified for this interacting protein in any organism in which it has been detected. Our results using the Sigma p21 antibody suggest that the p16-interacting protein is differentially expressed across regeneration with the greatest expression seen in unamputated tail, a down-regulation at 7 and 14 dpa, followed by a return to baseline levels at 21 days post amputation (see appendix for quantification, N_{Day0}=8 and N=5). Though not quantified with the required controls, this indicated pattern of expression follows a logical sequence that would presumably mimic the changing expression of p16 (or another CDK inhibitor) in response to a cell population that is re-entering the cell cycle and eventually undergoing differentiation. The discrepancy between p21-like mRNA transcript down-regulation at 14 and 21 dpa and the resurgence of p21-like protein or p16-interacting protein expression at 21 dpa, most likely indicates that the two experimental approaches are examining different genes and proteins, which has been hinted at with the discovery of the interacting protein. Further investigation into the novel newt p16 interacting protein is required to understand why it is present in the regenerating newt, and what function it performs during the regenerative process. Eventually, the inability of the Sigma p21 antibody to recognize the peptide for which its epitope was designed, despite identifying p16-interacting protein in the process, left no choice but to abandon this line of research, and begin testing the fourth and final antibody, CST p21.

Preliminary testing of the CST p21 antibody showed immediate success with recognizing p21 protein in the recommended positive control sample, the human neuroblastoma cell line, SHSY5Y (Poluha et al., 1996). This represented the first and only tested antibody to detect the

expression of p21 at 21 kDa in a sample, thereby validating the ability of the antibody to accurately identify p21 protein expression with our Western blotting procedure. When testing on regenerating newt tail tissue, the CST p21 antibody did not bind to any proteins. The profile of tissues examined was expanded to include those from the rat, zebrafish, and *Xenopus,* and all of the tested tissues, except for faint bands in *Xenopus* heart and hindlimb, showed no p21 expression. Given the lack of p21 expression in newt tissue, even in the high turnover cell population of gut tissue which has the greatest potential to express p21, there are three main conclusions that can be drawn (Bouvard et al., 2000; Macleod et al., 1995).

First, the CST p21 antibody, like the 3 others tested, does not cross react with the newt and therefore is incapable of recognizing newt p21 protein expression. Second, p21 protein is expressed at such low levels within the tested newt tissues that it would appear to be undetectable using standard Western blot protocols. The use of newt total protein concentrations as high as 40 ug and antibody concentrations as high as 1 in 100 failed to demonstrate expression. Alternatively, lack of detection of p21 protein via Western blotting could be due to only a small proportion of cells within the regenerate actively expressing p21. The uninjured and regenerating newt tail both represent heterogeneous cell populations containing bone, muscle, fibroblasts, connective tissue, nerves, and undifferentiated cells. Examination of p21 protein in other species is typically performed on homogeneous cell lines, which can make it more difficult to extrapolate the findings back to a whole system, *in vivo* context, but provides a clear signal when probed with an anti-p21 antibody. As well, studies in wild-type mice have shown that p21 expression can be isolated to a few select cells, making them easier to detect in tissue slices versus whole tissue extracts (Bouvard et al., 2000). Finally, it is possible that the newt does not express p21 protein, indicating that it lacks p21 similar to the MRL mouse and suggesting that the absence of p21 contributes to the regenerative phenotype of regeneration-competent species.

Testicular cells of the marbled newt, *Triturus marmoratus,* represent the only newt tissue that has been shown to express p21 protein at a molecular weight of approximately 20 kDa

(Ricote et al., 2002). The greatest expression of p21 is detected during the quiescent phase, at which point temperature and light reach the lowest values of the year, requiring little cell proliferation at this time (Ricote et al., 2002). The recognition of p21 in this newt tissue suggests that all antibodies tested in my project were simply incapable of cross reacting to newt tissue; however, *Triturus* (*Triton*) *marmoratus*, is described as one of the only newt species to lack regenerative capabilities. As described by Weismann in 1893, regeneration in *T. marmoratus* is minimal compared to all other species of *Triton*, as even slight injuries are not healed and when amputating an appendage or tail, the extremity failed to grow back to its original size and often resulted in a "deformed protuberance" (Towle, 1901; Weismann, 1893). The inability of *Triturus marmoratus* to successfully regenerate damaged tissue, combined with the strong expression of p21 protein, potentially explains our finding that p21 protein could not be detected in the regeneration-competent newt species, *Notophthalmus viridescens*.

The overall finding of changes in mRNA expression of a p21-like transcript during tail regeneration with no detected p21 protein expression suggests a role for potential post-transcriptional control of p21 expression in the newt. In one study of the specific mouse tissues that express p21, it was determined that no direct correlation exists between the rate of mRNA upregulation and the number of cells expressing p21 protein, particularly in response to ionizing radiation damage, implicating post-transcriptional regulation (Bouvard et al., 2000). A number of microRNAs have been implicated in the past to regulate p21 expression at the level of transcription and translation (Wu et al., 1996). Research by Dolezalova et al (2012) specifically demonstrated that following induction of the DNA damage response via Ultraviolet-C (UVC) irradiation, as indicated by increased levels of p53, human embryonic stem cells (hESCs) have up-regulated expression of p21 mRNA, but p21 protein is not detected. Further investigation directly linked the miR-302 family to the regulation of p21 protein expression in hESCs (Dolezalova et al., 2012). Potential microRNA regulation of p21 in the newt would represent an additional avenue to explore in order to understand p21 expression during regeneration.

Although our findings parallel those of Bedelbaeva et al (2010) with a lack of p21 protein detected in the newt as in the regenerative MRL mouse, the further study of p21 expression in *Notophthalmus viridescens*, using such approaches as additional antibodies, histological examination, and *in vivo* functional studies, is warranted to understand the role of the cell cycle regulator, p21, in the regenerative process.

Acknowledgements

I would like to thank Lucas Maddalena and Dr. Jeff Stuart for C2C12 and SHSY5Y cell lysate samples, and a trial of their Caspase-3 antibody. Thank you as well to Jonathan Simone and Dr. Cheryl McCormick for the use of the EZ View Gel Doc system, the rat hippocampus protein sample used in a variety of Western blots, and samples of their ERK and phospho-ERK antibodies. A final thank you to Dr. Nina Slavickova for her assistance with preparing the gel and samples for protein sequencing, and Dr. Charles Despres for the use of his Odyssey Infrared Imaging system.

CHAPTER 3:
5’-3’ RACE identifies a newt p21-like sequence with similarity to newt Histone H3a

Abstract

The ability to regenerate a variety of tissues as an adult makes the newt, *Notophthalmus viridescens,* an ideal model organism to study regeneration. Mammals are typically unable to undergo this phenomenon of regeneration; however, the MRL mouse is able to close ear hole punctures through a similar mechanism. A lack of the CDK inhibitor, p21, confers regenerative abilities in these mice. Given that the absence of p21 is linked to MRL mouse's ability to regenerate, it is imperative to determine the involvement of p21 in the newt, a regeneration-competent species. Presently, a full-length p21 gene has not been cloned from the newt, however a CDK inhibitor homologous to human p21 was detected in the closely related axolotl, *Ambystoma mexicanum*. This axolotl partial contiguous sequence (contig) shares 44% identity with the human p21 sequence showing the greatest similarity in the CDK binding domain – the region considered the most highly conserved in p21 sequences across species. Following an extensive search that was unable to locate a p21 antibody capable of detecting the expression of p21 protein in the newt - assuming it is expressed in detectable quantities - the need for a newt-specific p21 antibody was clear. In order to create this antibody, 5'-3' Rapid Amplification of cDNA Ends (RACE) was performed in attempt to obtain a p21 sequence from the newt. After three rounds of RACE, we were unable to identify a newt-specific p21 sequence. Sequence information returned from the amplified products identified a high degree of similarity with p21 from other species and the *N. viridescens* Histone H3a gene, unexpectedly complicating the process of primer design for further rounds of RACE. Despite being unable to identify a p21 sequence from the newt, the obtained sequence data shared some similarity with p21 sequences from other species, but it was insufficient information to establish a significant and meaningful match. Therefore, these initial rounds provided important preliminary findings and suggest that continued pursuit of the newt-specific p21 sequence using these methods is merited.

Introduction

The Eastern red-spotted newt, *Notophthalmus viridescens,* is an excellent model for

studying regeneration as it is the only tetrapod vertebrate capable of regenerating the spinal cord and limbs as an adult (Brockes and Kumar, 2003; Chernoff et al., 2003). However, in recent years, the difficulties in examining the molecular basis of this phenomenon due to a lack of genomic information have led to a decline in the use of this model organism (Bruckskotten et al., 2012). Our own inability to ascertain if p21 protein is expressed in the newt, whether due to either a lack of expressed protein or unsuitable antibodies, emphasizes the necessity for a newt-specific p21 antibody. Further to this point, the detection of a p16-interacting protein N-terminal like peptide sequence in regenerating newt tail, with no known record of p16 expression in the newt or other lower vertebrates, highlights the need for more transcriptome information made available by a sequenced newt genome (Abdullayev et al., 2013).

In order to create a newt-specific antibody, at least a partial sequence of newt p21 will be required and no p21 newt sequence has been identified to date. An axolotl (*Ambystoma. mexicanum*) Cip/Kip (CDK interacting protein/Kinase inhibitory protein) that is 44% identical to human p21 has been identified (Heber-Katz et al., 2012). Figure 3.1 shows the alignment of this 1713bp contig with p21 protein sequences from human, two *Xenopus* species, and the mouse. This contig, or contiguous sequence, is a set of overlapping DNA segments that collectively represent a consensus region of DNA. The highest degree of sequence conservation exists in the cyclin dependent kinase (CDK)-binding domain, where two key amino acid signatures of LFGPVD and WNFDF exist. Outside of this defined region, there are significant sequence differences between the axolotl, *Xenopus,* and mammalian p21 sequences examined. In hopes of finding p21 information from another urodele, we identified a sequence in the Japanese salamander, *Hynobius retardatus*, that through BLAST searches and alignments with human p21, we characterized as being p21-like. Figure 3.2 depicts a pairwise alignment between the *H. retardatus* sequence and human p21 with 37% identity and 51% similarity (92% query cover, Evalue 4e-35, and bit score 110). When performing BLAST alignments, the combination of an identity greater than 30%, an E value less than 0.001, and a bit score larger than 50 are typically

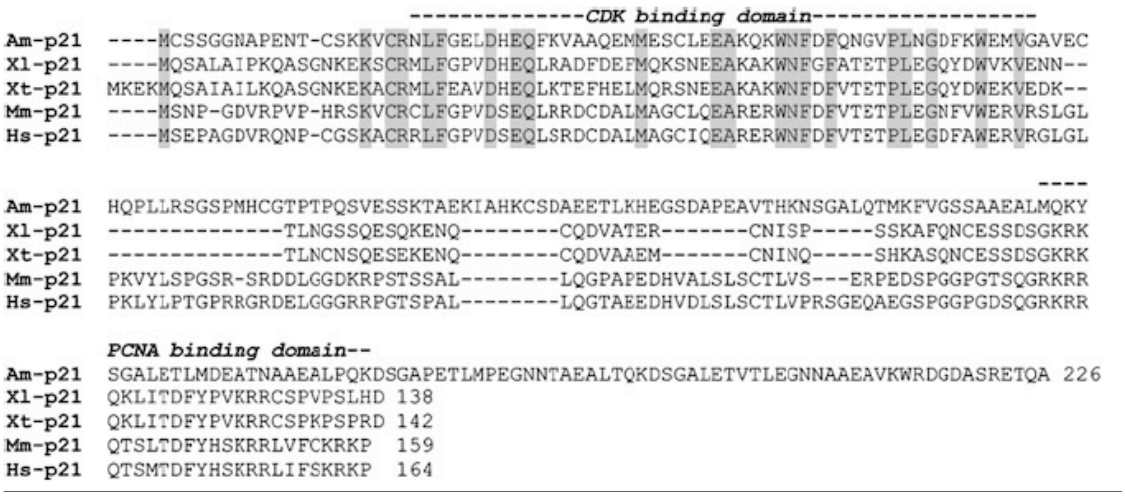

Figure 3.1: Multiple sequence alignment comparing the axolotl p21 contig with known mammalian and amphibian sequences. Taken from Heber-Katz et al (2012). The most highly conserved region can be seen in the cyclin dependent kinase (CDK) binding domain. Organisms included and their associated p21 accession numbers are as follows: Am=*Ambystoma mexicanum* (axolotl) (ID: C0207013); Xl=*Xenopus laevis* (NP_001087933); Xt=*Xenopus tropicalis* (XP_002935823); Mm=*Mus musculus* (NP_001104569); Hs=*Homo sapiens* (NP_000380).

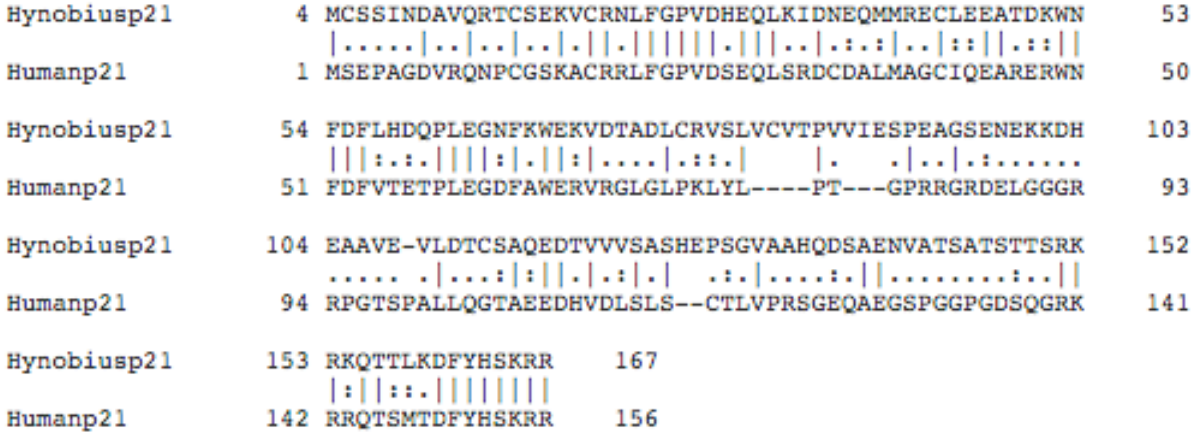

Figure 3.2: Sequence alignment of *Hynobius retardatus* p21-like sequence and Human p21. Sequence alignment using EMBL-EBI EMBOSS Water Pairwise Protein Sequence Alignment program. *H. retardatus* p21-like sequence obtained from the DNA DataBank of Japan and *H. sapiens* p21 sequence obtained from NCBI. (|) = positions with a single, fully conserved residue, (:) = conservation between groups of strongly similar properties, and (.) = conservation between groups of weakly similar properties.

considered indicative of similarity, with the potential for sequence homology; however, it is always best to proceed cautiously when inferring functional similarities from sequence alignments (Pearson, 2013). Similar to the axolotl, the area of highest sequence conservation between the Japanese salamander and human p21 is found in the CDK-binding domain. Although not implicated in the regenerative response, the zebrafish, *Danio rerio,* has been found to express both p21, and the related p20, in relation to circadian cell cycle timing of both the brain and intestine (Laranjeiro et al., 2013; Peyric et al., 2013). Figure 3.3 illustrates the high degree of conservation that exists between the zebrafish p21 and p20 sequences, and a variety of fish, bird, and reptile species. Common domains are shared amongst the p21 and p20 sequences, with p20 containing a unique VPAFY amino acid signature upstream of the CDK-binding domain (Laranjeiro et al., 2013).

The lack of a published newt sequence can be partially attributed to the extremely large genome of *Notophthalmus viridescens*, with a C-value of 38 picograms and a genome size estimated to reach $c*10^{10}$ bases, which is 10 times that of the human genome (Horner and Macgregor, 1983; Looso et al., 2013). The large size of the newt's genome is a significant hindrance to a *de novo* genome project; however research groups have assembled a comprehensive and central repository, known as Newt-omics, to collect expressed sequence tag (EST) data sets in addition to microarray data and peptides identified by mass spectrometry (Bruckskotten et al., 2012). As well, the Sandberg lab published a reference transcriptome with an inferred proteome for *N. viridescens* from extensive RNA sequencing analyses (Abdullayev et al., 2013). In searching this newt transcriptome, we identified a sequence termed 84181 that contained the same two amino acid signatures found in a variety of other p21 sequences (Figure 3.4). Interestingly, when directly comparing the *N. viridescens* 84181 p21-like and zebrafish p20 sequences (39% identity and 53% similarity), the additional amino acid signature of p20 is detected in the newt sequence upstream of the CDK-binding domain, suggesting that the newt sequence may be more closely related to p20 instead of p21 (Figure 3.5).

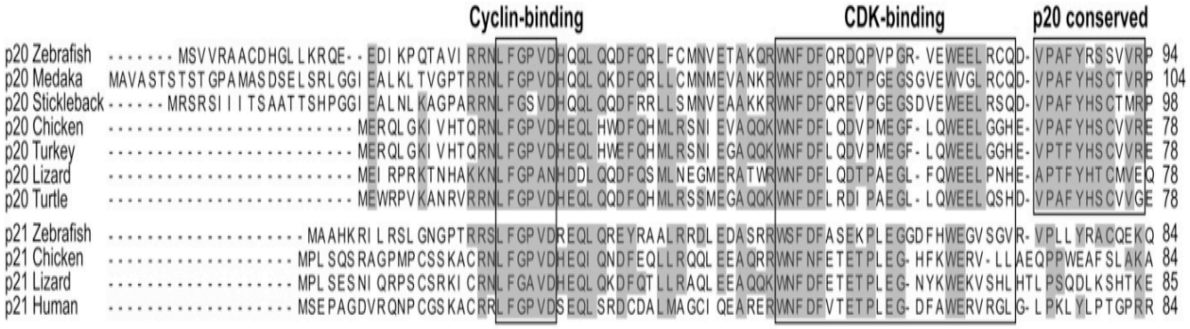

Figure 3.3: Multiple sequence alignment comparing p20 and p21 sequences from the zebrafish, *Danio rerio*, to fish, birds, and reptiles. Taken from Laranjeiro et al (2013). The cyclin-binding and CDK-binding domains are the regions of greatest sequence conservation across species. Notably, an eleven amino acid sequence upstream of the CDK-binding domain is highly conserved in p20 sequences and is considered the distinguishing factor between p21 (CDKN1A) and p20 (CDKN1D). Organisms included and their associated accession numbers are as follows: Zebrafish p21 (KC818434) and p20 (KC818433); Stickleback p21 (Ensembl ID ENSGACG00000001049) and p20 (Ensembl ID ENSGACG00000018951); Medaka p21 (KC818436) and p20 (KC818435); Chicken p21 (KC818438) and p20 (KC818437); Turkey p21 (Ensembl ID ENSMGAG00000013858); Human p21 (NP_000380). The sequences of other organisms were not specified.

Figure 3.4: Multiple sequence alignment of *Notophthalmus viridescens* p21-like sequence with the p21 and p20 sequences of various organisms. Sequence alignment using EMBL-EBI EMBOSS MUSCLE Multiple Protein Sequence Alignment program. *N. viridescens* p21-like sequence (84181) obtained from the Newt-omics transcriptome database. Zebrafish, human, and *Xenopus* sequences were obtained from NCBI. (*) = positions with a single, fully conserved residue, (:) = conservation between groups of strongly similar properties, and (.) = conservation between groups of weakly similar properties.

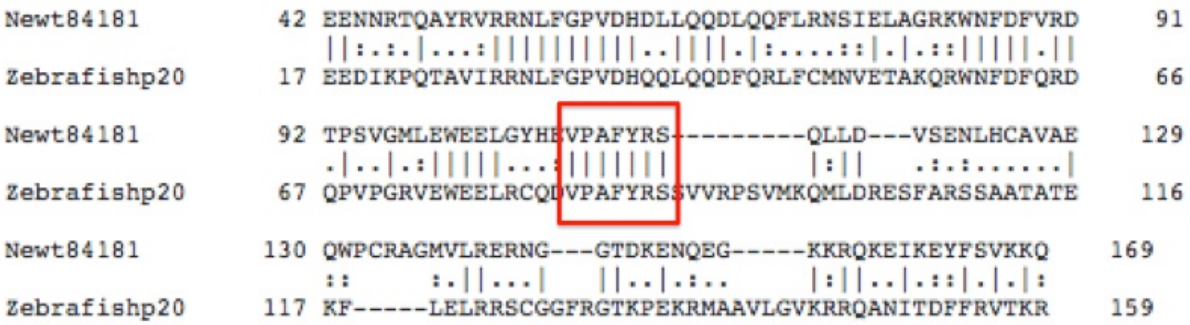

Figure 3.5: Sequence alignment of *Notophthalmus viridescens* p21-like sequence and Zebrafish p20. Sequence alignment using EMBL-EBI EMBOSS Water Pairwise Protein Sequence Alignment program. Red box highlights the conserved region between both sequences that matches the CDKN1D or p20-specific domain. *N. viridescens* p21-like sequence (84181) obtained from the Newt-omics transcriptome database and *D. rerio* p20 sequence obtained from NCBI. (|) = positions with a single, fully conserved residue, (:) = conservation between groups of strongly similar properties, and (.) = conservation between groups of weakly similar properties.

In order to resolve how p21 functions in the newt, *Notophthalmus viridescens,* compared to the regeneration-competent MRL mouse, a greater understanding of p21 in the newt is required. A crucial step in this process is the determination of the newt-specific p21 sequence given the vast differences observed in known p21 amino acid sequences, even when comparing closely-related species. This sequence information would also be invaluable for creating a newt-specific p21 antibody to examine the expression of p21 protein during regeneration. The task of trying to identify the newt p21 sequence was completed using the technique of 5'-3' RACE. Sequence information from our previously identified newt p21-like mRNA transcript, *H. retardatus*, human, axolotl, *Xenopus,* and the newt 84181 transcript were utilized to design primers for p21. After three rounds of RACE, a full p21 sequence was unable to be identified; however, sequence data obtained from the newt contained some similarities to established p21 sequences, indicating the necessity for further investigation.

Materials & Methods

Animal Care and Surgery

All animal handling and surgical procedures were approved by the Brock University Animal Care and Use Committee. See Chapter 2 for detailed methods of caudal tail amputations in the adult Eastern red-spotted newt, *Notophthalmus viridescens*.

5'-3' RACE

Primers were specifically defined for separate 5' and 3' reactions to identify unknown sequence information. DNA sequences were amplified from an mRNA template between a defined internal site and unknown sequences of either the 3' or 5' ends of the mRNA. Table 3.1 contains the primers designed for each round of RACE using Primer3.

Two primers are required for 5' RACE: first, a gene specific primer (GSP1) that will transcribe mRNA into first strand cDNA, and second, a nested primer (GSP2), located upstream of GSP1 that will be used for the PCR amplification. Only one gene-specific forward primer (GSP1) is necessary for 3' RACE as the natural poly-A tail of the sequence is used to prime the

reaction. All reactions were completed using the Roche 5'/3' RACE Kit - 2nd Generation - Version 12 (Cat No. 03353621001). The 5' reaction began with first strand cDNA synthesis with the GSP1 using total RNA from 7 dpa newt tail samples. Day 7 RNA was selected as it had the greatest concentration (ng/uL) and it produced clear bands when run on an agarose gel. It should be noted that previous findings (Chapter 2) indicate that p21 mRNA expression was greatest in unamputated tissue, with a significant decrease at 14 and 21 dpa. A general trend highlighted a decrease in p21 transcripts as early as day 3, potentially hindering the ability to detect p21 from reduced availability of transcript at 7 dpa.

Table 3.1: RACE Primer Sequences for each of the three rounds of 5'-3' RACE performed.

Round of RACE	Primer Name	Primer Sequence
1	FORWARDGSP1	CACTTCTTCACTGCCACCTGTATC
	FORWARDGSP2	TCCTTCGACTCTCTCCTGGG
	REVERSEGSP1	GATGTCGTGGAGGTTGCAGAG
	REVERSEGSP2	CGTGGAGGTTGCAGAGGTG
2	5PRIMEGSP1	CCATTCCAGCATGCCCACTG
	5PRIMEGSP2	AGTTCCATTTCCTGCCAGCC
	3PRIMEGSP1	ACCTTCAGCAGTTCCTTCGGA
3	5primeGSP1p21	TCCCTCAACACCATTCCAGC
	5primeGSP2p21	GTAACCCAGCTCCTCCCATT
	3primeGSP1p21	GATCCATAACCAAGGCGAGC

Next, the Roche High Pure PCR Product Purification Kit was used to purify the single-stranded cDNA. This purified cDNA was then submitted to Poly (A) tailing which added a homopolymeric A tail to the 3' end of the first strand cDNA. Finally, PCR amplification of the dA-tailed cDNA was performed using the Roche Expand High Fidelity PCR System with the GSP2. The 3' reaction also began with first strand cDNA synthesis using an oligo dT anchor primer. After this step, the cDNA was amplified directly without prior purification, utilizing the GSP1 primer and the Roche Expand High Fidelity PCR System.

Product Isolation and Sequencing

PCR products were stored at 4°C after running RACE reactions. Samples were analyzed

alongside a Minisizer DNA Ladder (Norgen) on 1-2% Agarose gels containing GelRed. Bands were excised from each sample lane following UV visualization and DNA was extracted using a Gel Extraction Kit (Sigma). All samples were shipped at room temperature to Nanuq – McGill University and Genome Quebec Innovation Centre for sequencing service.

Results

First RACE procedure detects N. viridescens Histone H3a gene

Initial primer design for RACE was attempted using the partial newt p21-like sequence information obtained from my earlier work to confirm the identity of the qPCR product (Chapter 2). However, the sequence length was insufficient for the primer parameters required for RACE. Thus, the first round of 5'-3' RACE utilized primers specific to the axolotl p21 contig and *H. retardatus* p21-like sequences. As shown in Figure 3.6, the 5' reaction produced a single bright band of approximately 400bp. Conversely, the 3' reaction appeared as a smear on the gel indicating an unsuccessful amplification (results not shown). Sequencing results of the 5' product indicated a high degree of similarity between the amplified DNA and the newt Histone H3a gene. The 5' RACE product sequence was 86.8% identical and 87.1% similar to the *Notophthalmus viridescens* Histone H3a gene partial coding sequence (Figure 3.7).

This unexpected result suggested that the newt p21 sequence, for which the primers were originally designed, might share sequence similarity with Histone H3a. To examine this possibility further, a series of pairwise sequence alignments were performed between the newt Histone H3a protein sequence, the human p21 sequence, and four amphibian p21 sequences (Figure 3.8). Although matches are detected between all pairs, Figure 3.8E shows that the axolotl p21 sequence shares the highest degree of similarity to the newt Histone H3a with 41.2% identity and 52.9% similarity. When performing a BLAST alignment, this translates to 16% query cover with 39% identity (E value 0.018 and bit score 19.2), indicating that despite sharing some similar amino acids, there is insufficient sequence information to identify the 5' RACE product as p21-like. Based upon these findings, it was imperative for the second round of primer design that

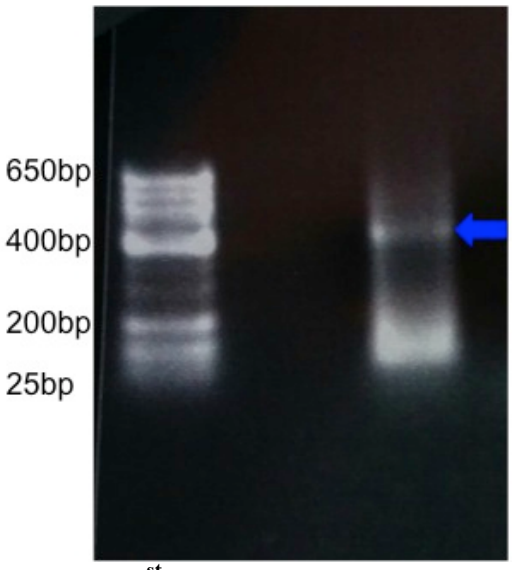

Figure 3.6: 5' RACE product from 1st RACE reaction after being subjected to agarose electrophoresis and UV irradiation. The arrow denotes 5' product excised for sequencing purposes. Norgen DNA Minisizer ladder indicates the product is approximately 400bp in length. The lower bands in the 5' product most likely represent artifacts caused by the nonspecific binding of primers to multiple primer sites or primer dimers and therefore, were not included in the analysis (SMARTer RACE Kit product information).

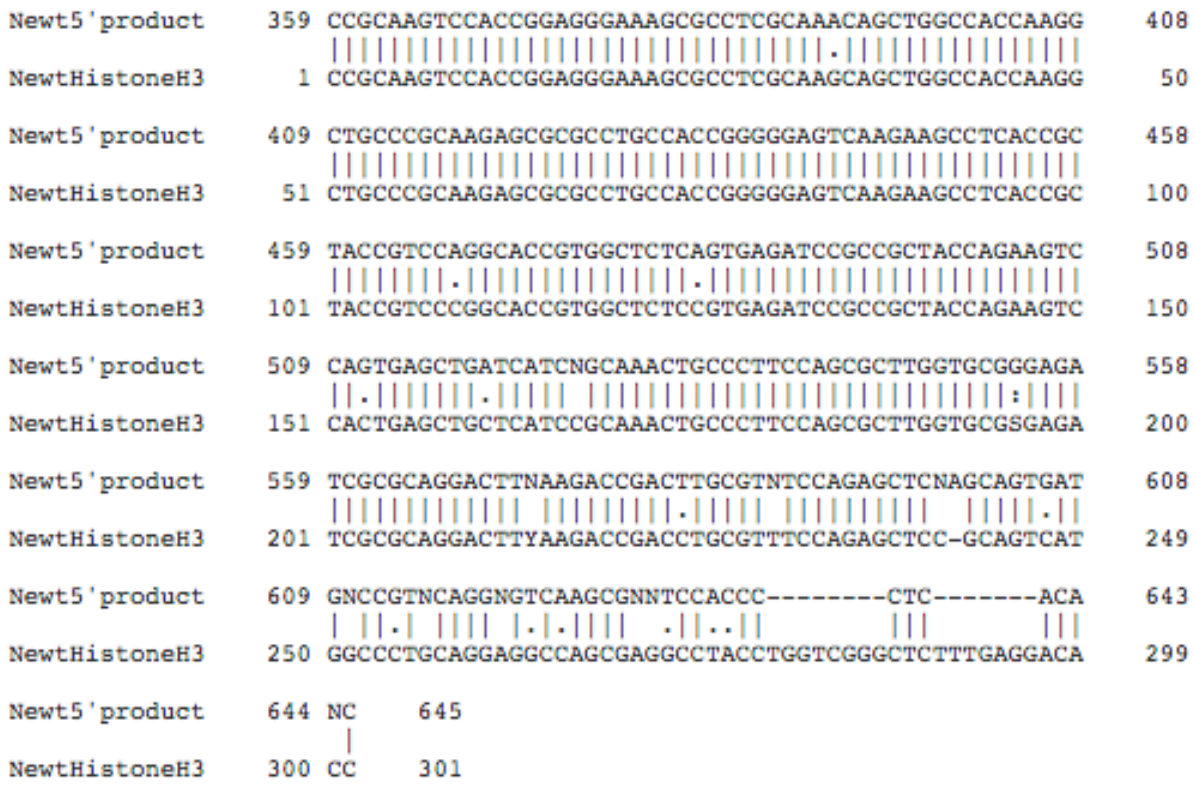

Figure 3.7: Sequence alignment of *N. viridescens* 5'RACE product and *N. viridescens* Histone H3a gene. Sequence alignment using EMBL-EBI EMBOSS Water Pairwise Protein Sequence Alignment program. *N. viridescens* histone H3a sequence obtained from NCBI after BLAST search with 5'RACE product. (|) = positions with a single, fully conserved residue, (:) = conservation between groups of strongly similar properties, and (.) = conservation between groups of weakly similar properties.

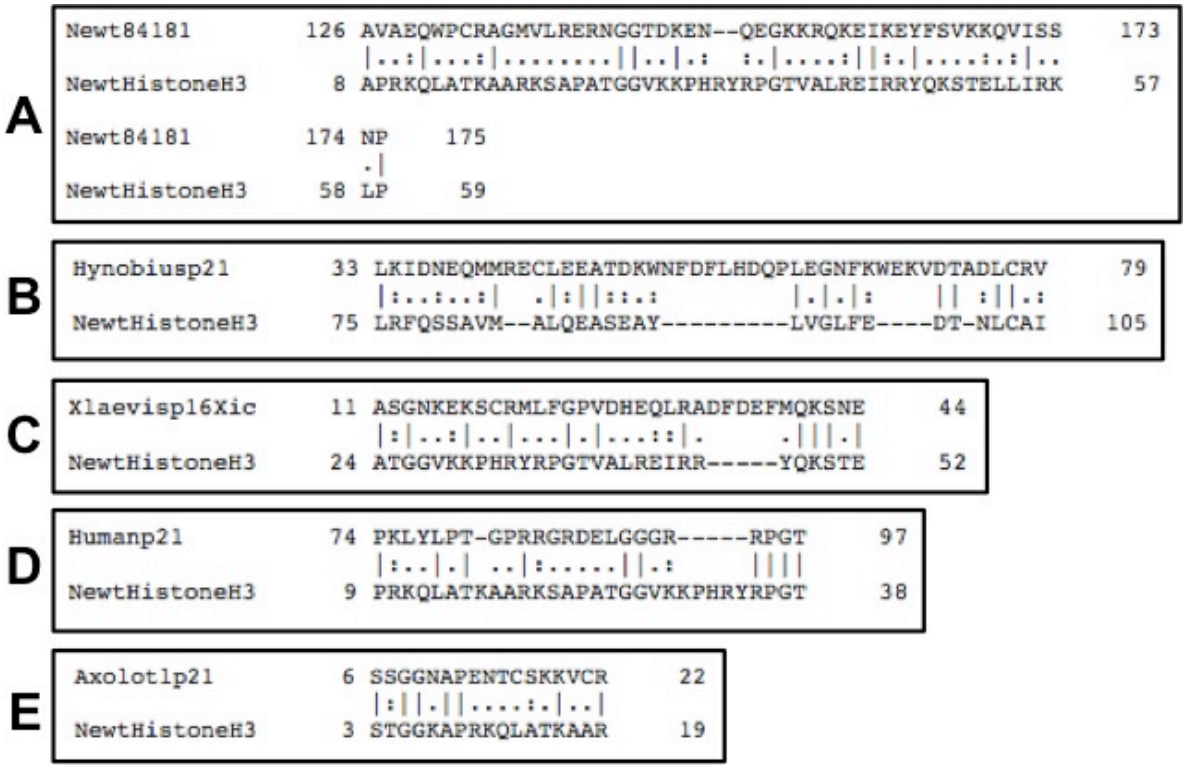

Figure 3.8: Multiple pairwise sequence alignments of *Notophthalmus viridescens* Histone H3a and p21 sequences from human and a variety of amphibians. Sequence alignment using EMBL-EBI EMBOSS Water Pairwise Protein Sequence Alignment program. *N. viridescens* p21-like sequence (84181) obtained from the Newt-omics transcriptome database. Axolotl p21 sequence obtained from SalSite database. *H. retardatus* p21-like sequence obtained from the DNA DataBank of Japan. *N. viridescens* Histone H3a sequence and p21 sequences from *Xenopus* and human obtained from NCBI. (|) = positions with a single, fully conserved residue, (:) = conservation between groups of strongly similar properties, and (.) = conservation between groups of weakly similar properties.

both the 5' and 3' sequences would target p21, while minimizing the likelihood of recognizing and binding to the Histone H3a sequence as well.

Second round of RACE recognizes C. elegans sequences

The task of designing p21-specific primers proved to be a difficult process, requiring that the 3' reaction be run at two different annealing temperatures in order to find the optimal temperature to increase specificity and minimize the potential of the primers dimerizing. The final 3' product can be seen in Figure 3.9. As indicated by the blue arrows to the right, the 3' RACE reaction underwent a step-wise sequencing process in which the sequence information from each smaller band was nested in the larger band directly above it. All five of the bands present in the sample were collected for sequencing. The presence of nested sequences was confirmed when reviewing the sequence chromatograms from Nanuq and observing that the sequence data from each of the smaller excised bands was contained in the larger bands above. The 5' reaction ran on the gel as a very bright smear and was excluded from this round of analysis.

Sequencing results from this round of RACE identified all of the 3' RACE products as *C. elegans* related sequences using BLAST (see appendix). The largest sequence fragment, of approximately 300 base pairs shares 95% identity with a *C. elegans* genome assembly complex; 98% identity with a *C. elegans* fosmid, which is an artificially constructed cloning vector based on a bacterial F plasmid; and 95% identity with a *C. elegans* uncharacterized protein. Interestingly, when trying to understand why the 3' RACE product was only recognizing *C. elegans* sequences when p21-specific primers were utilized, an alignment of the *Hynobius retardatus p21* sequence with the 3' product determined that they shared identity and similarity of 45.4%. Follow-up with a BLAST alignment found that with 63% query coverage the two sequences are 28% identical (E value 1.2 and bit score 13.1) indicating that the sequence similarity is just below the recommended 30% threshold. Figure 3.10 shows the pairwise alignment of the *H. retardatus p21* sequence and the 3' RACE product, and suggests that

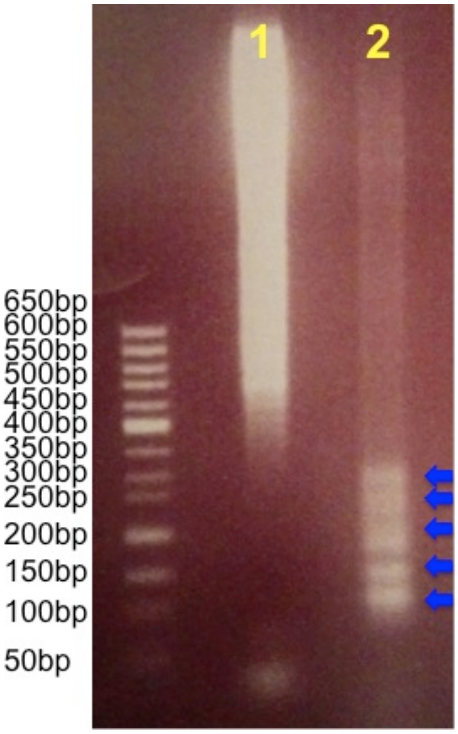

Figure 3.9: 3' RACE product from 2nd RACE reaction after being subjected to agarose electrophoresis and UV irradiation. Lane 1 contains a 5' RACE product that returned no sequence information. Lane 2 contains a 3' RACE product. The arrows indicate the stepwise sequencing of the 3' product in a series of nested fragments later excised for sequencing purposes. Norgen DNA Minisizer ladder indicates the 3' products range from 100 to approximately 300 bp.

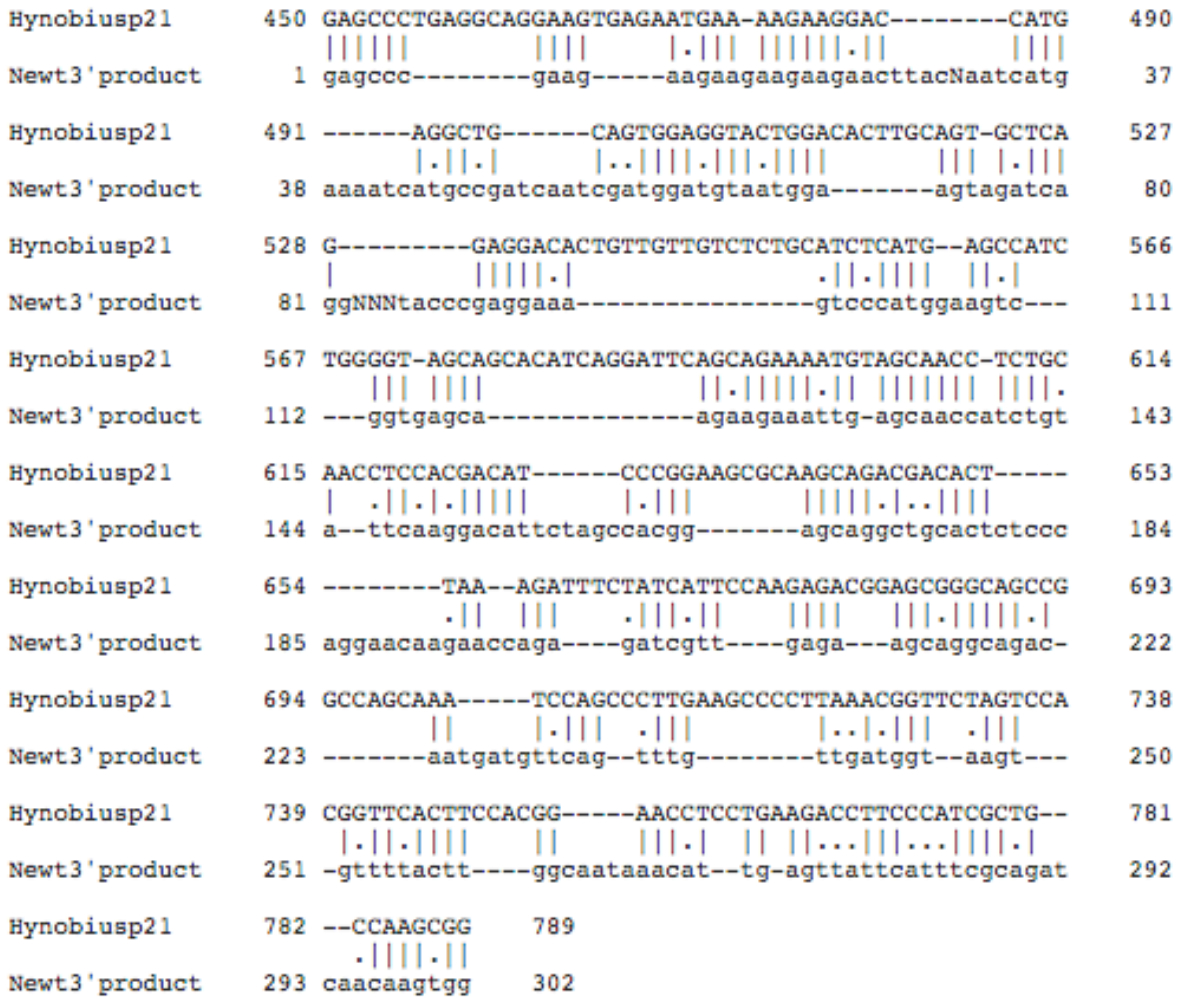

Figure 3.10: Sequence alignment of *N. viridescens* 3'RACE product and *H. retardatus* p21. Sequence alignment using EMBL-EBI EMBOSS Water Pairwise Protein Sequence Alignment program. *H. retardatus* p21-like sequence obtained from the DNA DataBank of Japan. (|) = positions with a single, fully conserved residue, (:) = conservation between groups of strongly similar properties, and (.) = conservation between groups of weakly similar properties.

although the sequence only returned results related to *C. elegans,* the sequence might contain more p21-like characteristics than previously thought.

Final round of RACE produces bright bands on the gel, but no sequence information found

After two unsuccessful rounds of RACE reactions trying to determine the newt p21 sequence, the final primer design process targeted the CDK-binding domain of the human p21 sequence and focused on those areas of this region that were most similar to the axolotl, *H. retardatus*, and newt transcriptome sequences. As can be seen in Figure 3.11, both the 5' and 3' RACE reactions resulted in products with bright bands on the gel that were isolated for sequencing. Unfortunately, no sequence information was returned from any of the samples. Another round of samples was sent for sequencing using the remainder of the PCR products from this third set of reactions, but once again no useful sequence information was returned.

Discussion

Perhaps one of the most challenging aspects of working with the Eastern Red Spotted newt, *Notophthalmus viridescens*, as a model organism is the fact that it remains largely unsequenced. In order to identify the newt p21 sequence, it was necessary to use the p21 sequences of related species to design the 5' and 3' RACE primers. The comparison of the newt transcriptome 84181 and the zebrafish p20 sequences suggested that the unidentified newt sequence could be more closely related to p20 (CDKN1D) than p21 (CDKN1A). In the zebrafish, *p20* expression is independent of p53 expression, implying that its role as a cell cycle regulator differs from that of the closely-related p21 (Laranjeiro et al., 2013). Further study of the newt transcriptome sequence will be required to determine if it can be formally identified as either p20 or p21.

The first round of RACE reactions, which resulted in an almost 400 base pair product resembling the newt Histone H3a gene, represented a good starting point for this new technique. Although not the product expected, the high degree of similarity between the p21 sequences and Histone H3a, which was unknown before this point, suggests that the amplified product might be

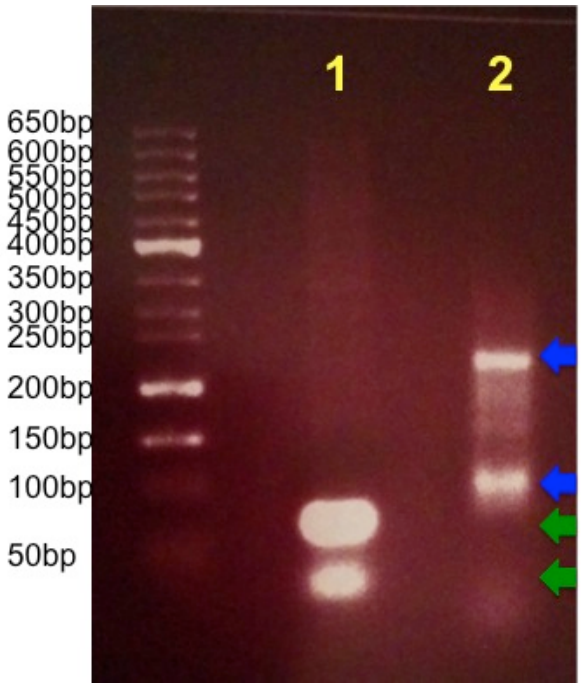

Figure 3.11: 3' and 5' RACE products from 3rd RACE reaction after being subjected to agarose electrophoresis and UV irradiation. Lane 1 contains the 5' RACE product. Lane 2 contains the 3' RACE product. Blue arrows denote the 3' products excised for sequencing purposes at approximately 225 and 100 base pairs. The Norgen DNA Minisizer ladder indicates the 5' products, highlighted with green arrows, are less than 100bp in length.

p21-like, it just also shares relatedness to newt histone. As well, while this has no bearing on the actual sequence of histone H3a and how it relates to p21, it is interesting to note that phosphorylated histone H3 has been used in a variety of regenerative studies as a marker for mitotic cells (Albors et al., 2015; Love et al., 2013; Tseng et al., 2007; Tweedell, 2010).

The second round of RACE leading primarily to *C. elegans* sequences from BLAST searches could be linked to the fact that databases lack sufficient newt-specific sequences to compare these products against. All of the *C. elegans* sequences were associated with unknown proteins or assemblages that contain large amounts of unassigned and unidentified sequence information. The 45.4% identity and similarity detected between the *Hynobius retardatus p21* sequence and the 3' RACE product indicate that the sequence data obtained from this reaction might contain p21-like characteristics that require additional comparison to known p21 sequences.

The final round of RACE showed the greatest promise of p21 sequence information when visualizing the bright bands on the gel; however, no sequence data was obtained from the products. The lack of data from these samples was concerning given that the procedures performed had been successful in the past, and PCR product that was not subjected to gel electrophoresis and excision, sent to control for the experimental conditions, failed to provide any quality sequence information. The inability to retrieve sequence information from the samples on the second attempt was not unexpected given that only 10 ul of each sample remained to be run on the gel and typically at least 20 ul of sample is used to aid in band isolation.

Taken together, the results from three rounds of 5'-3' RACE indicate that the amplified products contained sequence information related to p21 in the newt based upon their similarity to p21 sequences from a variety of organisms. Following the creation of new primers, perhaps including ones that focus on the amino acid signature related to zebrafish p20, additional rounds of RACE should be performed to gather more sequence information from the newt in hopes of

determining the newt-specific p21 sequence.

Acknowledgements

Thank you to Dr. Chris Carter for his assistance in locating the *Hynobius retardatus* sequence information and his technical notes for performing 5'-3' RACE.

CHAPTER 4:
Conclusions and Perspectives

Following my study, the role of the cell cycle regulator, p21, in newt tail and caudal spinal cord regeneration still remains unknown. It was found that a *p21*-like transcript is down-regulated in regenerating newt tail at 14 and 21 dpa compared to unamputated tissue, with a trend of decreased expression as early as 3 days post amputation (Figure 2.1). Sequencing analysis performed on the qPCR product revealed similarity with the axolotl p21 contig, suggesting the amplified product was p21-like. This small sequence fragment was then utilized as a starting point for determining the newt-specific p21 sequence using 5'-3' RACE. The difficulties associated with detecting p21 protein expression in the newt made efforts to sequence the newt p21 gene an important part of this project. Even though none of the sequence information returned from 5'-3' RACE was directly identified as p21 through BLAST searches, similarities between the products and p21 sequences from the axolotl, human, *Xenopus,* and Japanese newt, suggest that the newt amplified products have p21-like features and warrant additional rounds of RACE analysis (Figure 3.8).

In the process of searching for an antibody capable of identifying newt p21 expression, four separate antibodies were tested. The first two antibodies failed to recognize any of the recommended mammalian samples, making them unusable for detecting p21 expression. The third antibody tested was chosen from Sigma-Aldrich because the epitope sequence targeted a portion of the human p21 CDK-binding domain - the region bearing the greatest similarity between human and axolotl p21 sequences (Heber-Katz et al., 2012). Across all samples tested, this Sigma antibody failed to recognize p21 expression at the predicted weight of 21 kDa. However, a low molecular weight band of approximately 14-16 kDa was detected in both newt tail and limb over the course of regeneration (Figures 2.5, 2.6, and 2.8). This low molecular weight band was expressed in unamputated tissue, with a down-regulation seen at both 7 and 14 dpa, followed by a return of expression to almost basal levels by 21 days post amputation.

Protein identification analysis of this low molecular weight band revealed that it contained, among other proteins, the cell cycle related protein: CDKN2A N-terminal like

interacting protein or p16-interacting protein (Figures 2.10 and 2.11). Further testing of this antibody was unable to detect p21 expression in any control sample, leading to the use of a fourth and final p21 antibody. The CST p21 antibody was the only tested antibody to successfully detect p21 protein expression in one of the recommended control cell lines (SHSY5Y neuroblastoma cells), thereby validating the antibody and Western blotting techniques (Figure 2.14). A variety of newt, rat, *Xenopus,* and zebrafish tissues were tested with the CST p21 antibody, but p21 expression was not detected in any of the samples (Figures 2.15 and 2.16).

Collectively, this work represents a the first attempt to examine the expression of the cell cycle regulator, p21, during tail and caudal spinal cord regeneration in the newt, *Notophthalmus viridescens.* Results from qPCR analysis indicate that the down-regulation of a p21-like gene coincides temporally with some of the morphological and cellular changes occurring in the tail over the course of regeneration. Despite evidence for expression of the p21-like transcript, no protein could be detected. This could be due to a lack of p21 protein expression in the newt, similar to the MRL mouse, but the use of a newt-specific p21 antibody would be a definitive way to determine the expression of p21 during regeneration. The continued use of 5'-3' RACE to identify the newt-specific p21 sequence will be vital to this effort. The novel finding of a p16-interacting protein, which is differentially expressed across regeneration, represents a prospective new research avenue into the existence and role of p16 during regeneration. p16 is thought to have first arose in mammals and has not been found in salamanders, suggesting that the lack of p16 may be related to the robust regenerative capacities of urodeles (Khattak et al., 2013; Pajcini et al., 2010). Axolotl, *Xenopus*, and zebrafish all possess the gene for CDKN2A N-terminal like interacting proteins, but the functionality of this p16-interacting protein has yet to be determined. Ultimately, my investigation of p21 in caudal spinal cord and tail regeneration provides a foundation for future studies of the relationship between cell cycle regulation and regeneration in the newt.

Perspectives

The original aim of this thesis was to determine the role that the cell cycle regulator p21 plays in the regenerative process of the regeneration-competent species, *Notophthalmus viridescens*. After extensive attempts to find an antibody capable of cross-reacting in the newt, it became clear that this task would be much more difficult than originally thought. Despite testing a variety of tissue types, antibody and protein concentrations, incubation times and temperatures, secondary antibodies, and detection systems, I was unable to detect p21 protein in the newt in any of the tissues at any time points, used. When assessing these findings, some important future considerations come to mind.

First, it may be advantageous to attempt to detect p21 protein expression directly from caudal spinal cord and tail tissue sections rather than whole tissue protein extracts. Previous work in the mouse to establish the cellular localization of p21 expression determined that on several occasions, only a few cells in one particular region expressed p21 at any given point in time (Bouvard et al., 2000). This could be a similar situation in the newt, perhaps causing the combination of different tissues and cells in one extract to dilute the p21 signal. As a preliminary approach, fluorescence in situ hybridization (or FISH) could utilize probes matching the primers that recognized a p21-like transcript in newt homogenates. This procedure would allow for the identification of the transcripts *in vivo* and may facilitate determining where the p21 protein should be expressed. The majority of the antibodies I tested in this study were specifically designed solely for Western blotting applications, but the CST p21 antibody, which was the only antibody to recognize positive control samples, is suitable for immunofluorescence purposes. The next step in testing this antibody would be to collect a series of unamputated and regenerating newt tail histological sections, if FISH results detected p21 transcript expression, and incubate them with the CST p21 antibody to try and visualize p21 within the cells directly.

Second, my research also involved several attempts to perform comet assays to examine the degree of single and double strand breaks in newt DNA; however, technical issues prevented

continued pursuit of the project. The comet assay is a rapid and sensitive method for detecting the presence of both single and double strand DNA breaks by applying a current across a mini agarose gel containing a cell suspension on a microscope slide (Hartmann et al., 2003). The cells are exposed to a lysis solution and if strand breaks are present, the DNA loops out, eventually being pulled in one direction by the applied current, causing a 'comet' that is indicative of DNA damage. Work by Bedelbaeva et al (2010) demonstrated extensive single and double stranded DNA breaks in the MRL mouse compared to wild-type mice using comet assays, indicating that the regenerative ability comes at the expense of increased DNA damage. The DNA damage response is triggered upon detection of damage, leading to the activation of the oncogene p53 and subsequently stimulating *p21* expression in order to prevent further progression of the cell cycle (Dolezalova et al., 2012). Given that I was unable to detect expression of p21 protein in the newt under normal conditions, one suggestion would be to expose newts to irradiation or carcinogens for the purpose of triggering this cascade and provoking the expression of p21. A similar study was undertaken by Linklater (2011) to determine the expression of p53 in *Notophthalmus viridescens* in response to DNA damage, finding that a basal level of p53 was detected with virtually no change post irradiation. Interestingly, when MRL mice were exposed to gamma irradiation, no change in the expression of p21 was observed, indicating that even in response to DNA damage, the expression of p21 was not induced (Bedelbaeva et al., 2010). It will be of interest to see if p21 expression exhibits a similar pattern as p53 in the newt or as p21 in the MRL mouse.

More sensitive than the comet assay, the use of immunoblotting or immunostaining to examine the expression of phosphorylated histone H2AX (γH2AX) is the ideal way to assess DNA damage (Sharma et al., 2012). As a widespread marker of DNA damage, γH2AX directly reflects the extent of DNA damage as foci are formed within seconds of double strand break induction and a subsequent decrease in foci is observed as the DNA is repaired (Sharma et al., 2012). Previously, staining with γH2AX was significantly increased in the MRL mouse and in

newt A1 myotubes exposed to UV irradiation, indicating the presence of DNA damage (Bedelbaeva et al., 2010; Yun et al., 2013).

Third, the difficulties associated with detecting p21 protein strongly suggest the need for a newt-specific p21 antibody. As mentioned previously, the only instance of p21 expression in a newt was detected in the testicular tissue of *Triturus marmoratus marmoratus* (Ricote et al., 2002). The protein showed differential expression across the annual testicular cell cycle with the greatest levels observed during the quiescent period. However, *T. marmoratus* is unique since it is one of the only urodele amphibians that has limited regenerative ability (Towle, 1901; Weismann, 1893). This finding could be of interest if the strong expression of p21 is related to its lack of regenerative ability, as the absence of p21 confers regenerative capabilities in the MRL mouse. After contacting the researchers directly, we obtained the Santa Cruz p21 antibody utilized in their study. A preliminary test of this antibody utilized unamputated and regenerating newt tail, newt gut, heart, and brain, and SHSY5Y neuroblastoma cells. The expression of p21 was not detected in any of the tested tissues mirroring the previous results obtained with the other four antibodies. Although not shown to work with this antibody directly, SHSY5Y cells were utilized given their prior success as a positive control sample with the CST p21 antibody. A more appropriate positive control in this instance would be *T. marmoratus* testes tissue that has been shown to have a 21kDa protein recognized by this antibody. The next step will involve repeating this Western blot procedure in order to optimize the new antibody, as well as trying to obtain *Triturus marmoratus marmoratus* gonadal as well as limb and tail tissue to be able to directly test it alongside *Notophthalmus viridescens* tissue to compare and confirm the results of Ricote et al (2002).

Finally, there is the ultimate consideration of using other regeneration-competent species to determine the role of cell cycle regulators like p21 in the regenerative process. Zebrafish represent an excellent model organism, as they are also capable of undergoing extensive regeneration that occurs through a similar epimorphic phenomenon. The mRNA expression of

both p21 and p20 has been established in the brain and intestine, leaving the expression of p21 and p20 protein expression and the role of both CDK inhibitors in zebrafish regeneration unknown (Laranjeiro et al., 2013). As well, the use of *Xenopus* adults and tadpoles would allow for a comparative analysis of p21 expression through the changing regenerative capacity that occurs as the frog undergoes metamorphosis. The opportunity to examine these two regeneration competent species, in addition to the newt, would allow for a more comprehensive study of the role of p21 in regeneration-competent species and could aid in determining if a lack of p21 protein expression is in fact a key characteristic associated with the ability to regenerate.

References

Abdullayev, I., Kirkham, M., Björklund, Å. K., Simon, A. and Sandberg, R. (2013). A reference transcriptome and inferred proteome for the salamander Notophthalmus viridescens. *Exp. Cell Res.* 319, 1187–1197.

Albors, A. R., Tazaki, A., Rost, F., Nowoshilow, S., Chara, O. and Tanaka, E. M. (2015). Planar cell polarity-mediated induction of neural stem cell expansion during axolotl spinal cord regeneration. *Elife*.

Albrecht, J. H., Meyer, A. H. and Hu, M. Y. (1997). Regulation of cyclin-dependent kinase inhibitor p21(WAF1/Cip1/Sdi1) gene expression in hepatic regeneration. *Hepatology* 1–7.

Allen, S. P., Maden, M. and Price, J. S. (2002). A role for retinoic acid in regulating the regeneration of deer antlers. *Dev. Biol.* 251, 409–423.

Anderson, M. A., Burda, J. E., Ren, Y., Ao, Y., O'Shea, T. M., Kawaguchi, R., Coppola, G., Khakh, B. S., Deming, T. J. and Sofroniew, M. V (2016). Astrocyte scar formation aids central nervous system axon regeneration. *Nature* 532, 195–200.

Arthur, L. and Heber-Katz, E. (2011). The role of p21 in regulating mammalian regeneration. *Stem Cell Res. Ther.* 2, 30.

Arthur, L. M., Demarest, R. M., Clark, L., Gourevitch, D., Bedelbaeva, K., Anderson, R., Snyder, A., Capobianco, A. J., Lieberman, P., Feigenbaum, L., et al. (2010). Epimorphic regeneration in mice is p53-independent. *Cell Cycle* 9, 3667–3673.

Bedelbaeva, K., Snyder, A., Gourevitch, D., Clark, L., Zhang, X.-M., Leferovich, J., Cheverud, J. M., Lieberman, P. and Heber-Katz, E. (2010). Lack of p21 expression links cell cycle control and appendage regeneration in mice. *Proc. Natl. Acad. Sci. U. S. A.* 107, 5845–5850.

Benraiss, A., Arsanto, J. P., Coulon, J. and Thouveny, Y. (1999). Neurogenesis during caudal spinal cord regeneration in adult newts. *Dev. Genes Evol.* 209, 363–369.

Besson, A., Dowdy, S. F. and Roberts, J. M. (2008). CDK Inhibitors: Cell Cycle Regulators and Beyond. *Dev. Cell* 14, 159–169.

Boonstra, J. (2003). *Regulation of G1 Phase Progression*. Springer Science & Business Media.

Bouvard, V., Zaitchouk, T., Vacher, M., Duthu, a, Canivet, M., Choisy-Rossi, C., Nieruchalski, M. and May, E. (2000). Tissue and cell-specific expression of the p53-target genes: bax, fas, mdm2 and waf1/p21, before and following ionising irradiation in mice. *Oncogene* 19, 649–660.

Brockes, J. P. and Kumar, A. (2003). Plasticity and reprogramming of differentiated cells in amphibian regeneration. *Growth, Form Comput.* 3, 92–106.

Bruckskotten, M., Looso, M., Reinhardt, R., Braun, T. and Borchardt, T. (2012). Newt-omics: A comprehensive repository for omics data from the newt Notophthalmus viridescens. *Nucleic Acids Res.* 40, 895–900.

Brugarolas, J., Chandrasekaran, C., Gordon, J. I., Beach, D., Jacks, T. and Hannon, G. J. (1995). Radiation-induced cell cycle arrest compromised by p21 deficiency. *Nature* 377, 552–557.

Bryant, S. V., Endo, T. and Gardiner, D. M. (2002). Vertebrate limb regeneration and the origin of limb stem cells. *Int. J. Dev. Biol.* 46, 887–896.

Buckley, G., Wong, J., Metcalfe, A. D. and Ferguson, M. W. J. (2012). Denervation affects regenerative responses in MRL/MpJ and repair in C57BL/6 ear wounds. *J. Anat.* 220, 3–12.

Buzgariu, W., Crescenzi, M. and Galliot, B. (2014). Robust G2 pausing of adult stem cells in Hydra. *Differentiation* 87, 83–99.

Cayrol, C., Knibiehler, M. and Ducommun, B. (1998). p21 binding to PCNA causes G1 and G2 cell cycle arrest in p53-deficient cells. *Oncogene* 16, 311–320.

Chai, F., Evdokiou, a, Young, G. P. and Zalewski, P. D. (2000). Involvement of p21 Waf1 / Cip1 and its cleavage by DEVD-caspase during apoptosis of colorectal cancer cells induced by butyrate Butyrate. *Carcinogenesis* 21, 7–14.

Cheng, C.-H., Leferovich, J., Zhang, X.-M., Bedelbaeva, K., Gourevitch, D., Hatcher, C. J., Basson, C. T., Heber-Katz, E. and Marx, K. a. (2013). Keratin gene expression profiles after digit amputation in C57BL/6 vs. regenerative MRL mice imply an early regenerative keratinocyte activated-like state. *Physiol. Genomics* 45, 409–421.
Chernoff, E. A. G. and Stocum, D. L. (1995). Developmental aspects of spinal cord and limb regeneration. *Dev. Growth Differ.* 37, 133–147.
Chernoff, E. a G., Sato, K., Corn, A. and Karcavich, R. E. (2002). Spinal cord regeneration: Intrinsic properties and emerging mechanisms. *Semin. Cell Dev. Biol.* 13, 361–368.
Chernoff, E. a G., Stocum, D. L., Nye, H. L. D. and Cameron, J. A. (2003). Urodele spinal cord regeneration and related processes. *Dev. Dyn.* 226, 295–307.
Chinzei, N., Hayashi, S., Ueha, T., Fujishiro, T., Kanzaki, N., Hashimoto, S., Sakata, S., Kihara, S., Haneda, M., Sakai, Y., et al. (2015). P21 deficiency delays regeneration of skeletal muscular tissue. *PLoS One* 10, e0125765.
Chuykin, I. A., Lianguzova, M. S., Pospelova, T. V. and Pospelov, V. A. (2008). Activation of DNA damage response signaling in mouse embryonic stem cells. *Cell Cycle* 7, 2922–2928.
Clark, L. D., Clark, R. K. and Heber-katz, E. (1998). A New Murine Model for Mammalian Wound Repair and Regeneration. 88, 35–45.
Connolly, P. F., Jäger, R. and Fearnhead, H. O. (2014). New roles for old enzymes: Killer caspases as the engine of cell behavior changes. *Front. Physiol.* 5 APR, 149.
Copeland, N. A., Sercombe, H. E., Ainscough, J. F. X. and Coverley, D. (2010). Ciz1 cooperates with cyclin-A-CDK2 to activate mammalian DNA replication in vitro. *J. Cell Sci.* 123, 1108–15.
Coverley, D., Marr, J. and Ainscough, J. (2005). Ciz1 promotes mammalian DNA replication. *J. Cell Sci.* 118, 101–112.
Daniels, M., Dhokia, V., Richard-Parpaillon, L. and Ohnuma, S.-I. (2004). Identification of Xenopus cyclin-dependent kinase inhibitors, p16Xic2 and p17Xic3. *Gene* 342, 41–47.
David, C. N. and Gierer, a (1974). Cell cycle kinetics and development of Hydra attenuata. III. Nerve and nematocyte differentiation. *J. Cell Sci.* 16, 359–375.
Dent, J. N. (1962). Limb regeneration in larvae and metamorphosing individuals of the South African clawed toad. *J. Morphol.* 110, 61–77.
Dolezalova, D., Mraz, M., Barta, T., Plevova, K., Vinarsky, V., Holubcova, Z., Jaros, J., Dvorak, P., Pospisilova, S. and Hampl, A. (2012). MicroRNAs regulate p21Waf1/Cip1 protein expression and the DNA damage response in human embryonic stem cells. *Stem Cells* 30, 1362–1372.
Egar, M. and Singer, M. (1972). The role of ependyma in spinal cord regeneration in the urodele, Triturus. *Exp. Neurol.* 37, 422–430.
Eguchi, G., Eguchi, Y., Nakamura, K., Yadav, M. C., Millán, J. L. and Tsonis, P. a (2011). Regenerative capacity in newts is not altered by repeated regeneration and ageing. *Nat. Commun.* 2, 384.
Fan, X., Chen, P., Tan, H., Zeng, H., Jiang, Y., Wang, Y., Wang, Y., Hou, X., Bi, H. and Huang, M. (2014). Dynamic and coordinated regulation of KEAP1-NRF2-ARE and p53/p21 signaling pathways is associated with acetaminophen injury responsive liver regeneration. *Drug Metab. Dispos.* 42, 1532–1539.
Fausto, N. and Webber, E. M. (1994). Liver Regeneration. *liver Biol. Pathobiol.* 3rd, 1059–1084.
Ferretti, P. and Brockes, J. P. (1988). Culture of newt cells from different tissues and their expression of a regeneration-associated antigen. *J. Exp. Zool.* 247, 77–91.
Fitch, M. T., Doller, C., Combs, C. K., Landreth, G. E. and Silver, J. (1999). Cellular and molecular mechanisms of glial scarring and progressive cavitation: in vivo and in vitro analysis of inflammation-induced secondary injury after CNS trauma. *J. Neurosci.* 19, 8182–8198.
Gartel, A. L. and Tyner, A. L. (2002). The Role of the Cyclin-dependent Kinase Inhibitor p21 in

Apoptosis 1. *Mol. Cancer Ther.* 56283, 639–649.
Garza-Garcia, A. A., Driscoll, P. C. and Brockes, J. P. (2010). Evidence for the local evolution of mechanisms underlying limb regeneration in salamanders. *Integr. Comp. Biol.* 50, 528–535.
Gawriluk, T. R., Simkin, J., Thompson, K. L., Biswas, S. K., Clare-Salzler, Z., Kimani, J. M., Kiama, S. G., Smith, J. J., Ezenwa, V. O. and Seifert, A. W. (2016). Comparative analysis of ear-hole closure identifies epimorphic regeneration as a discrete trait in mammals. *Nat. Commun.* 7, 11164.
Geng, J., Gates, P. B., Kumar, A., Guenther, S., Garza-garcia, A., Kuenne, C., Zhang, P., Looso, M. and Brockes, J. P. (2015). Identification of the orphan gene Prod 1 in basal and other salamander families. *Evodevo* 6, 4–7.
Géraudie, J., Nordlander, R., Singer, M. and Singer, J. (1988). Early stages of spinal ganglion formation during tail regeneration in the newt, Notophthalmus viridescens. *Am. J. Anat.* 183, 359–370.
Gervais, J. L. M., Seth, P. and Zhang, H. (1998). Cleavage of CDK Inhibitor p21 Cip1 / Waf1 by Caspases Is an Early Event during DNA Damage-induced Apoptosis. *J. Biol. Chem.* 273, 19207–19212.
Gilley, J. and Fried, M. (2001). One INK4 gene and no ARF at the Fugu equivalent of the human INK4A/ARF/INK4B tumour suppressor locus. *Oncogene* 20, 7447–52.
Grimes, L. N. (1972). Tissue interactions in the regeneration of rabbit ear holes. 157, 151–157.
Grimes, L. N. and Goss, R. J. (1970). Regeneration of holes in rabbit ears. In *American Zoologist*, p. 537.
Habermann, B., Bebin, A.-G., Herklotz, S., Volkmer, M., Eckelt, K., Pehlke, K., Epperlein, H. H., Schackert, H. K., Wiebe, G. and Tanaka, E. M. (2004). An Ambystoma mexicanum EST sequencing project: analysis of 17,352 expressed sequence tags from embryonic and regenerating blastema cDNA libraries. *Genome Biol.* 5, R67.
Hampton, D. W., Seitz, a., Chen, P., Heber-Katz, E. and Fawcett, J. W. (2004). Altered CNS response to injury in the MRL/MpJ mouse. *Neuroscience* 127, 821–832.
Harper, J. W., Elledge, S. J., Keyomarsi, K., Dynlacht, B., Tsai, L. H., Zhang, P., Dobrowolski, S., Bai, C., Connell-Crowley, L. and Swindell, E. (1995). Inhibition of cyclin-dependent kinases by p21. *Mol. Biol. Cell* 6, 387–400.
Hartmann, a., Agurell, E., Beevers, C., Brendler-Schwaab, S., Burlinson, B., Clay, P., Collins, a., Smith, a., Speit, G., Thybaud, V., et al. (2003). Recommendations for conducting the in vivo alkaline Comet assay. *Mutagenesis* 18, 45–51.
Heber-Katz, E. and Naviaux, R. K. (2015). The MRL Mouse: A Model of Regeneration and Cancer. In *Energy Balance and Cancer* (ed. Berger, N. A.), pp. 47–64.
Heber-Katz, E., Leferovich, J., Bedelbaeva, K., Gourevitch, D. and Clark, L. (2004). The scarless heart and the MRL mouse. *Philos. Trans. R. Soc. Lond. B. Biol. Sci.* 359, 785–793.
Heber-Katz, E., Zhang, Y., Bedelbaeva, K., Song, F., Chen, X. and Stocum, D. L. (2012). Cell Cycle Regulation and Regeneration. *Curr. Top. Microbiol. Immunol.* 253–276.
Horner, H. a and Macgregor, H. C. (1983). C value and cell volume: their significance in the evolution and development of amphibians. *J. Cell Sci.* 63, 135–146.
Iten, L. E. and Bryant, S. V. (1976). Stages of Tail Regeneration in the Adult Newt, Notophthalmus viridescens. *J. Exp. Zool.* 196, 283–292.
Kazianis, S., Morizot, D. C., Coletta, L. D., Johnston, D. a, Woolcock, B., Vielkind, J. R. and Nairn, R. S. (1999). Comparative structure and characterization of a CDKN2 gene in a Xiphophorus fish melanoma model. *Oncogene* 18, 5088–5099.
Kench, J. A., Russell, D. M., Fadok, V. A., Young, S. K., Worthen, G. S., Jones-carson, J., Henson, J. E., Henson, P. M. and Nemazee, D. (1999). Aberrant Wound Healing and TGF-Beta Production in the Autoimmune-Prone MRL/+ Mouse. *Clin. Immunol.* 92, 300–310.
Khattak, S., Schuez, M., Richter, T., Knapp, D., Haigo, S. L., Sandoval-Guzm??n, T.,

Hradlikova, K., Duemmler, A., Kerney, R. and Tanaka, E. M. (2013). Germline transgenic methods for tracking cells and testing gene function during regeneration in the axolotl. *Stem Cell Reports* 1, 90–103.
Langheinrich, U., Hennen, E., Stott, G. and Vacun, G. (2002). Zebrafish as a model organism for the identification and characterization of drugs and genes affecting p53 signaling. *Curr. Biol.* 12, 2023–2028.
Laranjeiro, R., Tamai, T. K., Peyric, E., Krusche, P., Ott, S. and Whitmore, D. (2013). Cyclin-dependent kinase inhibitor p20 controls circadian cell-cycle timing. *Proc. Natl. Acad. Sci. U. S. A.* 110, 6835–40.
Lee, K.-C., Goh, W. L. P., Xu, M., Kua, N., Lunny, D., Wong, J. S., Coomber, D., Vojtesek, B., Lane, E. B. and Lane, D. P. (2008). Detection of the p53 response in zebrafish embryos using new monoclonal antibodies. *Oncogene* 27, 629–40.
Lee-Liu, D., Edwards-Faret, G., Tapia, V. S. and Larraín, J. (2013). Spinal cord regeneration: Lessons for mammals from non-mammalian vertebrates. *Genesis* 51, 529–544.
Leferovich, J. M. and Heber-Katz, E. (2002). The scarless heart. *Semin. Cell Dev. Biol.* 13, 327–333.
Leferovich, J. M., Bedelbaeva, K., Samulewicz, S., Zhang, X. M., Zwas, D., Lankford, E. B. and Heber-Katz, E. (2001). Heart regeneration in adult MRL mice. *Proc. Natl. Acad. Sci. U. S. A.* 98, 9830–9835.
Lefloch, R., Pouysségur, J. and Lenormand, P. (2008). Single and combined silencing of ERK1 and ERK2 reveals their positive contribution to growth signaling depending on their expression levels. *Mol. Cell. Biol.* 28, 511–27.
Lefloch, R., Pouysségur, J. and Lenormand, P. (2009). Total ERK1/2 activity regulates cell proliferation. *Cell Cycle* 8, 705–11.
Lepp, A. C. and Carlone, R. L. (2015). MicroRNA dysregulation in response to RARβ2 inhibition reveals a negative feedback loop between microRNAs 1, 133a and RARβ2 during tail and spinal cord regeneration in the adult newt. *Dev. Dyn.* 1519–1537.
Li, Y., Jenkins, C. W., Nichols, M. A. and Xiong, Y. (1994). Cell cycle expression and p53 regulation of the cyclin-dependent kinase inhibitor p21. *Oncogene* 9, 2261–2268.
Liggett, W. H. and Sidransky, D. (1998). Role of the p16 tumor suppressor gene in cancer. *J. Clin. Oncol.* 16, 1197–1206.
Linklater, S. (2011). The Effects of Carcinogens and Irradiation on Cells and Tissues of the Eastern Red Spotted Newt (Notophthalmus viridescens).
Looso, M., Preussner, J., Sousounis, K., Bruckskotten, M., Michel, C. S., Lignelli, E., Reinhardt, R., Höffner, S., Krüger, M., Tsonis, P. a, et al. (2013). A de novo assembly of the newt transcriptome combined with proteomic validation identifies new protein families expressed during tissue regeneration. *Genome Biol.* 14, R16.
Love, N. R., Chen, Y., Ishibashi, S., Kritsiligkou, P., Lea, R., Koh, Y., Gallop, J. L., Dorey, K. and Amaya, E. (2013). Amputation-induced reactive oxygen species are required for successful Xenopus tadpole tail regeneration. *Nat. Cell Biol.* 15, 222–228.
Lukas, J., Parry, D., Aagaard, L., Mann, D. J., Bartkova, J., Strauss, M., Peters, G. and Bartek, J. (1995). Retinoblastoma-protein-dependent cell-cycle inhibition by the tumour suppressor p16. *Nature* 375, 503–506.
Macleod, K., Sherry, N., Hannon, G., Beach, D., Tokino, T., Kinzler, K., Vogelstein, B. and Jacks, T. (1995). p53-Dependent and independent expression of p21 during cell growth, differentiation, and DNA damage. *Genes Dev.* 9, 935–944.
McCullough, W. D. and Tassava, R. a (1976). Determination of the Blastema Cell Cycle in Regenerating Limbs of the Larval Axolotl, Ambystoma Mexicanum. *Ohio J. Sci.* 76, 63–65.
Mescher, A. L. and Tassava, R. A. (1975). Denervation effects on DNA replication and mitosis during the initiation of limb regeneration in adult newts. *Dev. Biol.* 44, 187–197.
Mirzayans, R., Andrais, B., Scott, A. and Murray, D. (2012). New insights into p53 signaling and

cancer cell response to DNA damage: implications for cancer therapy. *J. Biomed. Biotechnol.* 2012, 1–16.

Mitsui, K., Matsumoto, A., Ohtsuka, S., Ohtsubo, M. and Yoshimura, A. (1999). Cloning and Characterization of a Novel p21Cip1/Waf1-Interacting Zinc Finger Protein, Ciz1. *Biochem. Biophys. Res. Commun.* 264, 457–464.

Niculescu, a B., Chen, X., Smeets, M., Hengst, L., Prives, C. and Reed, S. I. (1998). Effects of p21(Cip1/Waf1) at both the G1/S and the G2/M cell cycle transitions: pRb is a critical determinant in blocking DNA replication and in preventing endoreduplication. *Mol. Cell. Biol.* 18, 629–643.

Nishibe, R., Watanabe, W., Ueda, T., Yamasaki, N., Koller, R., Wolff, L., Honda, Z. I., Ohtsubo, M. and Honda, H. (2013). CIZ1, a p21Cip1/Waf1-interacting protein, functions as a tumor suppressor in vivo. *FEBS Lett.* 587, 1529–1535.

Noda, A., Ning, Y., Venable, S. F., Pereira-Smith, O. M. and Smith, J. R. (1994). Cloning of Senescent Cell-Derived Inhibitors of DNA Synthesis Using an Expression Screen. *Exp. Cell Res.* 211, 90–98.

Nordlander, R. H. and Singer, M. (1978). The role of ependyma in regeneration of the spinal cord in the urodele amphibian tail. *J. Comp. Neurol.* 180, 349–373.

Ollmann, M., Young, L. M., Di Como, C. J., Karim, F., Belvin, M., Robertson, S., Whittaker, K., Demsky, M., Fisher, W. W., Buchman, A., et al. (2000). Drosophila p53 is a structural and functional homolog of the tumor suppressor p53. *Cell* 101, 91–101.

Pajalunga, D., Mazzola, a, Franchitto, a, Puggioni, E. and Crescenzi, M. (2008). The logic and regulation of cell cycle exit and reentry. *Cell. Mol. Life Sci.* 65, 8–15.

Pajcini, K. V., Corbel, S. Y., Sage, J., Pomerantz, J. H. and Blau, H. M. (2010). Transient inactivation of Rb and ARF yields regenerative cells from postmitotic mammalian muscle. *Cell Stem Cell* 7, 198–213.

Park, J. A., Kim, K. W., Kim, S. Il and Lee, S. K. (1998). Caspase 3 specifically cleaves p21(WAF1/CIP1) in the earlier stage of apoptosis in SK-HEP-1 human hepatoma cells. *Eur. J. Biochem.* 257, 242–248.

Parker, S. B., Eichele, G., Zhang, P., Rawls, A., Sands, A. T., Olson, E. N., Harper, J. W., Elledge, S. J., Parker, S. B., Eichele, G., et al. (2015). p53-Independent Expression of p21 in Muscle and Other Terminally Differentiating Cells. *Science (80-.).* 267, 1024–1027.

Pearson, W. R. (2013). An Introduction to Sequence Similarity ("Homology") Searching. *Curr Protoc Bioinforma.* 3, 1–9.

Pearson, B. J. and Sánchez Alvarado, A. (2010). A planarian p53 homolog regulates proliferation and self-renewal in adult stem cell lineages. *Development* 137, 213–221.

Peyric, E., Moore, H. a. and Whitmore, D. (2013). Circadian Clock Regulation of the Cell Cycle in the Zebrafish Intestine. *PLoS One* 8, e73209.

Piccolo, M. T. and Crispi, S. (2012). The Dual Role Played by p21 May Influence the Apoptotic or Anti-Apoptotic Fate in Cancer. *J. Can. Res. Updates* 1, 189–202.

Poluha, W., Poluha, D. K., Chang, B., Crosbie, N. E., Schonhoff, C. M., Kilpatrick, D. L. and Ross, a H. (1996). The cyclin-dependent kinase inhibitor p21 (WAF1) is required for survival of differentiating neuroblastoma cells. *Mol. Cell. Biol.* 16, 1335–1341.

Rao, N., Jhamb, D., Milner, D. J., Li, B., Song, F., Wang, M., Voss, S. R., Palakal, M., King, M. W., Saranjami, B., et al. (2009). Proteomic analysis of blastema formation in regenerating axolotl limbs. *BMC Biol.* 7, 83.

Ricote, M., Alfaro, J. M., García-Tuñón, I., Arenas, M. I., Fraile, B., Paniagua, R. and Royuela, M. (2002). Control of the annual testicular cycle of the marbled-newt by p53, p21, and Rb gene products. *Mol. Reprod. Dev.* 63, 202–209.

Ruas, M. and Peters, G. (1998). The p16 INK4a / CDKN2A tumor suppressor and its relatives. *Biochim. Biophys. Acta* 1378, F115–F177.

Serrano, M. (1997). The Tumor Suppressor Protein p16 INK4a. *Exp. Cell Res.* 237, 7–13.

Serrano, M., Hannon, G. J. and Beach, D. (1993). A new regulatory motif in cell-cycle control causing specific inhibition of cyclin D/CDK4. *Nature* 366, 704–707.
Sharma, A., Singh, K. and Almasan, A. (2012). Histone H2AX Phosphorylation: A Marker for DNA Damage. In *Methods in Molecular Biology*, pp. 613–626.
Sherr, C. J. (1996). Cancer cell cycles. *Science (80-.).* 274, 1672–1677.
Silver, J. and Miller, J. H. (2004). Regeneration beyond the glial scar. *Nat. Rev. Neurosci.* 5, 146–156.
Sîrbulescu, R. F. and Zupanc, G. K. H. (2009). Dynamics of caspase-3-mediated apoptosis during spinal cord regeneration in the teleost fish, Apteronotus leptorhynchus. *Brain Res.* 1304, 14–25.
Stepniak, E., Ricci, R., Eferl, R., Sumara, G., Sumara, I., Rath, M., Hui, L. and Wagner, E. F. (2006). c-Jun / AP-1 controls liver regeneration by repressing p53 / p21 and p38 MAPK activity. *Genes Dev.* 20, 2306–2314.
Stocum, D. L. and Cameron, J. A. (2011). Looking proximally and distally: 100 years of limb regeneration and beyond. *Dev. Dyn.* 240, 943–968.
Tam, S. W., Shay, J. W. and Pagano, M. (1994). Differential expression and cell cycle regulation of the cyclin-dependent kinase 4 inhibitor p16Ink4. *Cancer Res.* 54, 5816–20.
Tanaka, E. M. (2003). Cell differentiation and cell fate during urodele tail and limb regeneration. *Curr. Opin. Genet. Dev.* 13, 497–501.
Tanaka, E. M., Gann, a. a F., Gates, P. B. and Brockes, J. P. (1997). Newt myotubes reenter the cell cycle by phosphorylation of the retinoblastoma protein. *J. Cell Biol.* 136, 155–165.
Tanaka, H., Yamashita, T., Yachi, K., Fujiwara, T., Yoshikawa, H. and Tohyama, M. (2004). Cytoplasmic p21Cip1/WAF1 enhances axonal regeneration and functional recovery after spinal cord injury in rats. *Neuroscience* 127, 155–164.
Tassava, R. A. and Mescher, A. L. (1976). Mitotic activity and nucleic acid precursor incorporation in denervated and innervated limb stumps of axolotl larvae. *J. Exp. Zool.* 195, 253–62.
Tassava, R. a, Goldhamer, D. J. and Tomlinson, B. L. (1987). Cell cycle controls and the role of nerves and the regenerate epithelium in urodele forelimb regeneration: possible modifications of basic concepts. *Biochem. Cell Biol.* 65, 739–749.
Taylor, S., Wakem, M., Dijkman, G., Alsarraj, M., Nguyen, M. and Laboratories, B. (2009). *A Practical Approach to RT-qPCR - Publishing Data That Conform to the MIQE Guidelines*.
Thuret, S., Thallmair, M., Horky, L. L. and Gage, F. H. (2012). Enhanced functional recovery in MRL/MpJ mice after spinal cord dorsal hemisection. *PLoS One* 7, e30904.
Tomlinson, B. L., Goldhamer, D. J., Barger, P. M. and Tassava, R. A. (1985). Punctuated cell cycling in the regeneration blastema of urodele amphibians. *Differentiation* 28, 195–199.
Towle, E. W. (1901). On Muscle Regeneration in the Limbs of Plethedon. *Biol. Bull.* 2, 289–299.
Tseng, A.-S., Adams, D. S., Qiu, D., Koustubhan, P. and Levin, M. (2007). Apoptosis is required during early stages of tail regeneration in Xenopus laevis. *Dev. Biol.* 301, 62–69.
Tucker, B., Klassen, H., Yang, L., Dong, F. C. and Young, M. J. (2008). Elevated MMP Expression in the MRL Mouse Retina Creates a Permissive Environment for Retinal Regeneration. *Investig. Opthalmology Vis. Sci.* 49, 1686–1695.
Tweedell, K. S. (2010). The urodele limb regeneration blastema: the cell potential. *ScientificWorldJournal.* 10, 954–971.
Vermeulen, K., Van Bockstaele, D. R. and Berneman, Z. N. (2003). The cell cycle: A review of regulation, deregulation and therapeutic targets in cancer. *Cell Prolif.* 36, 131–149.
Villiard, E., Brinkmann, H., Moiseeva, O., Mallette, F. a, Ferbeyre, G. and Roy, S. (2007). Urodele p53 tolerates amino acid changes found in p53 variants linked to human cancer. *BMC Evol. Biol.* 7, 1–14.
Vlaskalin, T., Wong, C. J. and Tsilfidis, C. (2004). Growth and apoptosis during larval forelimb development and adult forelimb regeneration in the newt (Notophthalmus viridescens). *Dev.*

Genes Evol. 214, 423–431.
Vousden, K. H. (2000). P53: Death Star. *Cell* 103, 691–694.
Weismann, A. (1893). The Germ-Plasm: A Theory of Heredity. 93–134.
Whited, J. L., Lehoczky, J. a., Austin, C. a. and Tabin, C. J. (2011). Dynamic expression of two thrombospondins during axolotl limb regeneration. *Dev. Dyn.* 240, 1249–1258.
Wu, H., Wade, M., Krall, L., Grisham, J., Xiong, Y. and Van Dyke, T. (1996). Targeted in vivo expression of the cyclin-dependent kinase inhibitor p21 halts hepatocyte cell-cycle progression, postnatal liver development and regeneration. *Genes Dev* 10, 245–260.
Xiong, Y., Hannon, G. J., Zhang, H., Casso, D., Kobayashi, R. and Beach, D. (1993). p21 is a universal inhibitor of cyclin kinases. *Lett. to Nat.* 366, 701–704.
Yamamoto, T., Ebisuya, M., Ashida, F., Okamoto, K., Yonehara, S. and Nishida, E. (2006). Continuous ERK Activation Downregulates Antiproliferative Genes throughout G1 Phase to Allow Cell-Cycle Progression. *Curr. Biol.* 16, 1171–1182.
Yun, M. H., Gates, P. B. and Brockes, J. P. (2013). Regulation of p53 is critical for vertebrate limb regeneration. *Proc. Natl. Acad. Sci. U. S. A.* 110, 17392–17397.
Yun, M. H., Gates, P. B. and Brockes, J. P. (2014). Sustained ERK activation underlies reprogramming in regeneration-competent salamander cells and distinguishes them from their mammalian counterparts. *Stem Cell Reports* 3, 15–23.
Zhang, Y., Fujita, N. and Tsuruo, T. (1999). Caspase-mediated cleavage of p21 Waf1 / Cip1 converts cancer cells from growth arrest to undergoing apoptosis. *Oncogene* 18, 1131–1138.
Zhu, X.-N., Kim, D. H., Lin, H.-R., Budhavarapu, V. N., Rosenbaum, H. B., Mueller, P. R. and Yew, P. R. (2013). Proteolysis of Xenopus Cip-type CDK inhibitor, p16Xic2, is regulated by PCNA binding and CDK2 phosphorylation. *Cell Div.* 8, 5.
Zukor, K. a, Kent, D. T. and Odelberg, S. J. (2011). Meningeal cells and glia establish a permissive environment for axon regeneration after spinal cord injury in newts. *Neural Dev.* 6, 1.

Appendix

1) Laemmli Buffer Recipe
    a. 5 mL 0.5M Tris HCl, pH 7.0 (3.49g Tris HCl and dH2O up to 50mL)
    b. 5 mL dH2O
    c. 1.2 g SDS
    d. 4 mL glycerol
    e. 2 mL bromophenol blue solution (1 mg bromophenol blue in 1 mL dH2O – store at room temperature)
    f. 620 mg dithiothreitol (DTT)
2) Protein Lysis Buffer Recipe
    a. 150 mM NaCl (5M stock) → 300 uL
    b. 50 mM Tris HCl pH 7.5-7.6 (1M stock) → 500 uL
    c. 10 mM EDTA (0.5M stock) → 200 uL
    d. 1 mL of 10% Triton X-100
    e. 100 uL of 100mM PMSF
    f. 100 uL of protease inhibitor cocktail (Sigma)
    g. 7.8 mL of MilliQ

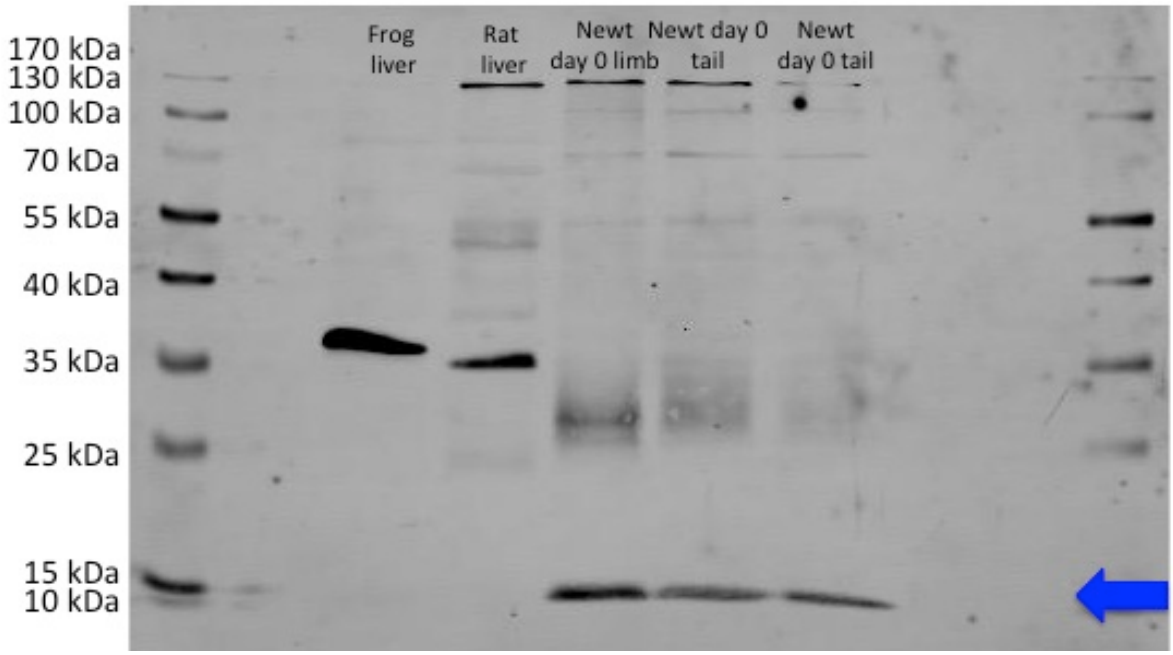

Figure A1: Western blot of frog, rat, and newt tissues probed with the Sigma p21 Antibody. The anti-p21 antibody used at a concentration of 5 ug/mL. Protein (40ug) from various tissues are as follows: frog liver tissue, rat liver tissue, pooled unamputated newt limb tissue, and two biological replicates of unamputated (day zero) newt tail tissue. The arrow on the right highlights a low molecular weight band recognized by the Sigma anti-p21 antibody at 14/15 kDa in only newt tail tissue.

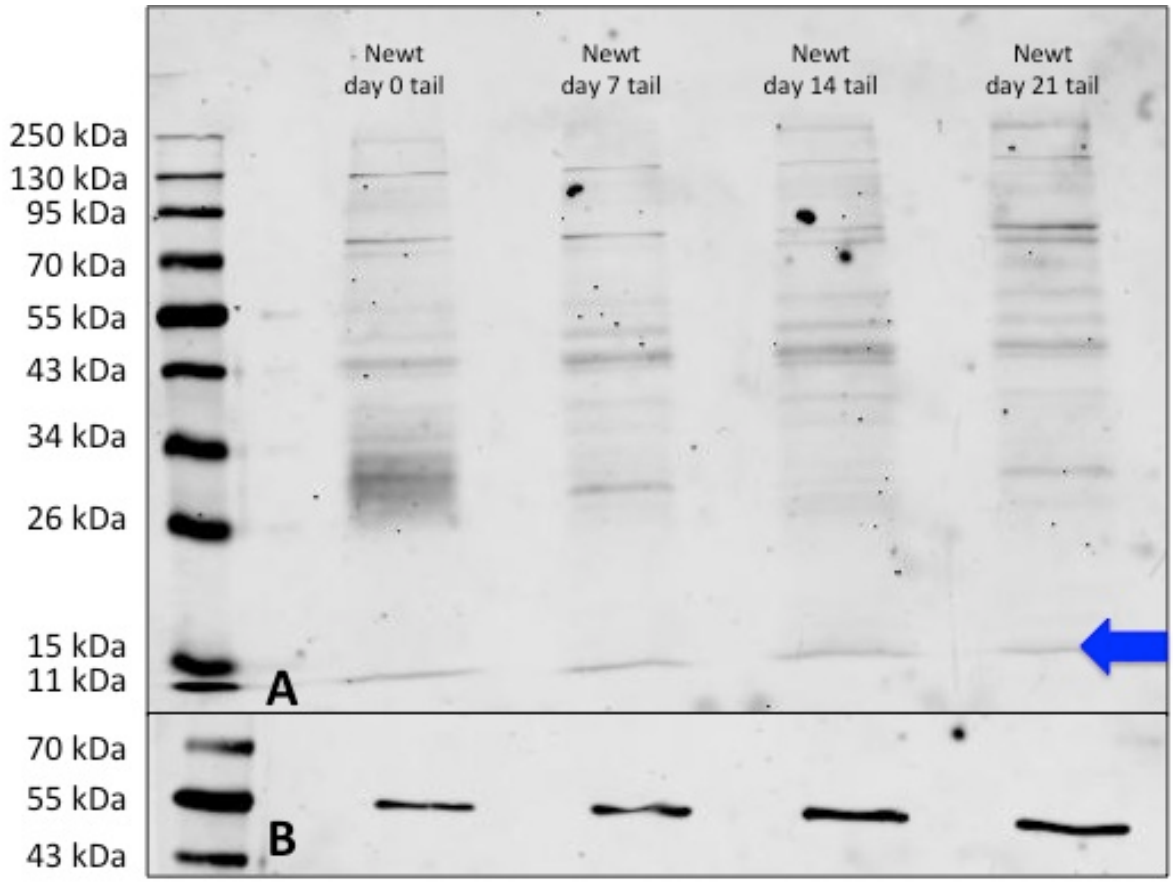

Figure A2: Western blot of newt tail tissues probed with the Sigma p21 Antibody. (A) The anti-p21 antibody used at a concentration of 5 ug/mL. (B) The anti-alpha tubulin antibody used at a 1/500 dilution. Protein (20 ug) from various tissues are as follows: unamputated (day zero) newt tail tissue and newt tail regenerate tissue from days 7, 14, and 21 dpa. The arrow on the right highlights a low molecular weight band recognized by the Sigma anti-p21 antibody at 14/15 kDa in all newt tail tissue samples.

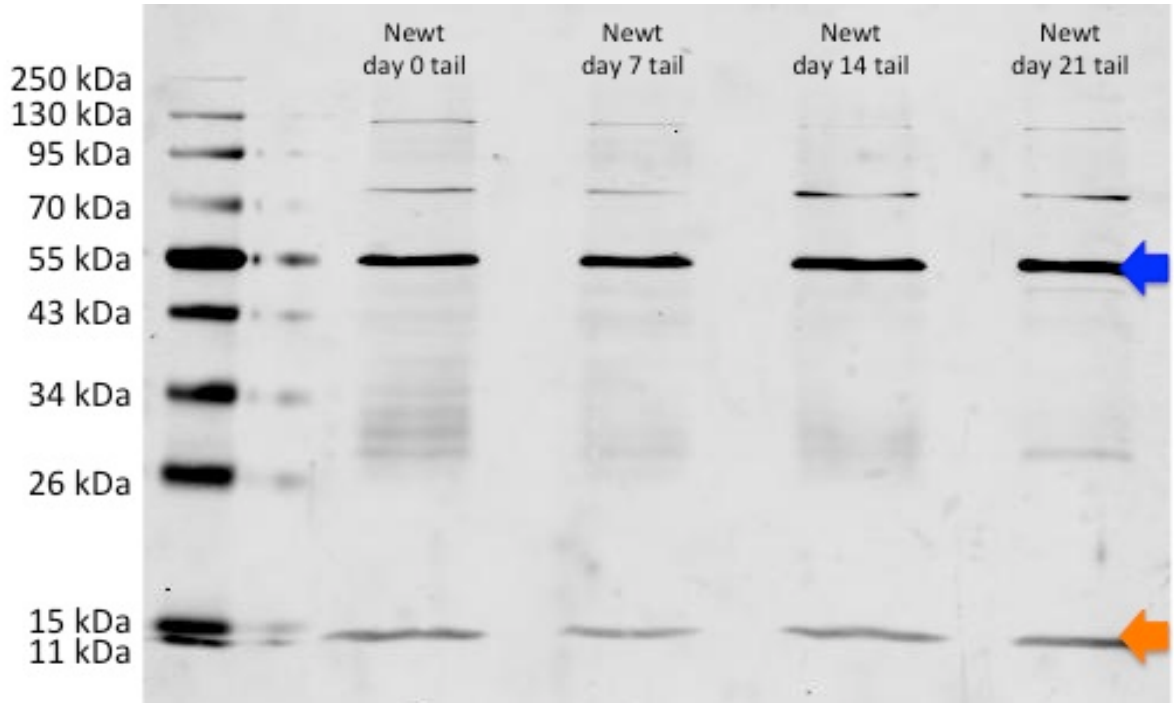

Figure A3: Western blot of newt tail tissues probed with the Sigma p21 Antibody and later reprobed with the anti-alpha tubulin antibody. The anti-p21 antibody used at a concentration of 5 ug/mL and the anti-alpha tubulin antibody used at a 1/500 dilution. Protein (20 ug) from various tissues are as follows: unamputated (day zero) newt tail tissue and newt tail regenerate tissue from days 7, 14, and 21 dpa. The lower arrow on the right highlights a low molecular weight band recognized by the Sigma anti-p21 antibody at 14/15 kDa in all newt tail tissue samples. The upper arrow on the right highlights alpha tubulin expression at 55 kDa in all newt tail tissue samples.

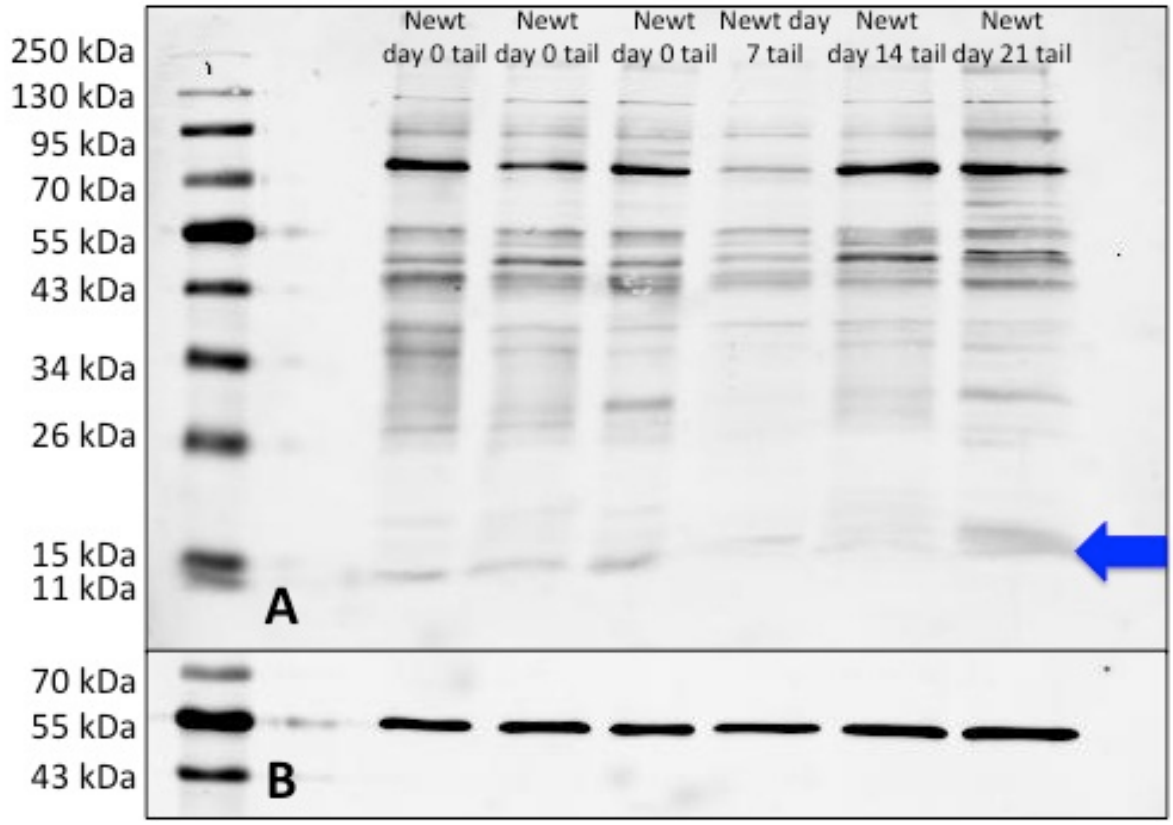

Figure A4: Western blot of newt tail tissues probed with the Sigma p21 Antibody. (A) The anti-p21 antibody used at a concentration of 5 ug/mL. (B) The anti-alpha tubulin antibody used at a 1/500 dilution. Protein (12 ug) from various tissues are as follows: three biological replicates of unamputated (day zero) newt tail tissue and newt tail regenerate tissue from days 7, 14, and 21 dpa. The arrow on the right highlights a low molecular weight band recognized by the Sigma anti-p21 antibody at 14/15 kDa in all newt tail tissue samples. This blot was incubated in a blocking serum made of 5% BSA instead of 3% Milk powder, producing brighter and cleaner bands that required less exposure for imaging.

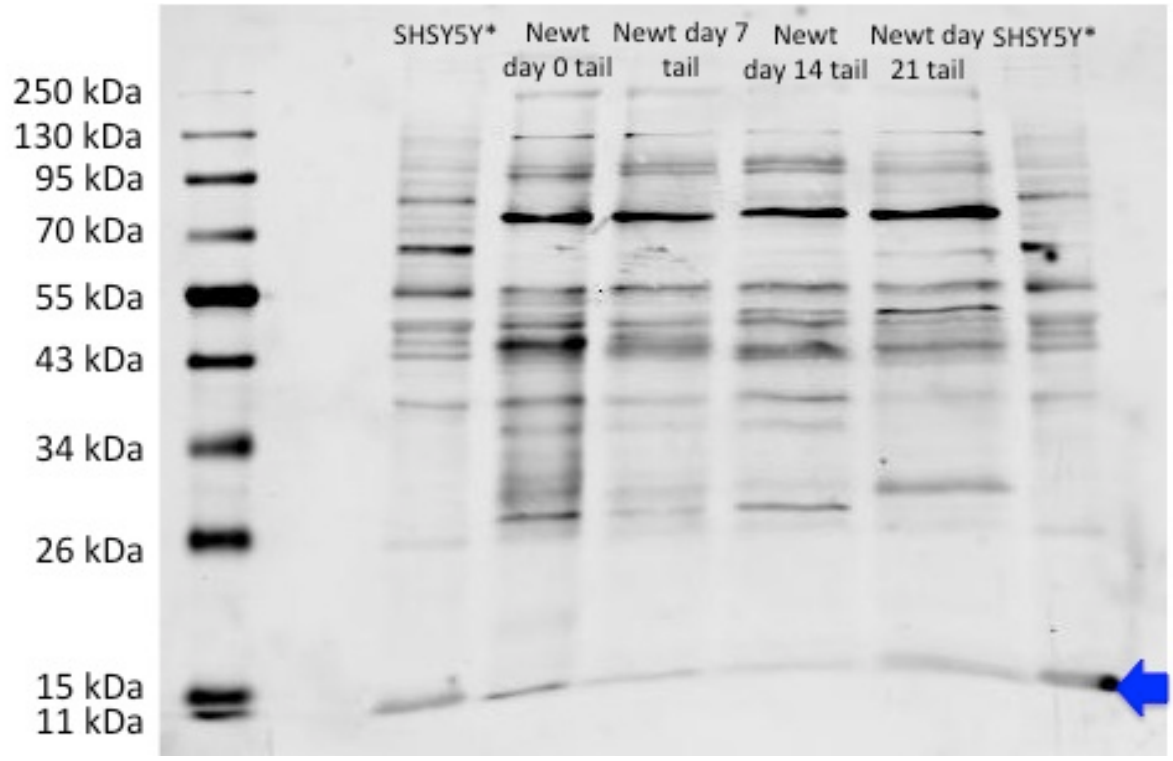

Figure A5: Western blot of SHSY5Y cells and newt tail tissues probed with the Sigma p21 Antibody. The anti-p21 antibody used at a concentration of 5 ug/mL. Protein (15 ug) from various tissues are as follows: two cell lysates from SHSY5Y cells cultured in media containing galactose, unamputated (day zero) newt tail tissue, and newt tail regenerate tissue from days 7, 14, and 21 dpa. The arrow on the right highlights a low molecular weight band recognized by the Sigma anti-p21 antibody at 14/15 kDa in all newt tail tissue samples and the SHSY5Y cell lysate samples.

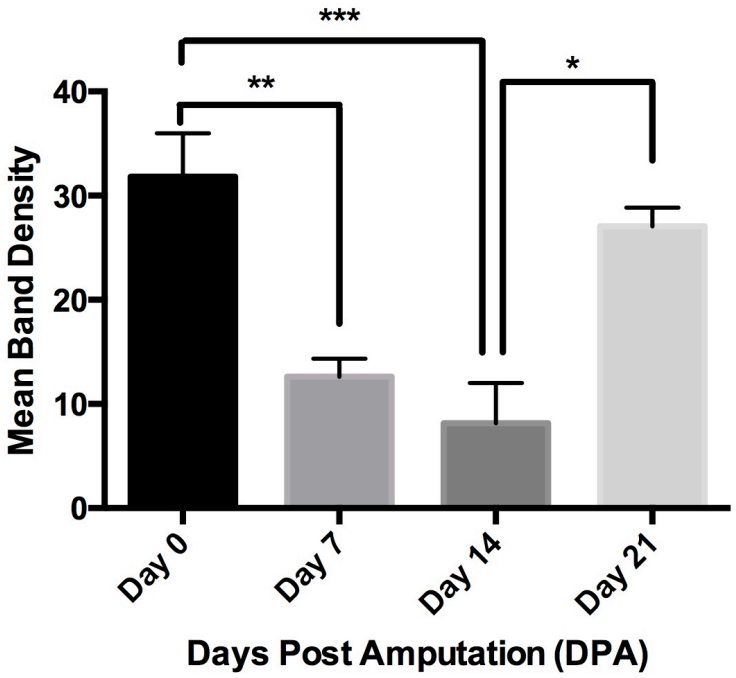

Figure A6: Quantification of Mean Band Density of low molecular weight band recognized in newt tail tissues by the Sigma p21 antibody. Significant differences are seen between day 0 and day 7 newt tail tissues and day 0 and day 14 newt tail tissues. There is also a significant difference in band density detected between day 14 and day 21 newt tails. N_{Day0}=8 and N=5 for all other time points, F=10.47, p value=0.0003; *<0.05, **<0.01, ***<0.001.

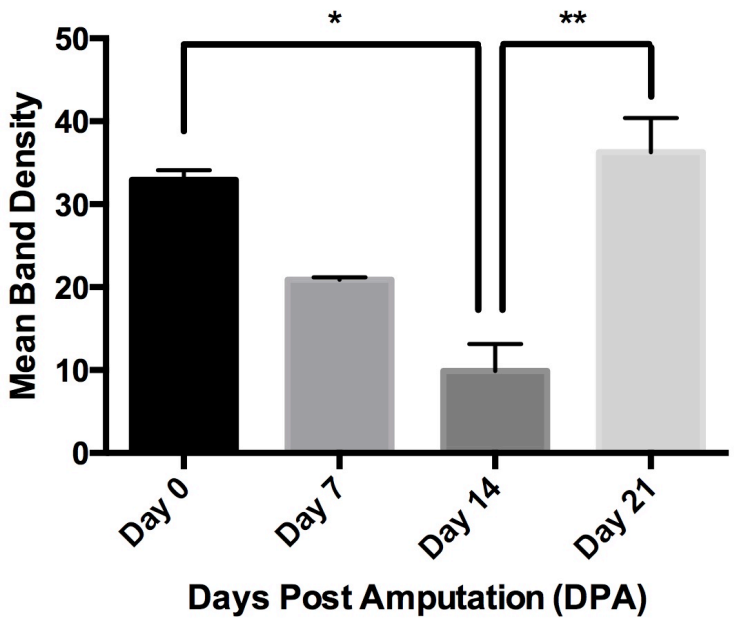

Figure A7: Quantification of Mean Band Density of low molecular weight band recognized in newt limb tissues by the Sigma p21 antibody. Significant differences are seen between day 0 and day 14 newt tail tissues and day 14 and day 21 newt tail tissues. N=2 for all time points, F=20.21, p value=0.0070; *<0.05, **<0.01.

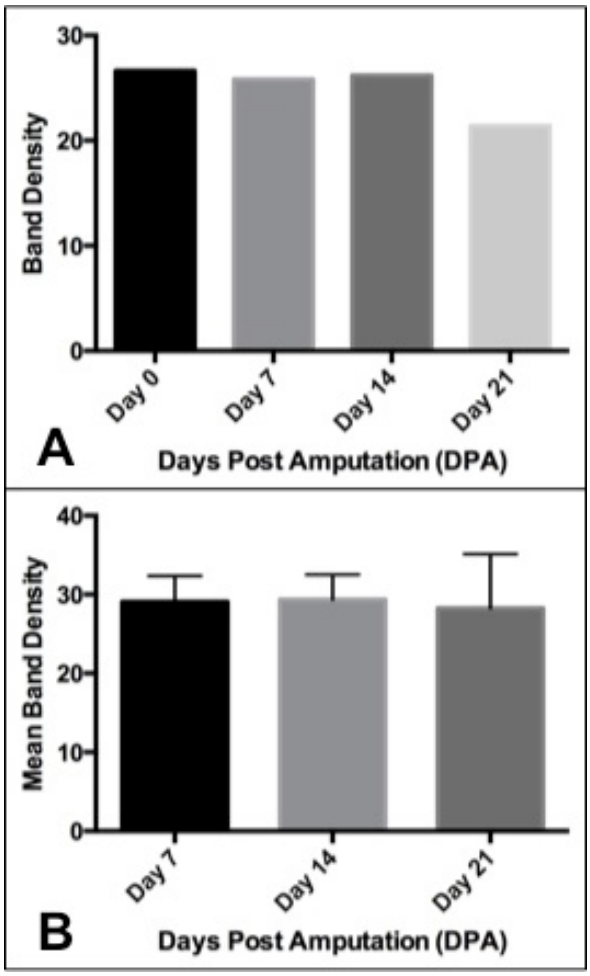

Figure A8: Quantification of Mean Band Density for ERK expression. (A) Band densities are similar across all newt tail time points tested (N=1). (B) No significant differences are seen between day 7, 14, and 21 newt tail tissues (N=2), suggesting that ERK expression is consistent across regenerative time points.

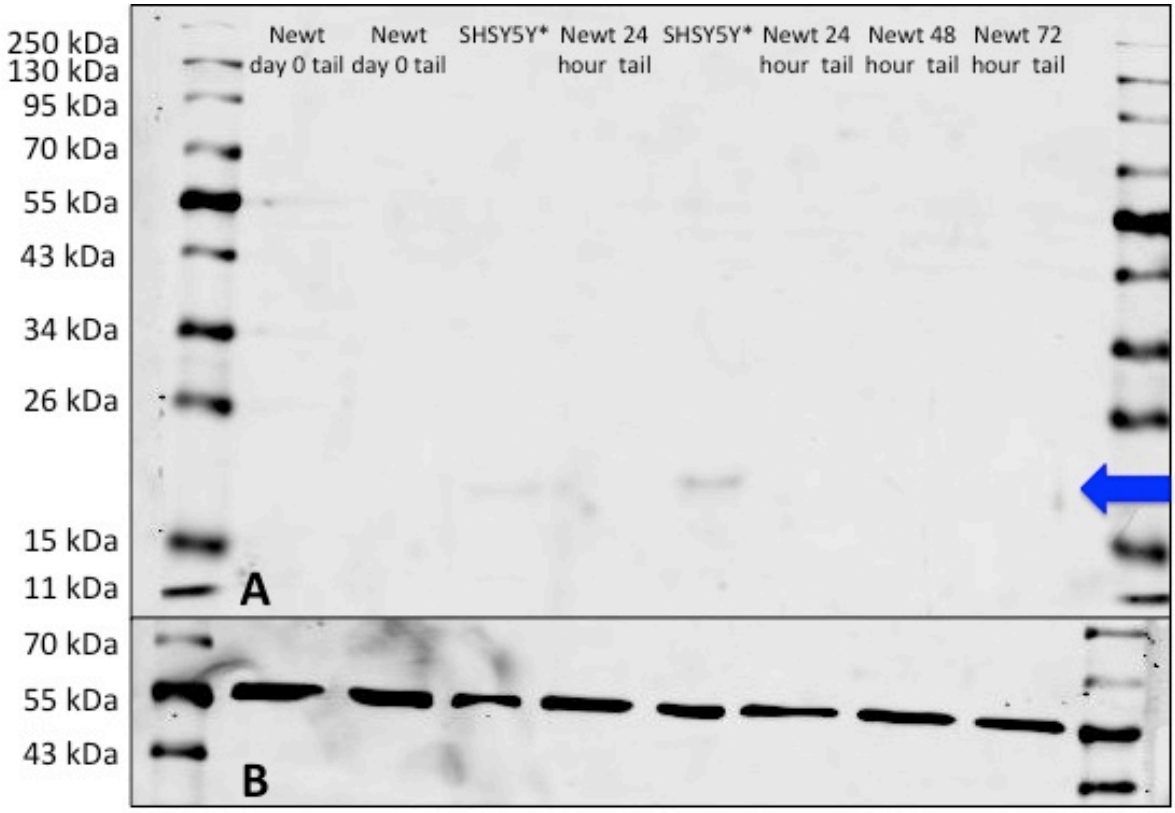

Figure A9: Western blot of SHSY5Y cells and newt tail tissues probed with the CST p21 Antibody. (A) The anti-p21 antibody used at a dilution of 1/500. (B) The anti-alpha tubulin antibody used at a 1/500 dilution. Protein (25 ug) from various tissues are as follows: two cell lysates of SHSY5Y cells cultured in media containing galactose, two biological replicates of unamputated (day zero) newt tail tissue, two biological replicates of 24 hour regenerate newt tail tissue, and newt tail regenerate tissue from 48 and 72 hours post amputation. The arrow on the right highlights p21 expression at approximately 20 kDa in only the SHSY5Y cell lysate samples.

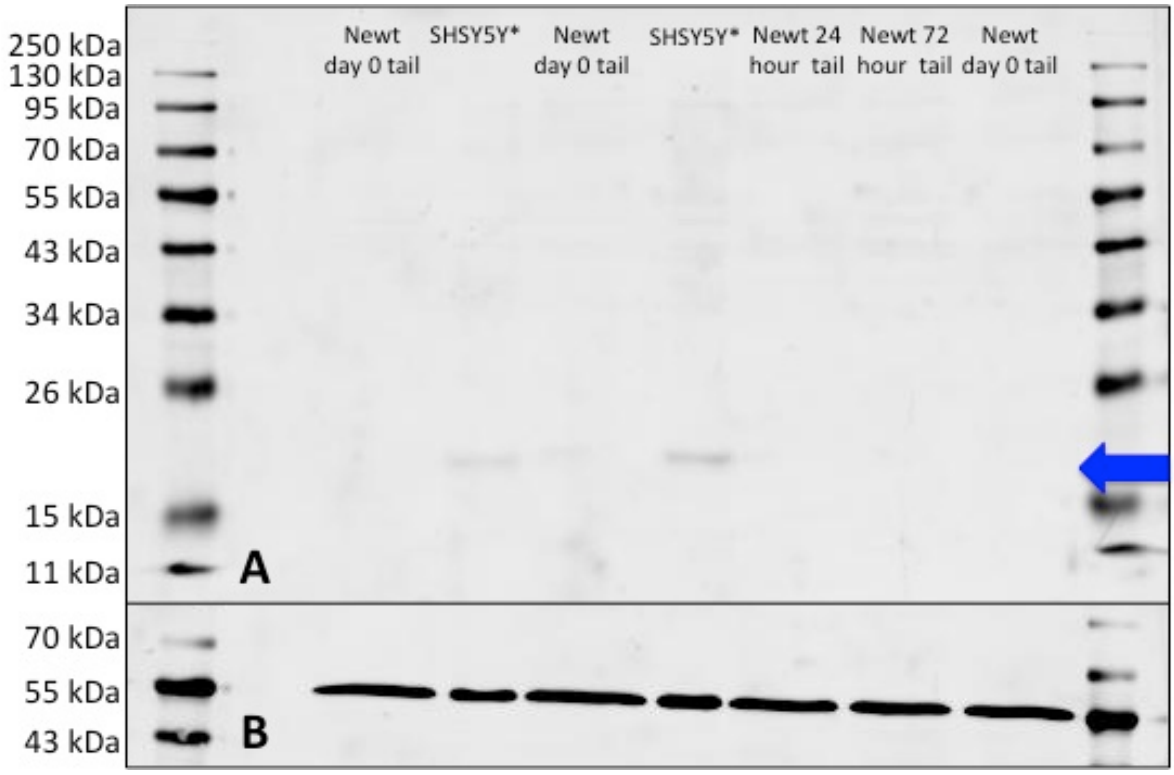

Figure A10: Western blot of SHSY5Y cells and newt tail tissues probed with the CST p21 Antibody. (A) The anti-p21 antibody used at a dilution of 1/500. (B) The anti-alpha tubulin antibody used at a 1/500 dilution. Protein (40 ug) from various tissues are as follows: two cell lysates of SHSY5Y cells cultured in media containing galactose, two biological replicates of unamputated (day zero) newt tail tissue, and newt tail regenerate tissue from 24 and 72 hours post amputation. The arrow on the right highlights p21 expression at approximately 20 kDa in only the SHSY5Y cell lysate samples.

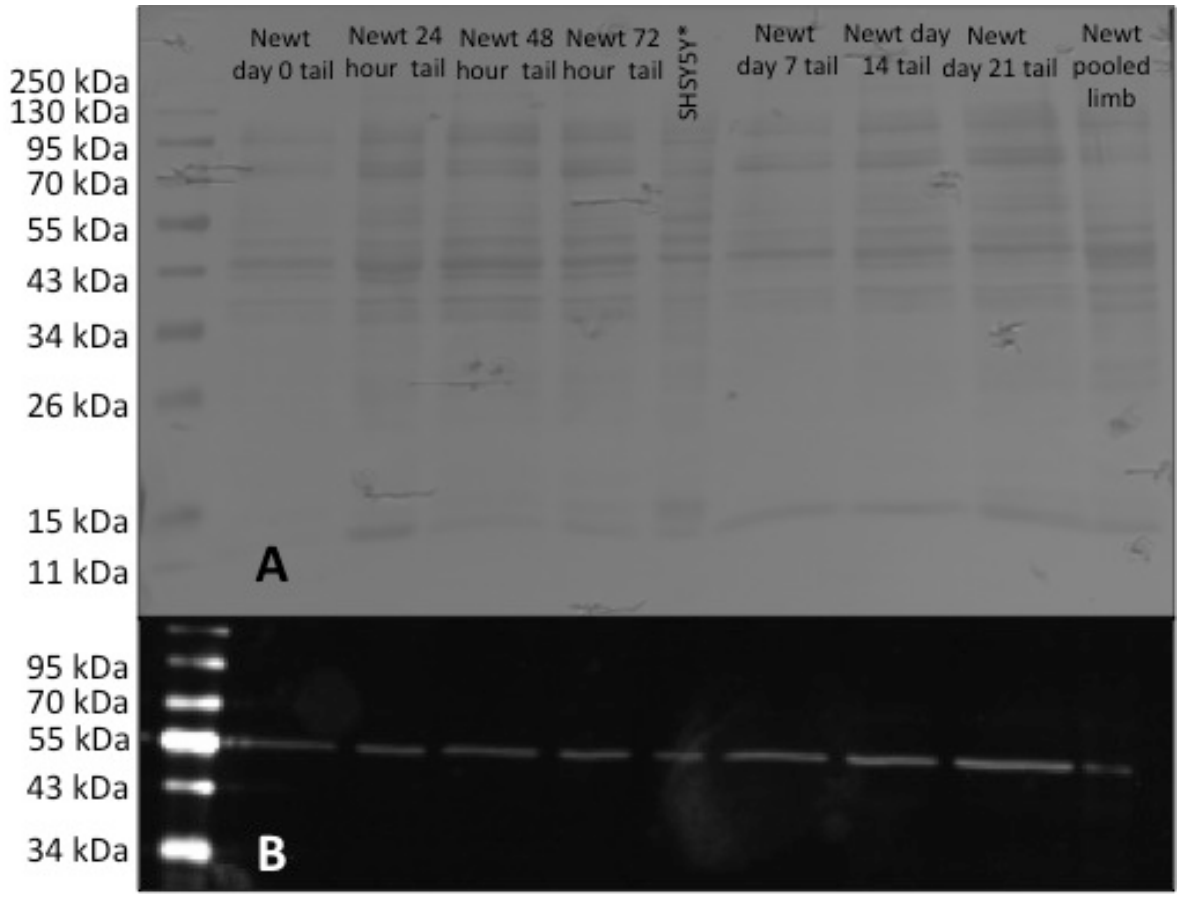

Figure A11: Ponceau-stained blot Western blot and imaged blot of various newt tissues and SHSY5Y cell lysate samples probed with the DSHB Alpha Tubulin Antibody. (A) Ponceau-stained image of Western blot before incubation with the primary antibody to stain for all proteins and validate that transfer was efficient. (B) Western blot image of anti-alpha tubulin antibody used at a 1/500 dilution and imaged as a negative using the BioRad GelDoc system. Protein (15 ug) from various tissues are as follows: newt tail tissue from 0, 24, 48, and 72 hours post amputation, newt tail tissue from 7, 14, and 21 days post amputation, pooled day 0 (unamputated) newt limb tissue, and a cell lysate from SHSY5Y cells cultured in media with galactose. This blot demonstrates that the transfer procedure was efficient, and that even low molecular weight proteins were effectively transferred.

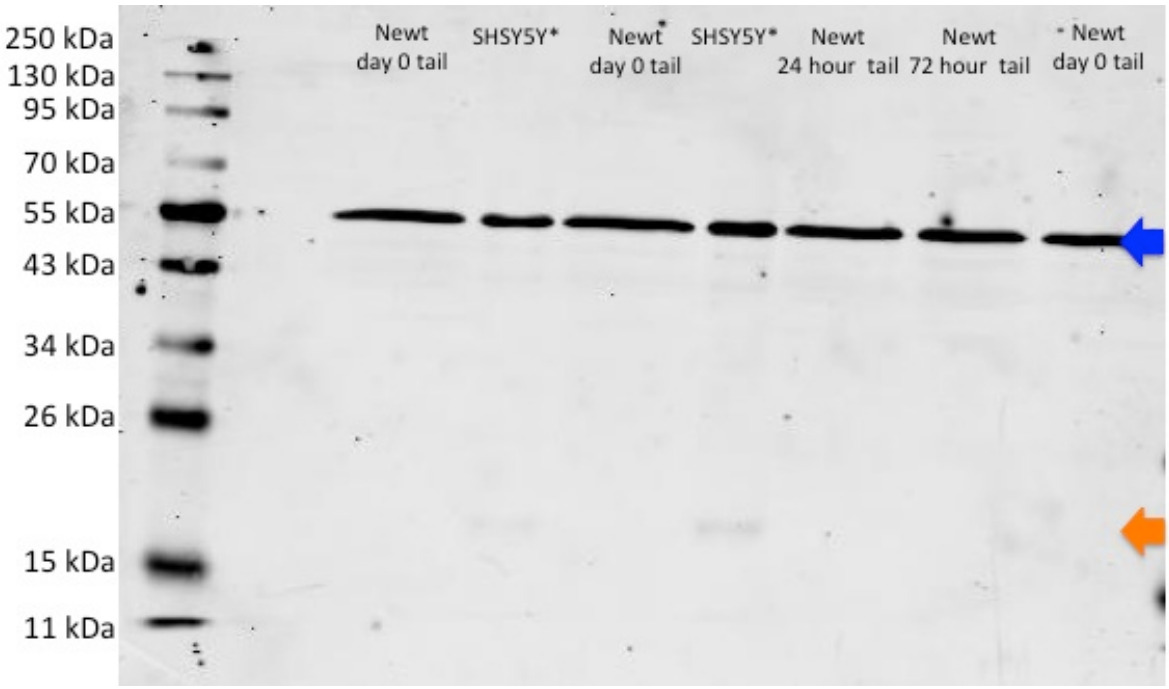

Figure A12: Western blot in Figure A10 of SHSY5Y cells and newt tail tissues probed with the CST p21 Antibody now reprobed with DSHB Alpha Tubulin Antibody. The anti-p21 antibody used at a 1/500 dilution and the anti-alpha tubulin antibody used at a 1/500 dilution. Protein (40 ug) from various tissues are as follows: two cell lysates of SHSY5Y cells cultured in media containing galactose, three biological replicates of unamputated (day zero) newt tail tissue, and newt tail regenerate tissue from 24 and 72 hours post amputation. The lower arrow on the right highlights p21 expression at approximately 20 kDa in only the SHSY5Y cell lysate samples. The upper arrow on the right highlights alpha tubulin expression at 55 kDa in all of the tested samples indicating that protein was successfully re-probed on the same blot and that protein samples were not degraded.

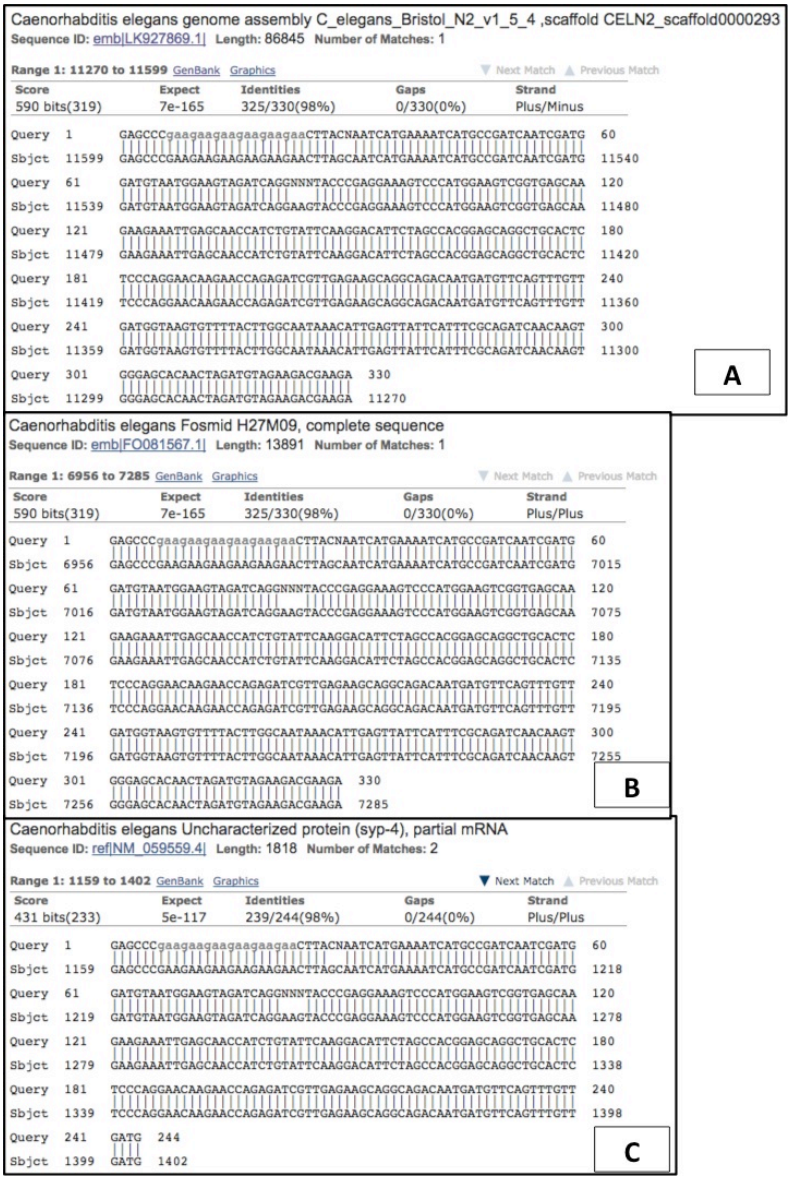

Figure A13: BLAST results finding that the 3'RACE product from primers designed to target p21 shares a high degree of similarity with 3 sequences from *C. elegans.* A) 3'RACE product shows 98% identity with *C. elegans* genome assembly complex. B) 3' RACE product shows 98% identity with *C. elegans* fosmid. A fosmid is an artificially constructed cloning vector, like a cosmid, but is based on the bacterial F plasmid. C) 3' RACE product shows 98% identity with the uncharacterized protein syp-4.